Supporting Information

Chiral inversion of macroscopic helical structures in coordination polymers induced by lanthanide ions

Zhi-Min Zhai, Song-Song Bao, Yan Xu, Qian Teng, and Li-Min Zheng*

1. Experimental details

Materials and physical measurements： *R*-(1-phenylethylamino)methyl-phosphonic acid (*R*-pempH$_2$) was prepared according to methods reported in the literature.[1,2] All other purchased materials and solvents were directly available without further treatment and purification. Elemental analyses for C, H and N were collected on a Elementar unicube (America). The Fourier infrared spectra (FTIR) spectra were recorded in the range of 400-4000 cm^{-1} by a Bruker Tensor 27 spectrometer (Bruker, Leipzig, Germany) with pressed KBr pellets. The pH value was detected with a Sartorius PB-10 pH metre. Thermogravimetric analyses (TGA) were carried out using METTLER TOLEDO TGA/DSC 1 instrument from 30 to 600 °C under a nitrogen atmosphere at a heating rate of 5 °C·min^{-1}. The powder X-ray diffraction (PXRD) patterns were collected using a Bruker D8 advance diffractometer. The scanning electron microscopy (SEM) measurements were performed on JEOL JEM-7800F. The circular dichroism (CD) spectra were recorded on a JASCO J-810 W (Tokyo, Japan) spectropolarimeter at room temperature. Vibrational circular dichroism (VCD) spectra were recorded on a Bruker VERTEX 80v Fourier transform infrared spectrometer (Bruker, Germany) equipped with a PMA 50 VCD/IRRAS module (Bruker, Germany). Single crystals were used for data collection on a Bruker D8 diffractometer using graphite monochromated Mo Kα radiation (λ=0.71073 Å) at 193 K. The photoluminescence spectra were obtained by Edinburgh FLS-980 spectrofluorometer with a xenon arc lamp (Xe900). The lifetimes of solid-state samples were obtained by fitting the decay curve with a single-exponential decay function. The quantum yields at room temperature were estimated using an integrating sphere (F-M101, Edinburgh) accessory in FLS-980 fluorescence spectrometer. The circularly polarized luminescence (CPL) was measured using a JASCO CPL-300 spectrometer.

Synthesis of helices of *R*-1h-Ln.

Synthesis of helices of Sm(*R*-pempH)$_3$·2H$_2$O (*R*-1h-Sm)： A mixture of Sm(NO$_3$)$_3$·6H$_2$O (0.066 mmol, 0.0293 g) and *R*-pempH$_2$ (0.4 mmol, 0.086 g) in 6 mL of H$_2$O was stirred for 30 min at room temperature, and then the pH of the mixture was adjusted to pH 3.5 with 0.5 M NaOH. Afterwards, the glass containing the mixture was kept in a Teflon-lined autoclave (10 mL), and incubated for hydrothermal reactions at 120 °C for 24 h. After cooling to room temperature, the flocculent precipitates of ***R*-1h-Sm** were collected and dried under air. Elemental analyses calcd (%) for C$_{27}$H$_{39}$N$_3$O$_9$P$_3$Sm·2H$_2$O: C 39.12, H 5.19, N 5.07; found: C 38.71, H 5.33, N 5.14. IR (KBr, cm^{-1}): 3416 (s), 3062 (m), 2984 (m), 2783 (m), 2520 (m), 2401

(w), 1619 (m), 1497 (m), 1456 (m), 1425 (w), 1383 (w), 1275 (m), 1159 (s), 1085 (s), 1015 (s), 985 (s), 765 (m), 698 (m), 565 (m), 534 (m), 503 (m), 473 (m) cm^{-1}. Thermal analysis revealed that the weight loss below 110 °C was 4.74%, in agreement with the release of two lattice water molecules (calcd. 4.34%).

Synthesis of helices of Eu(*R*-pempH)$_3$·2H$_2$O (*R*-1h-Eu)： Compound ***R*-1h-Eu** was obtained following the same procedure as for ***R*-1h-Sm** except that the metal salt was adjusted to Eu$(NO_3)_3$·6H$_2$O. The flocculent precipitates of ***R*-1h-Eu** were collected manually and dried under air. Elemental analyses calcd (%) for $C_{27}H_{39}N_3O_9P_3Eu·2H_2O$: C 39.05, H 5.18, N 5.06; found: C 38.79, H 5.29, N 5.17. IR (KBr, cm^{-1}): 3417 (s), 3062 (m), 2985 (m), 2787 (m), 2522 (m), 2402 (w), 1623 (m), 1497 (m), 1458 (m), 1425 (w), 1384 (w), 1275 (m), 1151 (s), 1085 (s), 1016 (s), 983 (s), 767 (m), 702 (m), 565 (m), 536 (m), 503 (m), 473 (m) cm^{-1}. Thermal analysis revealed that the weight loss below 110 °C was 4.64%, in agreement with the release of two lattice water molecules (calcd. 4.33%).

Synthesis of helices of Gd(*R*-pempH)$_3$·2H$_2$O (*R*-1h-Gd)： Compound ***R*-1h-Gd** was obtained following the same procedure as for ***R*-1h-Sm** except that the metal salt was adjusted to Gd$(NO_3)_3$·6H$_2$O. The flocculent precipitates of ***R*-1h-Gd** were collected manually and dried under air. Elemental analyses calcd (%) for $C_{27}H_{39}N_3O_9P_3Gd·2H_2O$: C 38.80, H 5.14, N 5.03; found: C 38.71, H 5.28, N 5.13. IR (KBr, cm^{-1}): 3418 (s), 3068 (m), 2985 (m), 2788 (m), 2522 (m), 2402 (w), 1620 (m), 1498 (m), 1458 (m), 1425 (w), 1384 (w), 1269 (m), 1151 (s), 1085 (s), 1020 (s), 987 (s), 763 (m), 702 (m), 570 (m), 536 (m), 503 (m), 470 (m) cm^{-1}. Thermal analysis revealed that the weight loss below 110 °C was 4.76%, in agreement with the release of two lattice water molecules (calcd. 4.30%).

Synthesis of helices of Tb(*R*-pempH)$_3$·2H$_2$O (*R*-1h-Tb)： Compound ***R*-1h-Tb** was obtained following the same procedure as for ***R*-1h-Sm** except that the metal salt was adjusted to Tb$(NO_3)_3$·6H$_2$O. The flocculent precipitates of ***R*-1h-Tb** were collected manually and dried under air. Elemental analyses calcd (%) for $C_{27}H_{39}N_3O_9P_3Tb·2H_2O$: C 38.72, H 5.13, N 5.02; found: C 38.50, H 5.24, N 5.13. IR (KBr, cm^{-1}): 3417 (s), 3065 (m), 2983 (m), 2787 (m), 2521 (m), 2402 (w), 1620 (m), 1498 (m), 1458 (m), 1429 (w), 1384 (w), 1277(m), 1151 (s), 1082 (s), 1020 (s), 987 (s), 767 (m), 702 (m), 565 (m), 532 (m), 503 (m), 474 (m) cm^{-1}. Thermal analysis revealed that the weight loss below 110 °C was 4.60%, in agreement with the release of two lattice water molecules (calcd. 4.30%).

Synthesis of helices of Dy(*R*-pempH)$_3$·2H$_2$O (*R*-1h-Dy)： Compound ***R*-1h-Dy** was obtained following the same procedure as for ***R*-1h-Sm** except that the metal salt was adjusted to Dy$(NO_3)_3$·6H$_2$O. The

flocculent precipitates of ***R*-1h-Dy** were collected manually and dried under air. Elemental analyses calcd (%) for $C_{27}H_{39}N_3O_9P_3Dy{\cdot}2H_2O$: C 38.56, H 5.11, N 5.00; found: C 38.72, H 5.36, N 5.13. IR (KBr, cm^{-1}): 3417 (s), 3062 (m), 2983 (m), 2785 (m), 2522 (m), 2402 (w), 1620 (m), 1498 (m), 1458 (m), 1429 (w), 1384 (w), 1272 (m), 1151 (s), 1082 (s), 1016 (s), 983 (s), 767 (m), 702 (m), 565 (m), 536 (m), 503 (m), 471 (m) cm^{-1}. Thermal analysis revealed that the weight loss below 110 °C was 4.69%, in agreement with the release of two lattice water molecules (calcd. 4.28%).

Synthesis of helices of Ho(*R*-pempH)$_3{\cdot}2H_2O$ (*R*-1h-Ho): Compound ***R*-1h-Ho** was obtained following the same procedure as for ***R*-1h-Sm** except that the metal salt was adjusted to $Ho(NO_3)_3{\cdot}6H_2O$. The flocculent precipitates of ***R*-1h-Ho** were collected manually and dried under air. Elemental analyses calcd (%) for $C_{27}H_{39}N_3O_9P_3Ho{\cdot}2H_2O$: C 38.45, H 5.10, N 4.98; found: C 38.36, H 5.20, N 5.13. IR (KBr, cm^{-1}): 3417 (s), 3065 (m), 2985 (m), 2787 (m), 2524 (m), 2401 (w), 1620 (m), 1498 (m), 1458 (m), 1425 (w), 1384 (w), 1272 (m), 1151 (s), 1082 (s), 1020 (s), 987 (s), 763 (m), 702 (m), 565 (m), 536 (m), 503 (m), 470 (m) cm^{-1}. Thermal analysis revealed that the weight loss below 110 °C was 4.49%, in agreement with the release of two lattice water molecules (calcd. 4.27%).

Synthesis of block-like crystals of *R*-2b-Ln

Synthesis of block-like crystals of $(H_3O)[Sm_6$(*R*-pempH$_2)_3$(*R*-pempH$)_{15}](NO_3)_4{\cdot}16H_2O$ (*R*-2b-Sm). Crystals of ***R*-2b-Sm** was obtained following the same procedure as for ***R*-1h-Sm** except that the pH of the mixture was adjusted to 3.0. The colourless block-like crystals of ***R*-2b-Sm** were collected manually and dried under air. Elemental analyses calcd (%) for $C_{162}H_{237}N_{22}O_{66}P_{18}Sm_6{\cdot}16H_2O(H_3O)$: C 36.60, H 5.12, N 5.80; found: C 36.96, H 5.13, N 5.78. IR (KBr, cm^{-1}): 3417(s), 3062(m), 2985(m), 2786(m), 2528(m), 2405(w), 1589 (m), 1494 (m), 1452 (m), 1384(s), 1311(w), 1265 (m), 1193 (s), 1128 (s), 1082 (s), 1018 (s), 756 (s), 702 (m), 565 (m), 536 (m), 503 (m), 473 (m) cm^{-1}. Thermal analysis revealed that the weight loss below 110 °C was 5.45%, in agreement with the release of seventeen lattice water molecules (calcd. 5.76%).

Synthesis of block-like crystals of $(H_3O)[Ho_6$(*R*-pempH$_2)_3$(*R*-pempH$)_{15}](NO_3)_4{\cdot}5H_2O$ (*R*-2b-Ho). Crystals of ***R*-2b-Ho** was obtained following the same procedure as for ***R*-1h-Ho** except that the pH of the mixture was adjusted to 3.0. The colourless block-like crystals of ***R*-2b-Ho** were collected manually and dried under air. Elemental analyses calcd (%) for $C_{162}H_{237}N_{22}O_{66}P_{18}Ho_6{\cdot}5H_2O(H_3O)$: C 37.38, H 4.80, N 5.92; found: C 37.25, H 4.80, N 5.81. IR (KBr, cm^{-1}): 3418(s), 3066(m), 2983(m), 2783(m), 2524(m),

2412(w), 1612 (m), 1496 (m), 1458 (m), 1385(s), 1315(w), 1276 (m), 1164 (s), 1120 (s), 1082 (s), 1016 (s), 754 (s), 702 (m), 565 (m), 538 (m), 503 (m), 472 (m) cm^{-1}. Thermal analysis revealed that the weight loss below 110 °C was 1.79%, in agreement with the release of six lattice water molecules (calcd. 2.07%).

Synthesis of rod-like crystals of *R*-3r-Ln

Synthesis of rod-like crystals of Sm(*R*-pempH)$_3$·H$_2$O (*R*-3r-Sm). Crystals of ***R*-3r-Sm** was obtained following the same procedure as for ***R*-1h-Sm** except that the pH of the mixture was adjusted to 5.0. The colourless rod-like crystals of ***R*-3r-Sm** were collected manually and dried under air. Elemental analyses calcd (%) for $C_{27}H_{39}N_3O_9P_3Sm·H_2O$: C 39.96, H 5.06, N 5.18; found: C 39.78, H 5.11, N 5.07. IR (KBr, cm^{-1}): 3417 (s), 3066 (m), 2985 (m), 2787 (m), 2522 (m), 2402 (w), 1621 (m), 1497 (m), 1456 (m), 1425 (w), 1384 (w), 1275 (m), 1159 (s), 1085 (s), 1015 (s), 985 (s), 766 (m), 700 (m), 565 (m), 536 (m), 503 (m), 473 (m) cm^{-1}. Thermal analysis revealed that the weight loss below 110 °C was 2.59%, in agreement with the release of one lattice water molecules (calcd. 2.22%).

Synthesis of rod-like crystals of Eu(*R*-pempH)$_3$·H$_2$O (*R*-3r-Eu)： Crystals of ***R*-3r-Eu** was obtained following the same procedure as for ***R*-1h-Eu** except that the pH of the mixture was adjusted to 5.0. The colourless rod-like crystals of ***R*-3r-Eu** were collected manually and dried under air. Elemental analyses calcd (%) for $C_{27}H_{39}N_3O_9P_3Eu·H_2O$: C 39.88, H 5.05, N 5.17; found: C 39.65, H 5.14, N 5.08. IR (KBr, cm^{-1}): 3414 (s), 3066 (m), 2982 (m), 2788 (m), 2522 (m), 2402 (w), 1621 (m), 1498 (m), 1456 (m), 1425 (w), 1384 (w), 1276 (m), 1159 (s), 1085 (s), 1016 (s), 985 (s), 766 (m), 700 (m), 564 (m), 536 (m), 503 (m), 472 (m) cm^{-1}. Thermal analysis revealed that the weight loss below 110 °C was 2.66%, in agreement with the release of one lattice water molecules (calcd. 2.21%).

Synthesis of rod-like crystals of Gd(*R*-pempH)$_3$·H$_2$O (*R*-3r-Gd)： Crystals of ***R*-3r-Gd** was obtained following the same procedure as for ***R*-1h-Gd** except that the pH of the mixture was adjusted to 5.0. The colourless rod-like crystals of ***R*-3r-Gd** were collected manually and dried under air. Elemental analyses calcd (%) for $C_{27}H_{39}N_3O_9P_3Gd·H_2O$: C 39.62, H 5.01, N 5.14; found: C 39.39, H 5.31, N 5.18. IR (KBr, cm^{-1}): 3417 (s), 3066 (m), 2981 (m), 2787 (m), 2526 (m), 2402 (w), 1621 (m), 1497 (m), 1455 (m), 1425 (w), 1385 (w), 1275 (m), 1154 (s), 1085 (s), 1015 (s), 985 (s), 765 (m), 700 (m), 565 (m), 536 (m), 503 (m), 471 (m) cm^{-1}. Thermal analysis revealed that the weight loss below 110 °C was 2.61%, in agreement with the release of one lattice water molecules (calcd. 2.20%).

Synthesis of rod-like crystals of Tb(*R*-pempH)$_3$·H$_2$O (*R*-3r-Tb): Crystals of ***R*-3r-Tb** was obtained following the same procedure as for ***R*-1h-Tb** except that the pH of the mixture was adjusted to 5.0. The colourless rod-like crystals of ***R*-3r-Tb** were collected manually and dried under air. Elemental analyses calcd (%) for $C_{27}H_{39}N_3O_9P_3Tb·H_2O$: C 39.54, H 5.00, N 5.13; found: C 39.36, H 5.11, N 5.03. IR (KBr, cm^{-1}): 3417 (s), 3066 (m), 2985 (m), 2787 (m), 2522 (m), 2402 (w), 1621 (m), 1497 (m), 1456 (m), 1425 (w), 1384 (w), 1275 (m), 1162 (s), 1085 (s), 1015 (s), 983 (s), 766 (m), 701 (m), 565 (m), 534 (m), 503 (m), 472 (m) cm^{-1}. Thermal analysis revealed that the weight loss below 110 °C was 2.59%, in agreement with the release of one lattice water molecules (calcd. 2.19%).

Synthesis of rod-like crystals of Dy(*R*-pempH)$_3$·H$_2$O (*R*-3r-Dy): Crystals of ***R*-3r-Dy** was obtained following the same procedure as for ***R*-1h-Dy** except that the pH of the mixture was adjusted to 5.0. The colourless rod-like crystals of ***R*-3r-Dy** were collected manually and dried under air. Elemental analyses calcd (%) for $C_{27}H_{39}N_3O_9P_3Dy·H_2O$: C 39.37, H 4.98, N 5.10; found: C 39.40, H 5.26, N 5.17. IR (KBr, cm^{-1}): 3418 (s), 3066 (m), 2985 (m), 2785 (m), 2522 (m), 2401 (w), 1621 (m), 1497 (m), 1460 (m), 1425 (w), 1384 (w), 1275 (m), 1159 (s), 1088 (s), 1015 (s), 985 (s), 764 (m), 700 (m), 565 (m), 531 (m), 503 (m), 474 (m) cm^{-1}. Thermal analysis revealed that the weight loss below 110 °C was 2.67%, in agreement with the release of one lattice water molecules (calcd. 2.18%).

Synthesis of rod-like crystals of Ho(*R*-pempH)$_3$·H$_2$O (*R*-3r-Ho): Crystals of ***R*-3r-Ho** was obtained following the same procedure as for ***R*-1h-Ho** except that the pH of the mixture was adjusted to 5.0. The colourless rod-like crystals of ***R*-3r-Ho** were collected manually and dried under air. Elemental analyses calcd (%) for $C_{27}H_{39}N_3O_9P_3Ho·H_2O$: C 39.25, H 4.97, N 5.09; found: C 38.77, H 5.14, N 5.14. IR (KBr, cm^{-1}): 3415 (s), 3066 (m), 2984 (m), 2787 (m), 2522 (m), 2401 (w), 1621 (m), 1497 (m), 1455 (m), 1425 (w), 1384 (w), 1275 (m), 1154 (s), 1085 (s), 1015 (s), 984 (s), 766 (m), 700 (m), 562 (m), 535 (m), 503 (m), 471 (m) cm^{-1}. Thermal analysis revealed that the weight loss below 110 °C was 2.60%, in agreement with the release of one lattice water molecules (calcd. 2.18%).

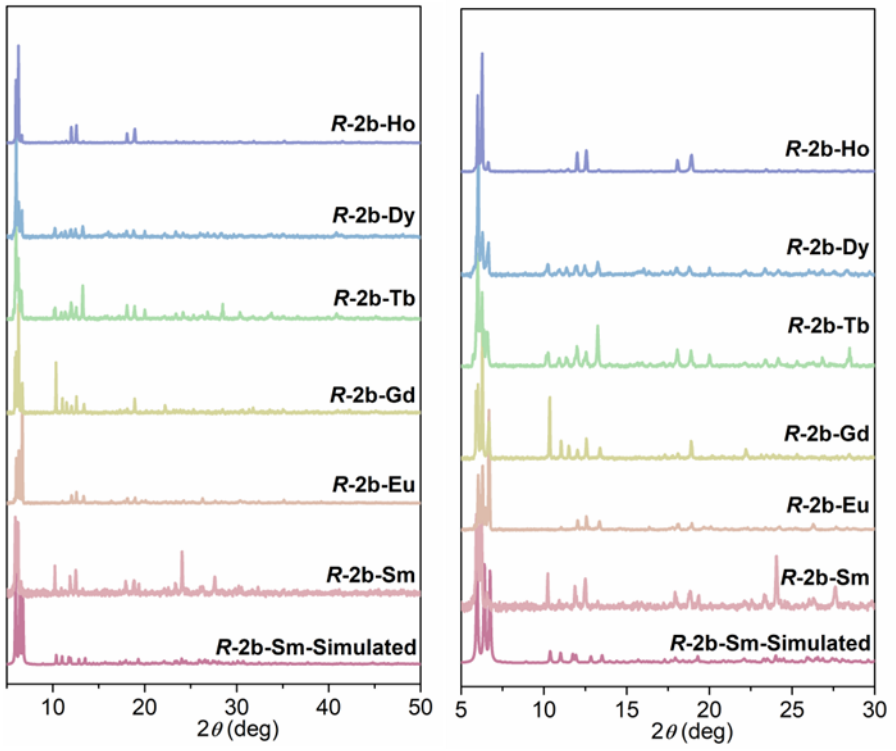

Figure S1. The PXRD patterns of ***R*-2b-Ln** (Ln = Sm, Eu, Gd, Tb, Dy, Ho). The patterns simulated from single crystal data are given for comparison.

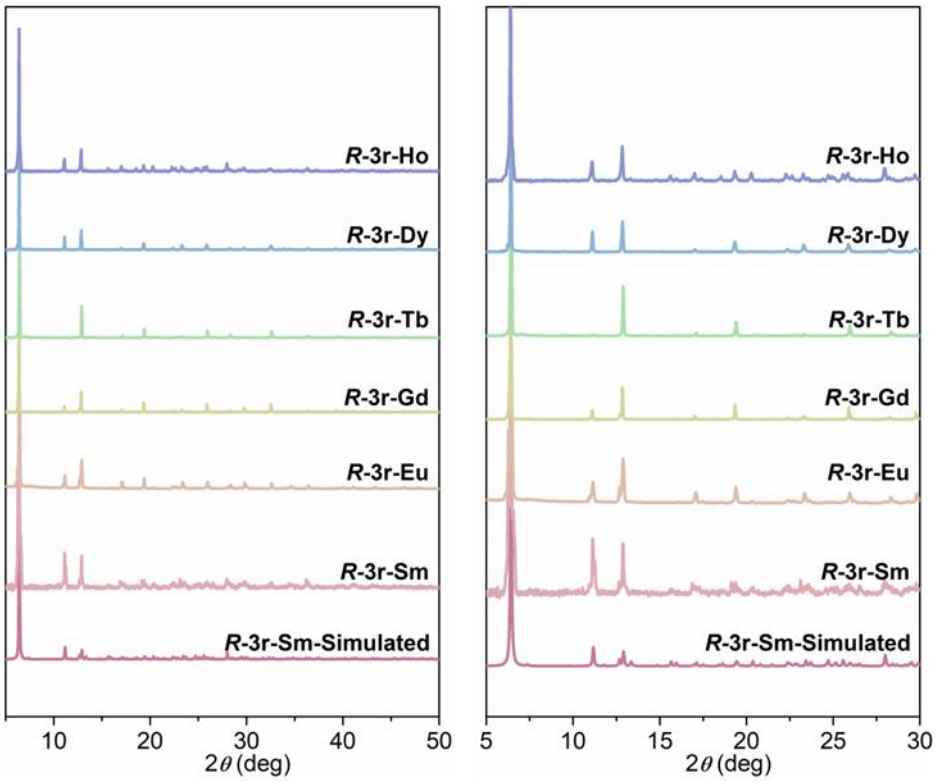

Figure S2. The PXRD patterns of ***R*-3r-Ln** (Ln = Sm, Eu, Gd, Tb, Dy, Ho). The patterns simulated from single crystal data are given for comparison.

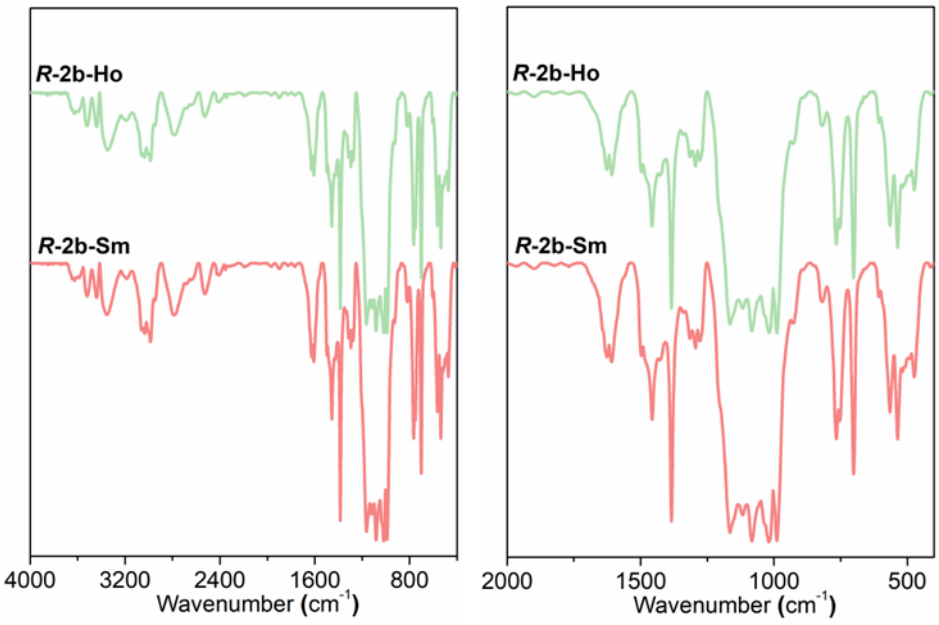

Figure S3. The IR spectra of ***R*-2b-Ln** (Ln = Sm, Ho).

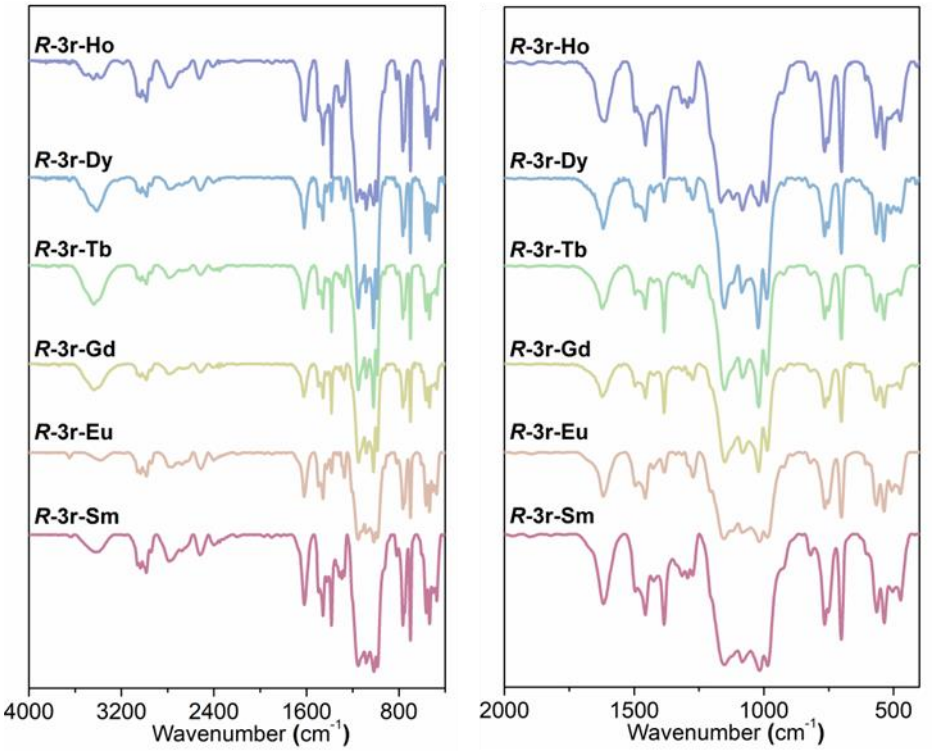

Figure S4. The IR spectra of ***R*-3r-Ln** (Ln = Sm, Eu, Gd, Tb, Dy, Ho).

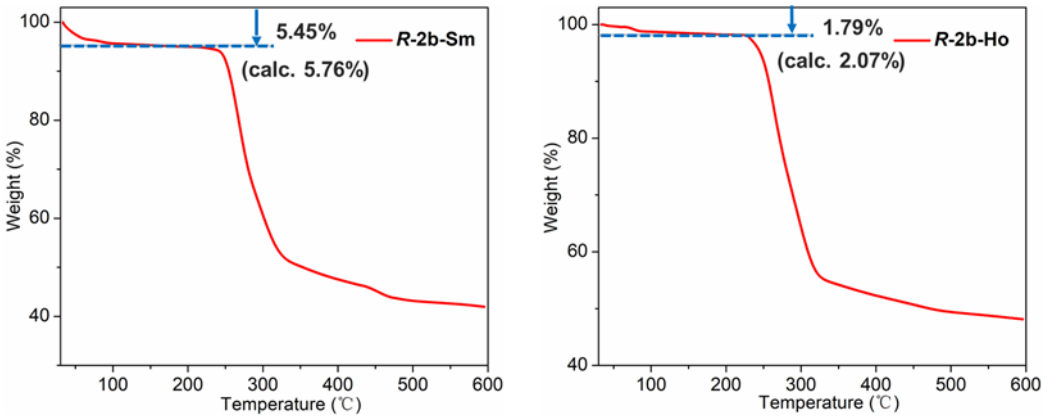

Figure S5. TGA curves of ***R*-2b-Ln** (Ln = Sm, Ho). The weight losses in the temperature 30-110 °C agree well with the valued expected for the removal of seventeen and six lattice water molecules for ***R*-2b-Sm** and ***R*-2b-Ho**, respectively.

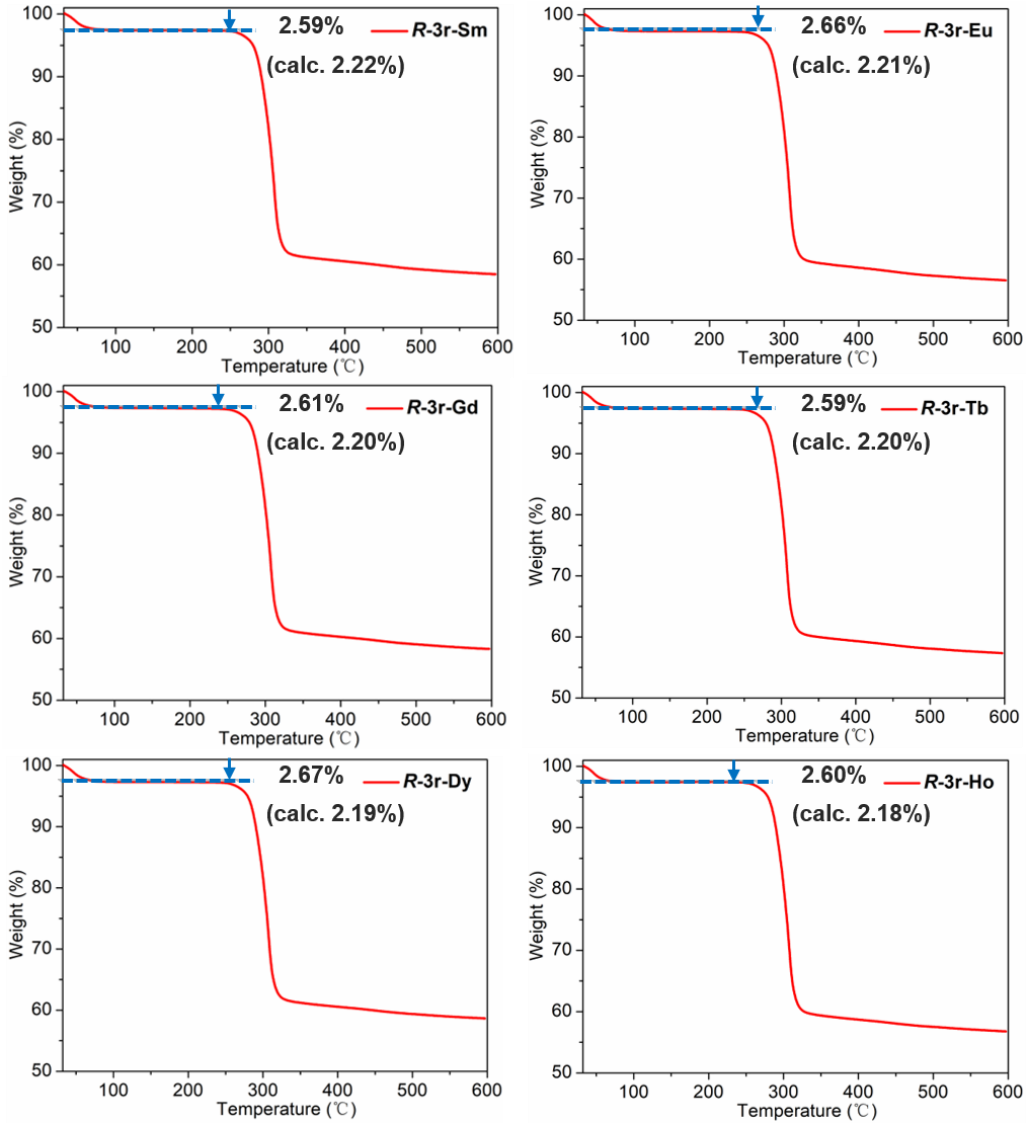

Figure S6. TGA curves of ***R*-3r-Ln** (Ln = Sm, Eu, Gd, Tb, Dy, Ho). The weight losses in the temperature 30-110 °C agree well with the valued expected for the removal of one lattice water molecules.

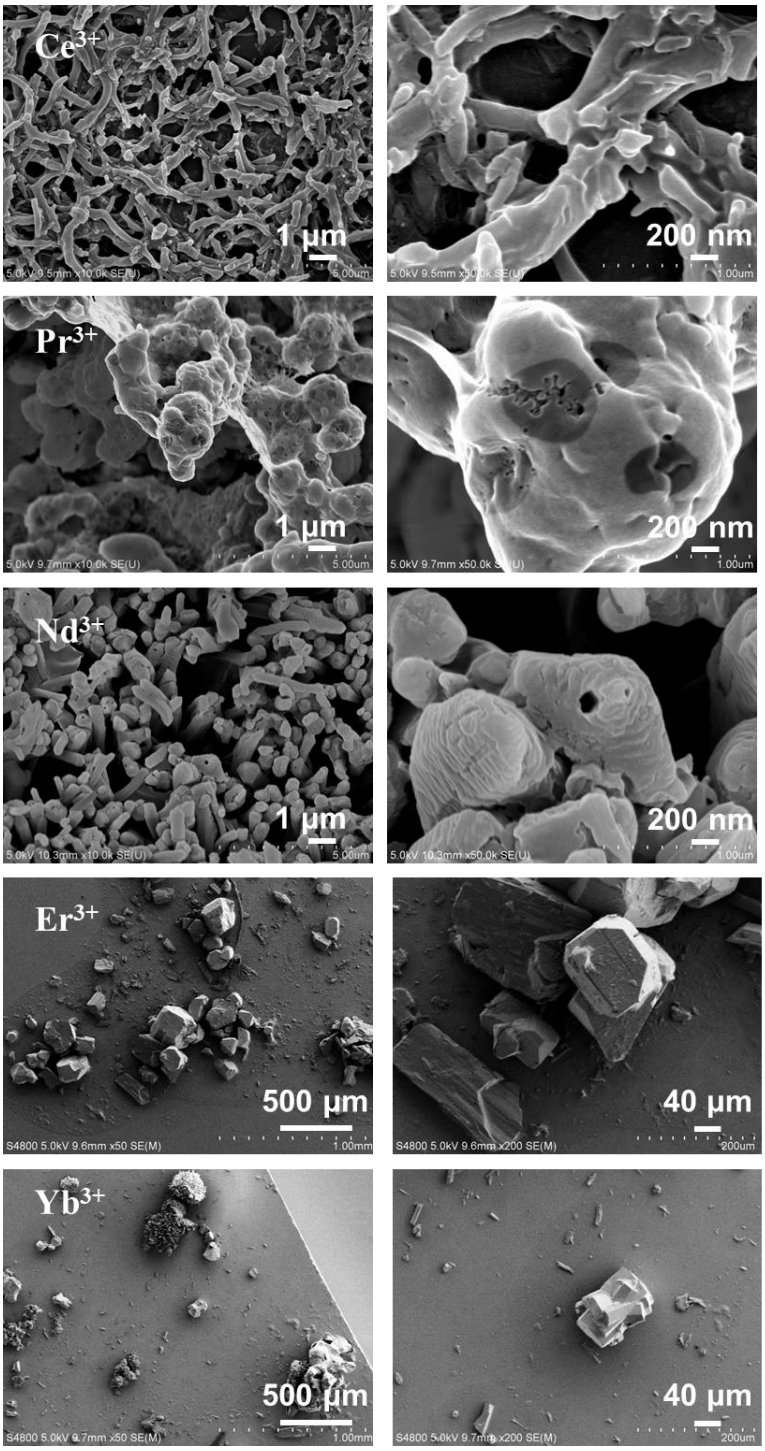

Figure S7. SEM images of products after hydrothermal reactions of $Ln(NO_3)_3$ (Ln = Ce, Pr, Nd, Er, Yb) and *R*-pempH$_2$ (M:L molar ratio 1:6, pH 3.5, autoclave filling degree 60 %) at 120 °C for 24 h.

Table S1. Crystal data of ***R*-2b-Sm**, ***R*-2b-Eu**, ***R*-2b-Gd**, ***R*-2b-Tb**, ***R*-2b-Dy** and ***R*-2b-Ho**.[a]

Compounds	***R*-2b-Sm**	***R*-2b-Eu**	***R*-2b-Gd**	***R*-2b-Tb**	***R*-2b-Dy**	***R*-2b-Ho**
Formula	$C_{162}H_{272}N_{22}O_{83}P_{18}Sm_6$	$C_{162}H_{262}N_{22}O_{78}P_{18}Eu_6$	$C_{162}H_{262}N_{22}O_{78}P_{18}Gd_6$	$C_{162}H_{262}N_{22}O_{78}P_{18}Tb_6$	$C_{162}H_{262}N_{22}O_{78}P_{18}Dy_6$	$C_{162}H_{262}N_{22}O_{78}P_{18}Ho_6$
M	5315.68	5235.23	5266.88	5276.90	5298.44	5291.86
Crystal system	Monoclinic	Monoclinic	Monoclinic	Monoclinic	Monoclinic	Monoclinic
Space group	$P2_1$	$P2_1$	$P2_1$	$P2_1$	$P2_1$	$P2_1$
T (K)	150	193	193	150	170	193
a (Å)	17.080(5)	17.045(6)	17.107(16)	17.196(3)	16.973(3)	17.041(17)
b (Å)	24.524(7)	24.219(9)	24.209(2)	24.279(4)	24.111(4)	24.075(2)
c (Å)	26.270(8)	26.173(10)	26.190(3)	26.223(5)	26.452(4)	26.614(3)
α (°)	90	90	90	90	90	90
β (°)	94.552(5)	92.618(1)	92.434(15)	92.282(4)	92.859(2)	92.619(3)
γ (°)	90	90	90	90	90	90
V (Å^3)	10969(5)	10792.9(7)	10836.0(18)	10940(3)	10812(3)	10907.2(19)
D_c [g cm^{-3}]	1.598	1.607	1.614	1.602	1.620	1.619
μ[mm^{-1}]	1.804	1.941	2.033	2.315	2.271	2.372
F(000)	5334	5310	5332	5344	5306	5350
R_{int}	0.078	0.060	0.040	0.153	0.055	0.121
R_1, wR_2 [$I>2\sigma(I)$]	0.0682, 0.1452	0.048, 0.123	0.0374, 0.0774	0.099, 0.181	0.073, 0.183	0.101, 0.253
CCDC number	2086972	2312659	2086976	1501001	1850509	Not deposit

$R_1 = \Sigma||F_o| - |F_c||/\Sigma|F_o|$, $wR_2 = [\Sigma w(F_o^2 - F_c^2)^2/\Sigma w(F_o^2)^2]^{1/2}$

[a] The structures of ***R*-2b-Eu**, ***R*-2b-Gd**, ***R*-2b-Tb** and ***R*-2b-Dy** have already been reported in our previous work, [2-4] while those of compounds ***R*-2b-Sm** and ***R*-2b-Ho** are unreported structures.

Table S2. Partial bond lengths [Å] and bond angles [°] of ***R*-2b-Ln**.

Compounds	***R*-2b-Sm**	***R*-2b-Ho**		***R*-2b-Sm**	***R*-2b-Ho**
Ln1-O4	2.322(11)	2.322(11)	P2-O6	1.511(13)	1.511(13)
Ln1-O1	2.386(11)	2.386(11)	P2-O5	1.517(13)	1.517 (12)
Ln1-O8	2.409(12)	2.409(12)	P3-O9	1.537(14)	1.536(13)
Ln1-O20A	2.419(12)	2.422(12)	P3-O8	1.535(13)	1.529(12)
Ln1-O26A	2.426(12)	2.426(12)	P3-O7	1.524(13)	1.522(12)
Ln1-O24A	2.420(11)	2.420(11)	P4-O12	1.502(15)	1.504(14)
Ln1-O7	2.541(12)	2.543(11)	P4-O10	1.520(12)	1.518(12)
Ln1-O22A	2.612(12)	2.616(12)	P4-O11	1.540(13)	1.541(12)
Ln2-O5	2.327(13)	2.325(12)	P5-O15	1.490(13)	1.489(13)
Ln2-O16	2.392(13)	2.388(11)	P5-O14	1.509(13)	1.507(12)
Ln2-O13	2.389(12)	2.390(12)	P5-O13	1.537(13)	1.539(13)
Ln2-O7	2.395(12)	2.397(11)	P6-O17	1.502(13)	1.508(13)
Ln2-O2	2.401(10)	2.401(10)	P6-O16	1.490(13)	1.492(13)
Ln2-O11	2.476(11)	2.475(11)	P6-O18	1.577(14)	1.578(14)
Ln2-O1	2.604(11)	2.601(11)	P7-O21	1.510(16)	1.510(14)
Ln2-O10	2.657(12)	2.656(12)	P7-O19	1.512(13)	1.508(12)
Ln3-O10	2.394(12)	2.396(11)	P7-O20	1.541(12)	1.537(12)
Ln3-O22	2.372(12)	2.367(12)	P8-O23	1.518(12)	1.518(12)
Ln3-O25	2.409(12)	2.409(12)	P8-O24	1.549(13)	1.549(13)
Ln3-O19	2.443(11)	2.438(11)	P8-O22	1.552(12)	1.554(12)
Ln3-O17	2.403(13)	2.400(12)	P9-O25	1.515(13)	1.515(12)
Ln3-O14	2.427(10)	2.425(11)	P9-O26	1.523(13)	1.528(13)
Ln3-O13	2.530(12)	2.527(12)	P9-O27	1.559(13)	1.560(13)
Ln3-O20	2.603(12)	2.601(12)	P10-O29	1.491(14)	1.490(14)
Ln4-O28	2.340(15)	2.338(15)	P10-O28	1.526(15)	1.529(15)
Ln4-O34	2.343(13)	2.342(12)	P10-O30	1.49(2)	1.50(2)
Ln4-O40	2.381(12)	2.381(13)	P11-O32	1.515(14)	1.515(13)
Ln4-O53B	2.366(12)	2.370(12)	P11-O31	1.537(13)	1.536(13)
Ln4-O31	2.437(13)	2.436(12)	P11-O33	1.535(15)	1.539(13)
Ln4-O37	2.441(11)	2.439(12)	P12-O35	1.520(13)	1.519(12)
Ln4-O38	2.573(12)	2.571(12)	P12-O36	1.507(13)	1.503(13)
Ln5-O35	2.390(13)	2.393(11)	P12-O34	1.498(14)	1.501(12)
Ln5-O49	2.396(12)	2.397(12)	P13-O39	1.483(14)	1.483(14)
Ln5-O38	2.384(12)	2.384(12)	P13-O37	1.548(13)	1.551(13)
Ln5-O43	2.400(12)	2.396(12)	P13-O38	1.536(14)	1.538(13)
Ln5-O41	2.423(12)	2.424(12)	P14-O42	1.453(16)	1.452(15)

Ln5-O46	2.454(11)	2.453(11)	P14-O41	1.543(13)	1.540(13)
Ln5-O47	2.529(12)	2.525(12)	P14-O40	1.534(13)	1.535(13)
Ln5-O40	2.619(12)	2.616(12)	P15-O45	1.494(14)	1.497(13)
Ln6-O44	2.368(12)	2.366(12)	P15-O44	1.537(13)	1.534(14)
Ln6-O47	2.350(11)	2.352(11)	P15-O43	1.514(13)	1.520(12)
Ln6-O29C	2.362(15)	2.360(14)	P16-O48	1.497(13)	1.500(12)
Ln6-O32C	2.425(12)	2.424(12)	P16-O47	1.527(12)	1.527(11)
Ln6-O52	2.456(10)	2.456(11)	P16-O46	1.543(13)	1.544(12)
Ln6-O49	2.580(12)	2.580 (12)	P17-O51	1.501(14)	1.502(12)
Ln6-O50	2.470(11)	2.471(11)	P17-O49	1.532(12)	1.531(12)
Ln6-O53	2.581(12)	2.583(12)	P17-O50	1.544(13)	1.543(14)
P1-O3	1.516(12)	1.516(12)	P18-O54	1.506(13)	1.504(12)
P1-O2	1.520(13)	1.522(12)	P18-O52	1.548(13)	1.548(13)
P1-O1	1.552(11)	1.554(11)	P18-O53	1.558(13)	1.555(12)
P2-O4	1.527(13)	1.528(12)			
O1-Ln1-O7	68.8(3)	68.8(3)	O25-Ln3-O17	78.6(4)	78.6(4)
O1-Ln1-O8	124.6(4)	124.5(4)	O25-Ln3-O19	98.7(4)	98.7(4)
O1-Ln1-O20A	154.6(4)	154.6(4)	O25-Ln3-O20	72.7(4)	72.7(4)
O1-Ln1-O22A	119.1(4)	119.1(4)	O28-Ln4-O31	96.6(5)	96.6(5)
O1-Ln1-O24A	78.0(4)	77.9(4)	O28-Ln4-O34	87.7(5)	87.7(5)
O1-Ln1-O26A	79.8(4)	79.8(4)	O28-Ln4-O37	151.9(4)	151.9(4)
O4-Ln1-O1	78.9(4)	78.9(4)	O28-Ln4-O38	149.8(4)	149.8(4)
O4-Ln1-O7	77.1(4)	77.1(4)	O28-Ln4-O40	84.6(5)	84.6(5)
O4-Ln1-O8	103.3(4)	103.3(4)	O28-Ln4-O53B	80.3(4)	80.3(4)
O4-Ln1-O20A	82.9(4)	82.9(4)	O31-Ln4-O37	77.6(4)	77.6(4)
O4-Ln1-O22A	145.9(4)	145.9(4)	O31-Ln4-O38	92.1(4)	92.1(4)
O4-Ln1-O24A	154.1(4)	154.0(4)	O34-Ln4-O31	161.4(4)	161.4(4)
O4-Ln1-O26A	88.4(4)	88.3(4)	O34-Ln4-O37	106.6(4)	106.6(4)
O7-Ln1-O22A	135.0(3)	135.0(3)	O34-Ln4-O38	75.7(4)	75.7(4)
O8-Ln1-O7	58.4	58.4	O34-Ln4-O40	88.1(4)	88.1(4)
O8-Ln1-O20A	76.8(4)	76.9(4)	O34-Ln4-O53B	82.6(4)	82.6(4)
O8-Ln1-O22A	89.9(3)	89.9(3)	O37-Ln4-O38	58.3(4)	58.3(4)
O8-Ln1-O24A	80.5(4)	80.6(4)	O40-Ln4-O31	74.3(4)	74.3(4)
O8-Ln1-O26A	154.2(4)	154.4(4)	O40-Ln4-O37	119.1(4)	119.1(4)
O20-Ln1-O7	123.9(4)	123.9(4)	O40-Ln4-O38	69.9(4)	69.9(4)
O20A-Ln1-O22A	69.6(4)	69.6(4)	O40-Ln4-O53B	162.6(4)	162.6(4)
O20A-Ln1-O24A	122.6(4)	122.7(4)	O53B-Ln4-O31	116.0(4)	116.0(4)
O20A-Ln1-O26A	82.1(4)	82.1(4)	O53B-Ln4-O37	77.9(4)	77.9(4)

O24A-Ln1-O7	83.7(4)	83.7(4)	O53B-Ln4-O38	121.2(4)	121.2(4)
O24A-Ln1-O22A	58.3(4)	58.3(4)	O35-Ln5-O38	78.7(4)	78.7(4)
O26A-Ln1-O7	147.2(4)	147.2(4)	O35-Ln5-O40	78.0(4)	78.0(4)
O26A-Ln1-O22A	68.9(3)	68.9(3)	O35-Ln5-O41	106.0(4)	106.0(4)
O26A-Ln1-O24A	98.9(4)	98.9(4)	O35-Ln5-O43	89.1(4)	89.1(4)
O1-Ln2-O10	139.3(3)	139.3(3)	O35-Ln5-O46	154.5(4)	154.5(4)
O2-Ln2-O1	58.7(4)	58.7(4)	O35-Ln5-O47	145.7(4)	145.7(4)
O2-Ln2-O10	86.5(4)	86.5(4)	O35-Ln5-O49	82.1(4)	82.1(4)
O2-Ln2-O11	80.2(4)	80.2(4)	O38-Ln5-O40	69.1(4)	69.1(4)
O5-Ln2-O1	71.9(4)	71.9(4)	O38-Ln5-O41	122.7(4)	122.7(4)
O5-Ln2-O2	103.3(4)	103.3(4)	O38-Ln5-O43	80.5(4)	80.5(4)
O5-Ln2-O7	86.2(4)	86.2(4)	O38-Ln5-O46	77.8(4)	77.8(4)
O5-Ln2-O10	142.6(4)	142.6(4)	O38-Ln5-O47	123.1(4)	123.1(4)
O5-Ln2-O11	159.8(4)	159.8(4)	O41-Ln5-O40	57.0(4)	57.0(4)
O5-Ln2-O13	80.5(4)	80.5(4)	O41-Ln5-O46	79.1(4)	79.1(4)
O5-Ln2O16	86.4(4)	86.4(4)	O41-Ln5-O47	85.0(4)	85.0(4)
O7-Ln2-O1	67.6(4)	67.6(4)	O43-Ln5-O40	148.7(4)	148.7(4)
O7-Ln2-O2	118.0(4)	118.0(4)	O43-Ln5-O41	154.0(4)	154.0(4)
O7-Ln2-O10	121.2(4)	121.2(4)	O43-Ln5-O46	96.5(4)	96.5(4)
O7-Ln2-O11	74.9(4)	74.9(4)	O43-Ln5-O47	71.2(4)	71.2(4)
O11-Ln2-O1	94.0(4)	94.0(4)	O46-Ln5-O40	84.6(4)	84.6(4)
O11-Ln2-O10	56.8(4)	56.8(4)	O46-Ln5-O47	58.4(4)	58.4(4)
O13-Ln2-O1	122.6(4)	122.6(4)	O47-Ln5-O40	132.2(4)	132.2(4)
O13-Ln2-O2	81.4(4)	81.4(4)	O49-Ln5-O38	156.5(4)	156.5(4)
O13-Ln2-O7	158.7(4)	158.7(4)	O49-Ln5-O40	119.7(4)	119.7(4)
O13-Ln2-O10	65.1(4)	65.1(4)	O49-Ln5-O41	75.6(4)	75.6(4)
O13-Ln2-O11	119.6(4)	119.6(4)	O49-Ln5-O43	85.9(4)	85.9(4)
O16-Ln2-O1	144.1(4)	144.1(4)	O49-Ln5-O46	123.0(4)	123.0(4)
O16-Ln2-O2	156.9(4)	156.9(4)	O49-Ln5-O47	69.1(4)	69.1(4)
O16-Ln2-O7	83.1(4)	83.1(4)	O29C-Ln6-O32C	85.2(4)	85.2(4)
O16-Ln2-O10	73.6(4)	73.6(4)	O29C-Ln6-O49	136.9(4)	136.9(4)
O16-Ln2-O11	98.0(4)	98.0(4)	O29C-Ln6-O50	158.5(4)	158.5(4)
O16-Ln2-O13	79.5(4)	79.5(4)	O29C-Ln6-O52	114.1(4)	114.1(4)
O10-Ln3-O13	67.2(4)	67.2(4)	O29C-Ln6-O53	77.5(4)	77.5(4)
O10-Ln3-O14	119.0(4)	119.0(4)	O32C-Ln6-O49	122.5(4)	122.5(4)
O10-Ln3-O17	78.3(4)	78.3(4)	O32C-Ln6-O50	73.5(4)	73.5(4)
O10-Ln3-O19	74.5(4)	74.5(4)	O32C-Ln6-O52	117.1(4)	117.1(4)
O10-Ln3-O20	121.8(4)	121.8(4)	O32C-Ln6-O53	69.3(4)	69.3(4)

O10-Ln3-O22	156.7(4)	156.7(4)	O44-Ln6-O29	79.8(4)	79.8(4)
O10-Ln3-O25	85.5(4)	85.5(4)	O44-Ln6-O32C	82.9(4)	82.9(4)
O13-Ln3-O20	141.0(4)	141.0(4)	O44-Ln6-O47	87.4(4)	87.4(4)
O14-Ln3-O13	58.6(4)	58.6(4)	O44-Ln6-O49	72.8(4)	72.8(4)
O14-Ln3-O20	88.9(3)	88.9(3)	O44-Ln6-O50	94.1(4)	94.1(4)
O17-Ln3-O13	73.9(4)	73.9(4)	O44-Ln6-O52	155.5(4)	155.5(4)
O17-Ln3-O14	109.3(4)	109.3(4)	O44-Ln6-O53	145.2	145.2
O17-Ln3-O20	142.6(4)	142.6(4)	O47-Ln6-O29	77.5(4)	77.5(4)
O19-Ln3-O13	95.6(4)	95.6(4)	O47-Ln6-O32C	161.4(4)	161.4(4)
O19-Ln3-O14	84.7(4)	84.7(4)	O47-Ln6-O49	68.8(4)	68.8(4)
O19-Ln3-O17	152.8(4)	152.8(4)	O47-Ln6-O50	123.1(4)	123.1(4)
O19-Ln3-O20	57.4(4)	57.4(4)	O47-Ln6-O52	76.8(4)	76.8(4)
O22-Ln3-O13	117.1(4)	117.1(4)	O47-Ln6-O53	112.6(4)	112.6(4)
O22-Ln3-O14	78.2(4)	78.2(4)	O49-Ln6-O50	57.8(4)	57.8(4)
O22-Ln3-O17	81.2(4)	81.2(4)	O49-Ln6-O53	112.6(4)	112.6(4)
O22-Ln3-O19	125.4(4)	125.4(4)	O50-Ln6-O53	97.5(4)	97.5(4)
O22-Ln3-O20	70.7(4)	70.7(4)	O52-Ln6-O49	84.0(4)	84.0(4)
O22-Ln3-O25	79.8(4)	79.8(4)	O52-Ln6-O50	79.5(4)	79.5(4)
O25-Ln3-O13	144.4(4)	144.4(4)	O52-Ln6-O53	59.3(4)	59.3(4)
O25-Ln3-O14	155.0(4)	155.0(4)			

Symmetry transformations used to generate equivalent atoms: A: 1-x, -1/2+y, 1-z; B: -x, -1/2+y, 2-z; C: -x, 1/2+y, 2-z.

Table S3. Hydrogen bonds among phosphonate groups, -NH_2- groups, -CH_2- groups, phenyl groups, water molecules and NO_3^- anions in ***R*-2b-Sm**.

D-H···A	*d*(D-H) (Å)	*d*(H···A) (Å)	*d*(D···A) (Å)	∠ DHA (°)
O18-H18d···O55	0.84	1.91	2.75(2)	174
O27-H27b···O63	0.84	1.82	2.65(3)	171
N1-H1d···O15	0.90	1.86	2.746(19)	169
N1-H1c···O6	0.90	1.87	2.739(19)	161
N2-H2c···O3W	0.90	1.88	2.78(2)	176
N3-H3e···O11	0.90	1.86	2.710(19)	157
N4-H4b···O19	0.90	1.93	2.70(2)	143
N4-H4a···O10W	0.90	2.08	2.82(8)	139
N5-H5c···O23	0.90	1.74	2.638(19)	173
N6-H6b···O12	0.90	1.95	2.80(2)	156
N7-H7c···O8^{ii}	0.90	1.95	2.72(2)	143
N7-H7a···O4W	0.90	1.97	2.83(2)	160
N8-H8c···O3^{ii}	0.90	1.73	2.623(19)	171
N9-H9c···O63	0.90	1.88	2.74(3)	161
N9-H9b···O6^{ii}	0.90	1.90	2.763(19)	161
N10-H10r···O13Wi	0.90	2.00	2.89(3)	171
N10-H10q···O45^{iii}	0.90	1.94	2.80(2)	160
N11-H11o···O50^{iii}	0.90	1.84	2.721(19)	166
N11-H11n···O37	0.90	1.76	2.651(19)	169
N12-H12r···O2W^{i}	0.90	1.86	2.76(3)	177
N13-H13m···O54^{iii}	0.90	1.82	2.712(19)	171
N13-H13l···O36	0.90	1.85	2.720(19)	161
N14-H14o···O31	0.90	1.79	2.668(19)	164
N14-H14n···O46	0.90	1.99	2.812(19)	151
N15-H15o···O9W^{iv}	0.90	1.92	2.81(2)	167
N15-H15n···O36	0.90	1.88	2.751(19)	163
N16-H16f···O39	0.90	1.88	2.755(19)	165
N16-H16e···O43	0.90	2.08	2.96(2)	164
N17-H17c···O41	0.90	1.78	2.666(19)	167
N18-H18c···O48	0.90	1.78	2.664(19)	168

Symmetry transformations used to generate equivalent atoms: i: +x, +y, 1+z; ii: 1-x, 1/2+y, 1-z; iii: -x, -1/2+y, 2-z; iv: -1+x, +y, +z.

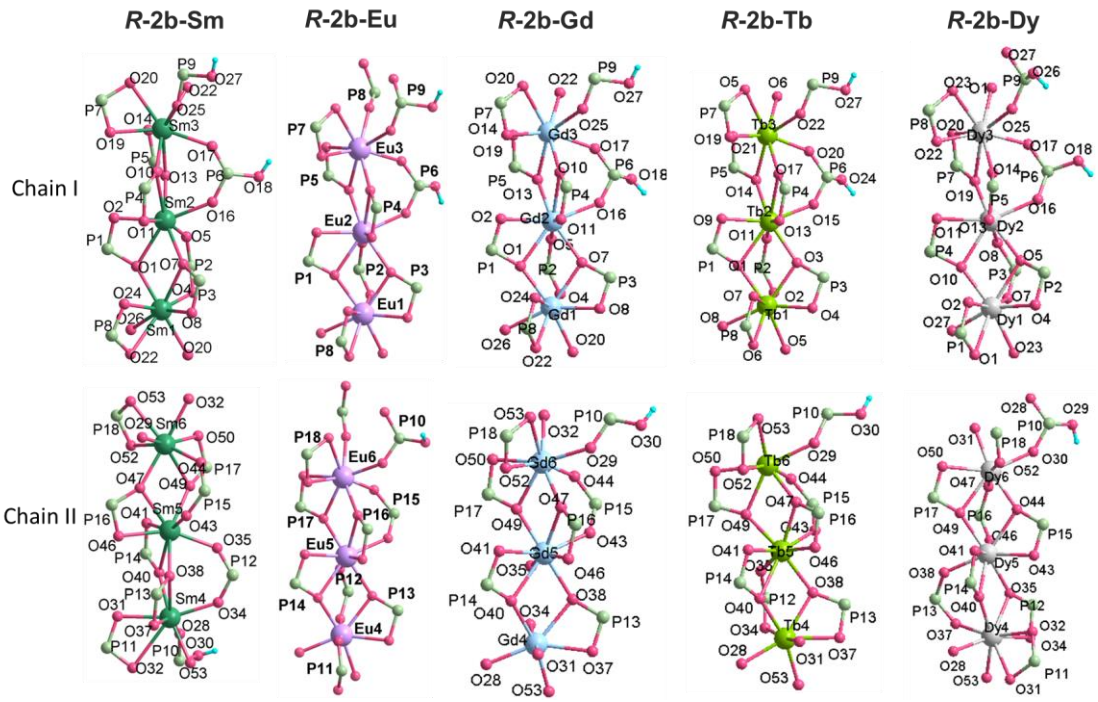

Figure S8. Chain (I and II) structures with atomic labelling of structure ***R*-2b-Ln** (Ln = Sm, Eu, Gd, Tb, Dy).

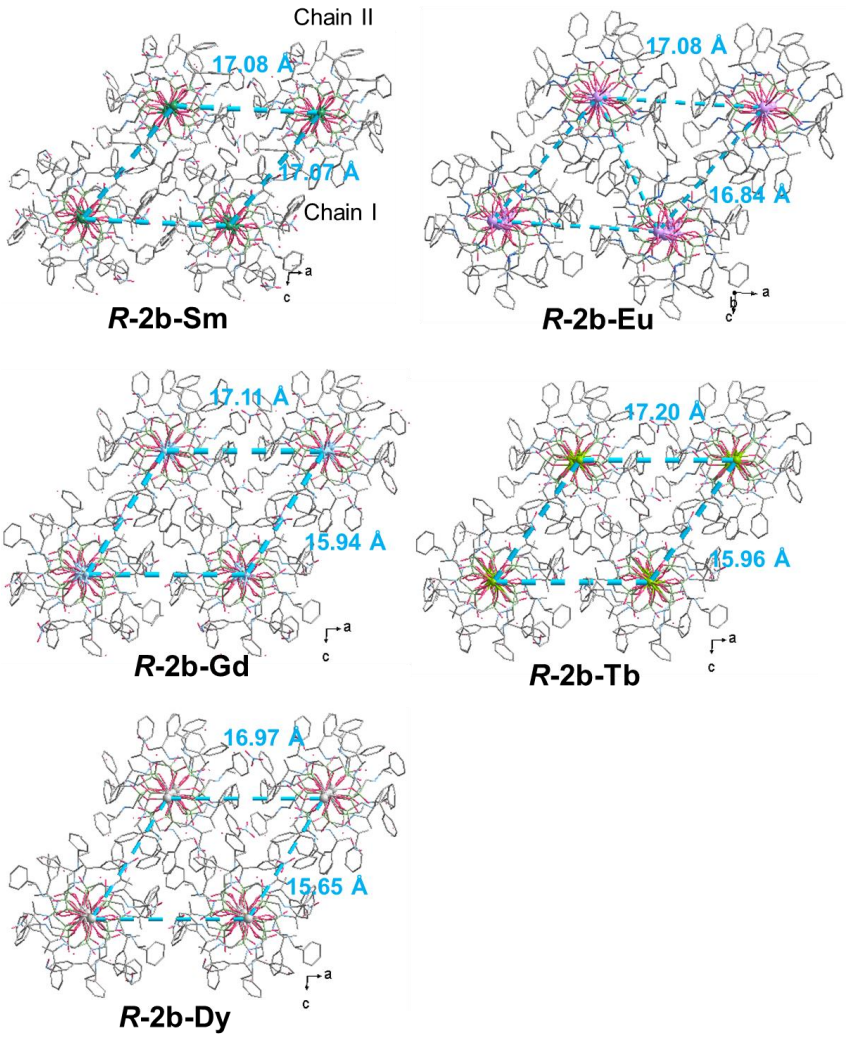

Figure S9. Packing diagrams of structure ***R*-2b-Ln** (Ln = Sm, Eu, Gd, Tb, Dy).

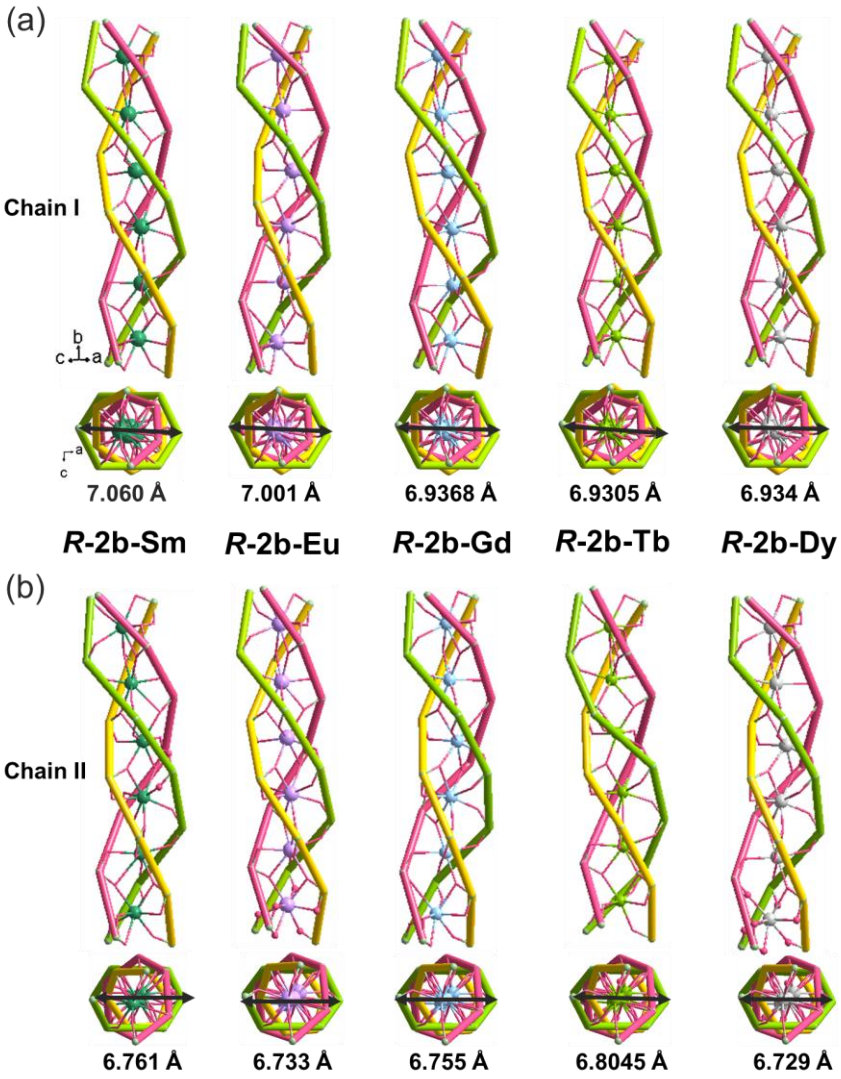

Figure S10. Side and top views of the inorganic triple helical chains of ***R*-2b-Ln** (Ln = Sm, Eu, Gd, Tb, Dy), the shortest diameters of each helical chain are also given.

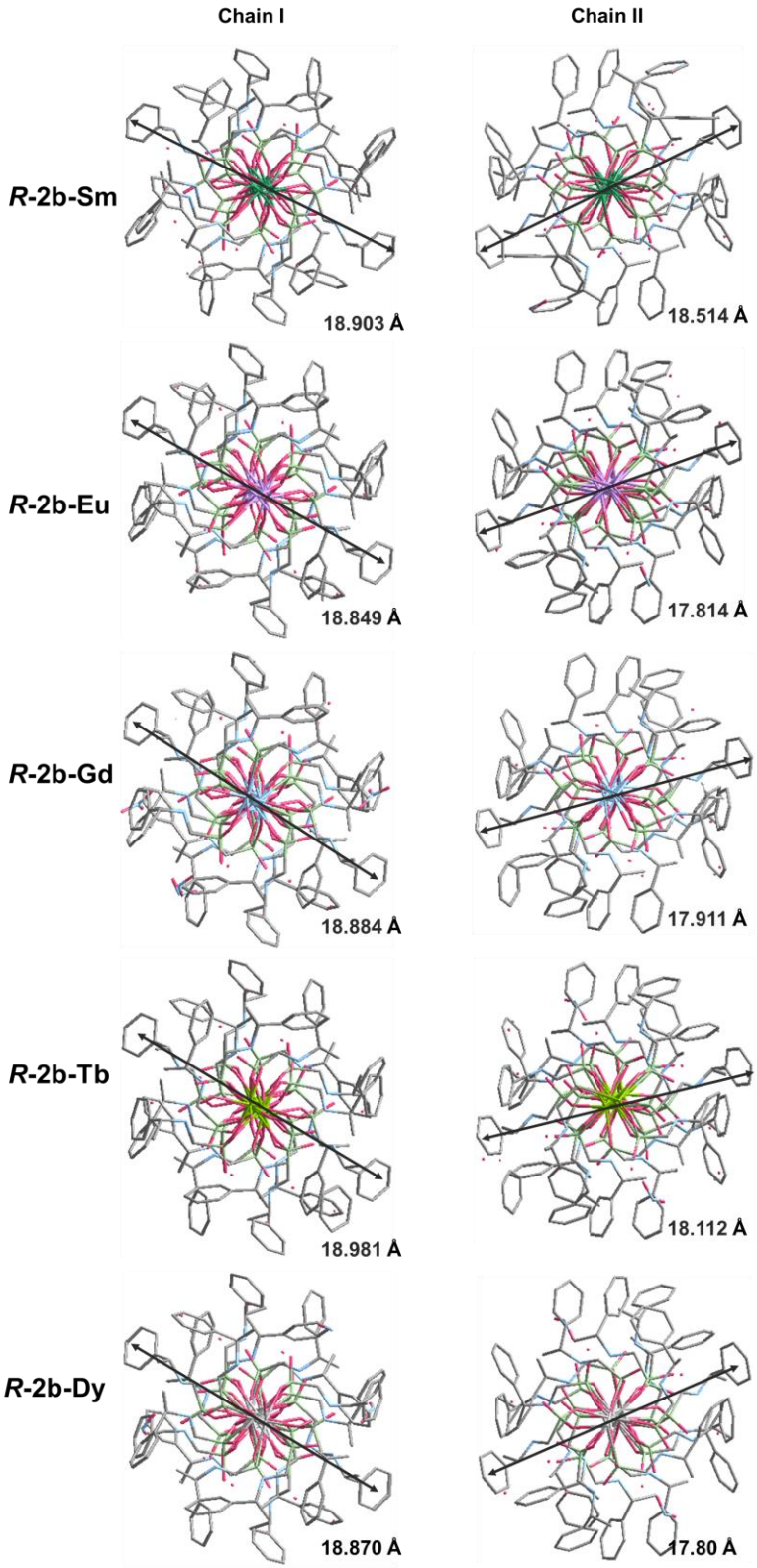

Figure S11. The outer diameters of helical chains of ***R*-2b-Ln** (Ln = Sm, Eu, Gd, Tb, Dy)**.**

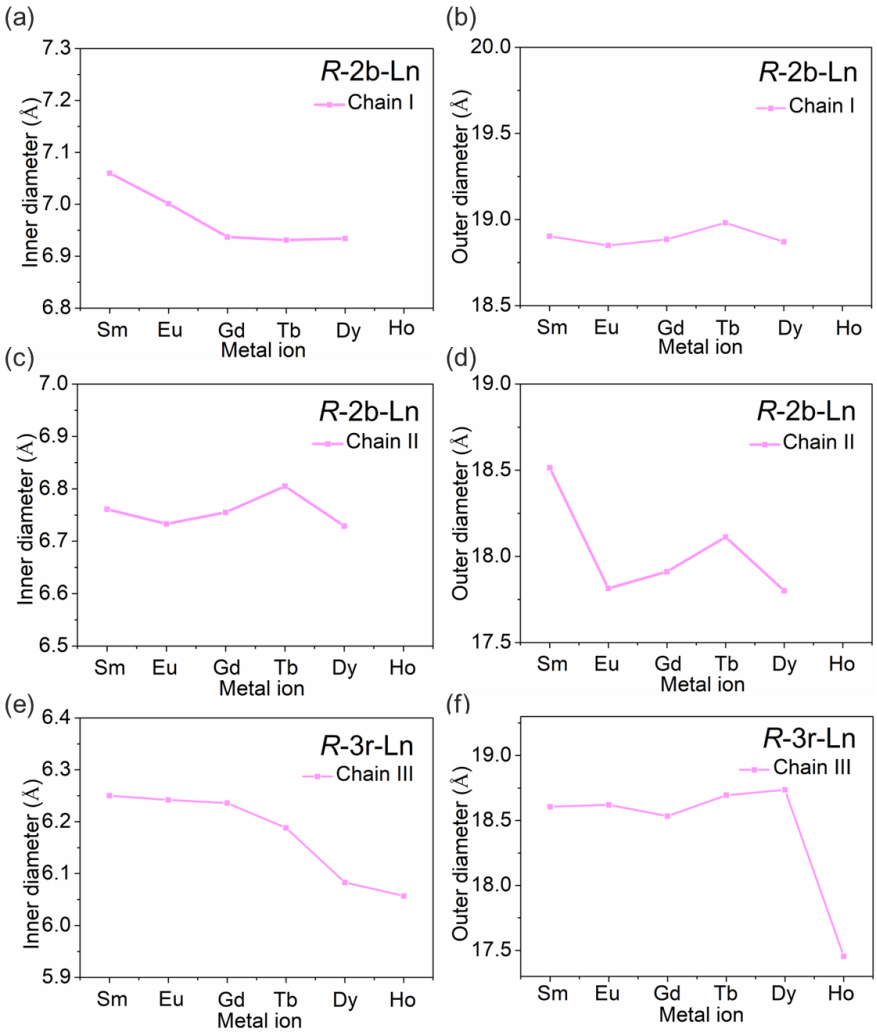

Figure S12. The variation trend of the diameters of helical chains of ***R*-2b-Ln** and ***R*-3r-Ln**.

Table S4. Crystal data of ***R*-3r-Sm**, ***R*-3r-Eu**, ***R*-3r-Gd**, ***R*-3r-Tb**, ***R*-3r-Dy** and ***R*-3r-Ho**.[a]

Compounds	***R*-3r-Sm**	***R*-3r-Eu**	***R*-3r-Gd**	***R*-3r-Tb**	***R*-3r-Dy**	***R*-3r-Ho**
Formula	$C_{27}H_{39}N_3O_9P_3$ Sm·H_2O	$C_{27}H_{39}N_3O_9P_3$ Eu·H_2O	$C_{27}H_{39}N_3O_9P_3$ Gd·H_2O	$C_{27}H_{39}N_3O_9P_3$ Tb·H_2O	$C_{27}H_{39}N_3O_9P_3$ Dy·H_2O	$C_{27}H_{39}N_3O_9P_3$ Ho·H_2O
M	810.89	812.50	817.78	819.46	823.04	825.48
Crystal system	Hexagonal	Hexagonal	Hexagonal	Hexagonal	Hexagonal	Hexagonal
Space group	$P6_5$	$P6_5$	$P6_5$	$P6_5$	$P6_5$	$P6_5$
T (K)	193	193	193	193	193	193
a (Å)	15.759(3)	15.746(3)	15.756(6)	15.758(3)	15.803(5)	15.751(6)
b (Å)	15.759(3)	15.746(3)	15.756(6)	15.758(3)	15.803(5)	15.751(6)
c (Å)	24.213(6)	24.158(8)	24.114(12)	24.073(7)	24.127(9)	24.070(11)
α (°)	90	90	90	90	90	90
β (°)	90	90	90	90	90	90
γ (°)	120	120	120	120	120	120
V (Å^3)	5207.5(2)	5187.2(3)	5184.1(5)	5176.9(2)	5218.0(4)	5174.4(5)
D_c [g cm^{-3}]	1.551	1.561	1.554	1.577	1.572	1.556
μ[mm^{-1}]	1.884	2.007	2.110	2.243	2.340	2.485
F(000)	2466	2472.0	2448.0	2484.0	2490.0	2436.0
R_{int}	0.046	0.045	0.060	0.072	0.041	0.052
R_1, wR_2 [$I>2\sigma(I)$]	0.061, 0.172	0.057, 0.159	0.061, 0.171	0.065, 0.178	0.091, 0.244	0.111, 0.308
CCDC number	2508335	2313014	2081949	2512347	2514394	2508336

$R_1 = \Sigma||F_o| - |F_c||/\Sigma|F_o|$, $wR_2 = [\Sigma w(F_o^2 - F_c^2)^2/\Sigma w(F_o^2)^2]^{1/2}$

[a] The structures of ***R*-3r-Eu**, ***R*-3r-Gd, *R*-3r-Tb** and ***R*-3r-Dy** have already been reported in our previous work. [2,4-6] To ensure the consistency of the testing conditions, we re-examined the crystals of ***R*-3r-Tb** and ***R*-3r-Dy** in this work. In addition, ***R*-3r-Sm** and ***R*-3r-Ho** are unreported structures.

Table S5. Partial bond lengths [Å] and bond angles [°] of ***R*-3r-Ln**.

Compound	***R*-3r-Sm**	***R*-3r-Eu**	***R*-3r-Gd**	***R*-3r-Tb**	***R*-3r-Dy**	***R*-3r-Ho**
Ln1-O9A	2.320(12)	2.309(12)	2.301(13)	2.271(14)	2.247(18)	2.25(2)
Ln1-O7	2.351(11)	2.335(11)	2.328(12)	2.318(13)	2.293(18)	2.28(2)
Ln1-O4B	2.380(10)	2.361(10)	2.351(12)	2.343(12)	2.329(16)	2.33(2)
Ln1-O1A	2.389(10)	2.383(10)	2.365(11)	2.348(11)	2.323(16)	2.28(3)
Ln1-O2	2.433(11)	2.418(10)	2.401(11)	2.385(12)	2.367(14)	2.34(2)
Ln1-O5	2.467(9)	2.452(9)	2.440(10)	2.416(11)	2.402(17)	2.41(2)
Ln1-O4	2.502(10)	2.498(10)	2.488(12)	2.487(12)	2.456(16)	2.44(2)
Ln1-O1	2.599(12)	2.591(12)	2.590(14)	2.608(13)	2.650(19)	2.67(3)
P1-O1	1.548(10)	1.541(10)	1.551(11)	1.541(12)	1.547(19)	1.57(3)
P1-O2	1.528(13)	1.531(12)	1.528(14)	1.524(13)	1.514(17)	1.52(2)
P1-O3	1.502(13)	1.502(13)	1.504(14)	1.497(16)	1.51(2)	1.52(3)
P2-O4	1.513(10)	1.522(10)	1.525(11)	1.510(12)	1.522(17)	1.50(2)
P2-O5	1.520(11)	1.520(11)	1.515(12)	1.522(11)	1.527(14)	1.52(2)
P2-O6	1.481(11)	1.480(11)	1.476(12)	1.478(12)	1.480(16)	1.47(2)
P3-O7	1.506(12)	1.515(12)	1.518(13)	1.511(14)	1.47(2)	1.45(3)
P3-O8	1.387(17)	1.371(17)	1.409(17)	1.377(18)	1.39(3)	1.45(3)
P3-O9	1.485(12)	1.486(12)	1.482(13)	1.496(13)	1.499(17)	1.51(2)
O1A-Ln1-O1	124.7(3)	124.8(3)	125.2(4)	124.4(4)	123.3(6)	123.0(9)
O1A-Ln1-O2	76.3(4)	76.2(4)	76.5(4)	77.0(5)	78.1(6)	78.0(9)
O1A-Ln1-O4	68.3(3)	67.9(3)	67.8(4)	68.3(4)	68.4(6)	68.7(9)
O1A-Ln1-O5	119.6(4)	119.6(4)	119.7(4)	120.3(4)	121.6(6)	120.8(9)
O2-Ln1-O1	57.7(4)	57.8(3)	58.1(4)	57.4(4)	57.2(5)	56.9(8)
O2-Ln1-O4	92.6(4)	92.6(3)	93.0(4)	93.2(4)	92.5(6)	91.9(7)
O2-Ln1-O5	80.2(4)	80.3(4)	80.7(4)	80.2(4)	80.1(6)	78.6(7)
O4-Ln1-O1	135.9(3)	136.1(3)	136.7(4)	137.1(4)	138.1(6)	137.2(7)
O4B-Ln1-O1	66.8(3)	66.6(3)	66.3(4)	66.5(4)	65.0(6)	64.1(8)
O4B-Ln1-O1A	159.7(3)	159.9(3)	159.5(4)	159.2(4)	159.0(6)	160.3(8)
O4B-Ln1-O2	121.4(4)	121.3(4)	121.3(4)	120.7(4)	118.5(6)	117.1(8)
O4B-Ln1-O4	116.7(3)	117.0(3)	117.3(3)	117.7(4)	120.0(5)	120.3(7)
O4B-Ln1-O5	76.0(3)	75.8(3)	76.0(3)	76.3(4)	76.2(5)	76.6(7)
O5-Ln1-O1	83.4(4)	83.2(4)	83.7(4)	83.9(4)	85.6(5)	84.9(7)
O5-Ln1-O4	58.0(3)	58.5(3)	58.5(4)	58.8(4)	59.2(5)	58.6(7)
O7-Ln1-O1	73.8(4)	73.9(4)	73.4(4)	73.3(5)	72.3(6)	71.2(8)
O7-Ln1-O1A	84.0(4)	83.7(4)	83.6(4)	83.1(5)	81.3(6)	82.3(9)
O7-Ln1-O2	97.1(5)	96.5(5)	96.2(5)	96.6(6)	96.8(8)	96.3(10)
O7-Ln1-O4	147.6(4)	147.1(4)	147.0(4)	146.7(5)	145.7(6)	147.5(7)

O7-Ln1-O4B	84.0(4)	84.6(4)	84.3(4)	83.9(5)	83.9(6)	83.4(7)
O7-Ln1-O5	154.2(4)	154.3(4)	154.4(4)	154.4(4)	155.0(5)	153.9(7)
O9A-Ln1-O1	139.7(3)	139.6(3)	139.3(4)	139.3(4)	139.3(5)	138.8(8)
O9A-Ln1-O1A	87.3(4)	87.1(4)	86.8(4)	86.7(4)	86.2(6)	88.6(9)
O9A-Ln1-O2	162.2(4)	162.2(4)	162.2(4)	162.6(4)	163.0(6)	164.2(8)
O9A-Ln1-O4B	76.0(4)	76.3(4)	76.2(4)	76.3(4)	78.3(6)	77.9(8)
O9A-Ln1-O4	74.4(4)	75.1(4)	74.6(4)	75.1(4)	75.4(6)	75.3(7)
O9A-Ln1-O5	102.5(4)	103.2(4)	102.7(4)	103.3(5)	103.0(7)	101.7(8)
O9A-Ln1-O7	87.9(5)	87.7(5)	88.1(5)	87.7(5)	87.2(8)	90.1(10)

Symmetry transformations used to generate equivalent atoms: A: 1+y, -x+y, 1/6+z; B: -y+x, -1+x, -1/6+z.

Table S6. Hydrogen bonds among water molecules, phosphonate groups, -NH_2- groups, -CH_2- groups and phenyl groups in ***R*-3r-Sm**.

D-H···A	*d*(D-H) (Å)	*d*(H···A) (Å)	*d*(D···A) (Å)	∠ DHA (°)
N1-H1d···O2^{i}	0.91	1.80	2.697(18)	166
N1-H1c···O5	0.91	1.89	2.776(18)	164
N2-H2b···O6^{i}	0.91	1.75	2.653(18)	171
N2-H2a···O8^{ii}	0.91	2.18	3.040(2)	156
N3-H3e···O8^{i}	0.91	1.91	2.808(2)	168
N3-H3d···O1W	0.91	2.16	2.850(3)	133

Symmetry transformations used to generate equivalent atoms: i: -y+x, -1+x, -1/6+z; ii: 1+y, -x+y, 1/6+z.

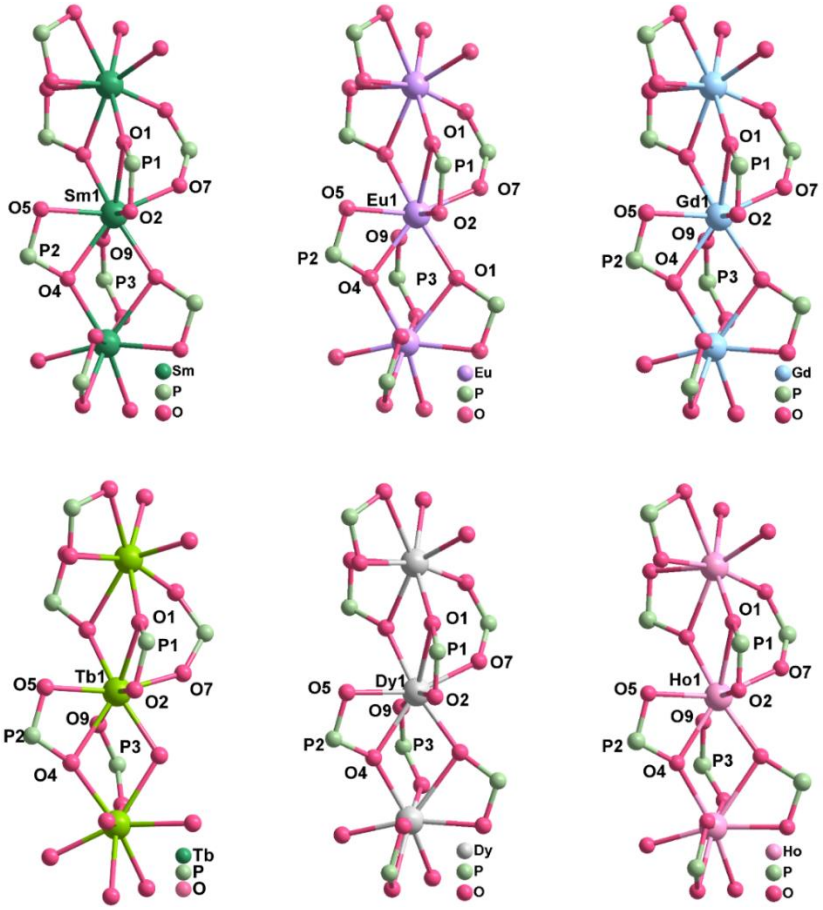

Figure S13. Chain structures with atomic labelling of structure ***R*-3r-Ln** (Ln = Sm, Eu, Gd, Tb, Dy, Ho).

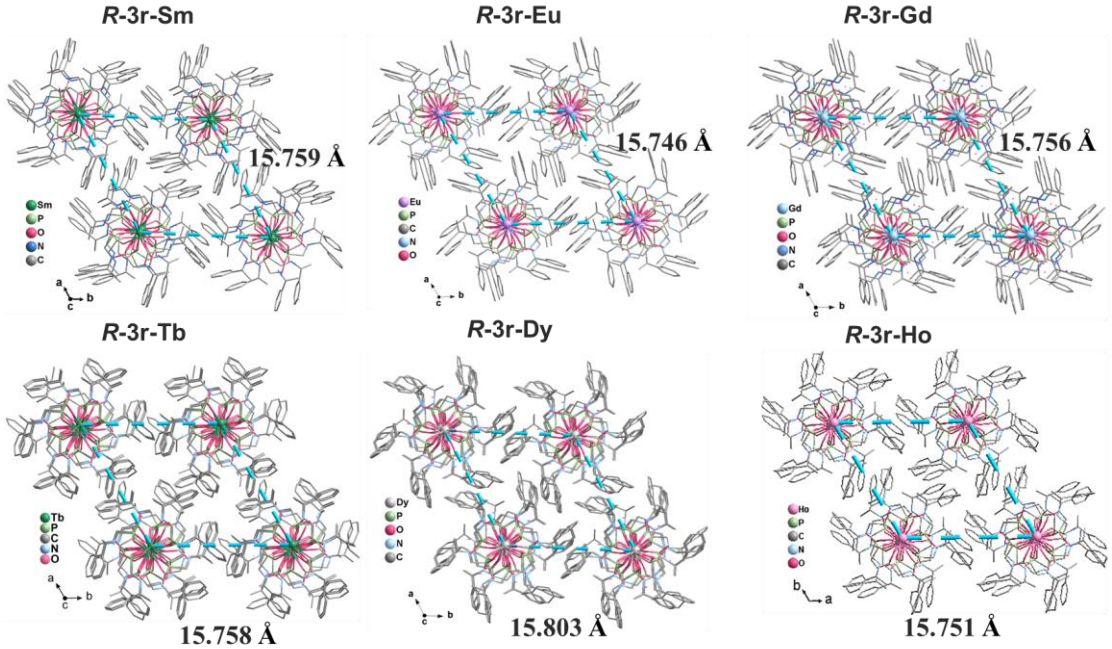

Figure S14. Packing diagrams of structure ***R*-3r-Ln** (Ln = Sm, Eu, Gd, Tb, Dy, Ho).

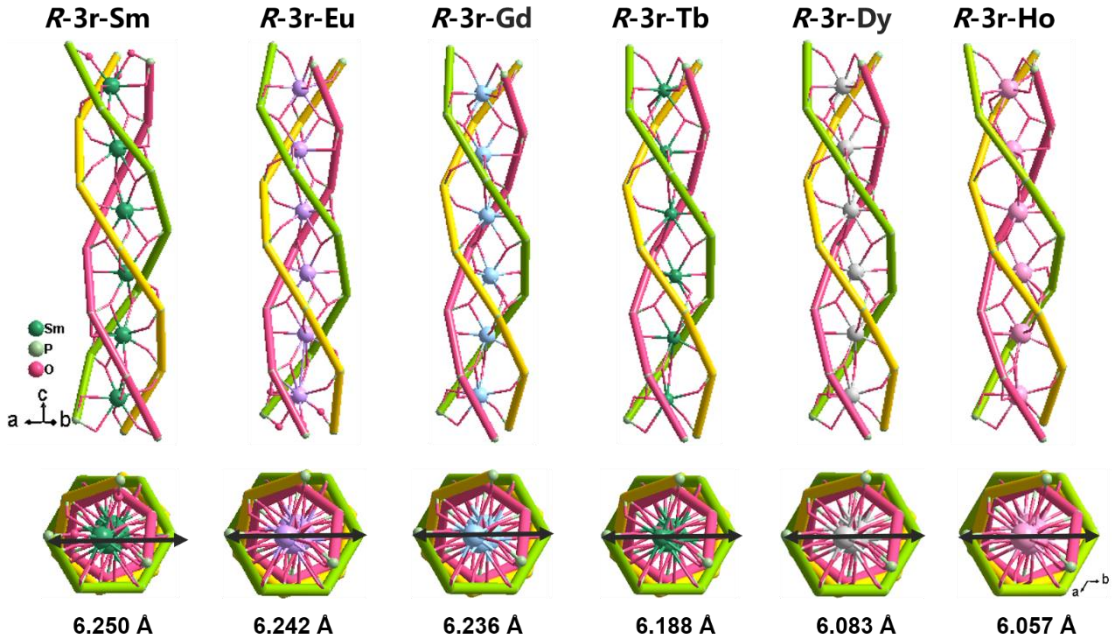

Figure S15. Side and top views of the inorganic triple helical chains of ***R*-3r-Ln** (Ln = Sm, Eu, Gd, Tb, Dy, Ho), the shortest diameters of each helical chain are also given.

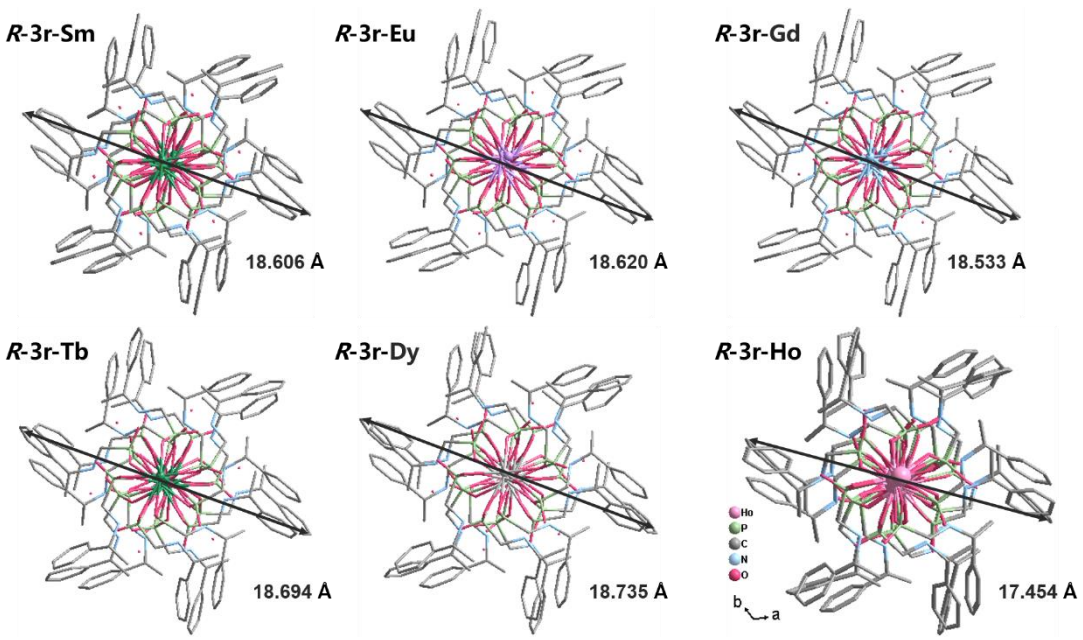

Figure S16. The outer diameters of helical chains of ***R*-3r-Ln** (Ln = Sm, Eu, Gd, Tb, Dy, Ho).

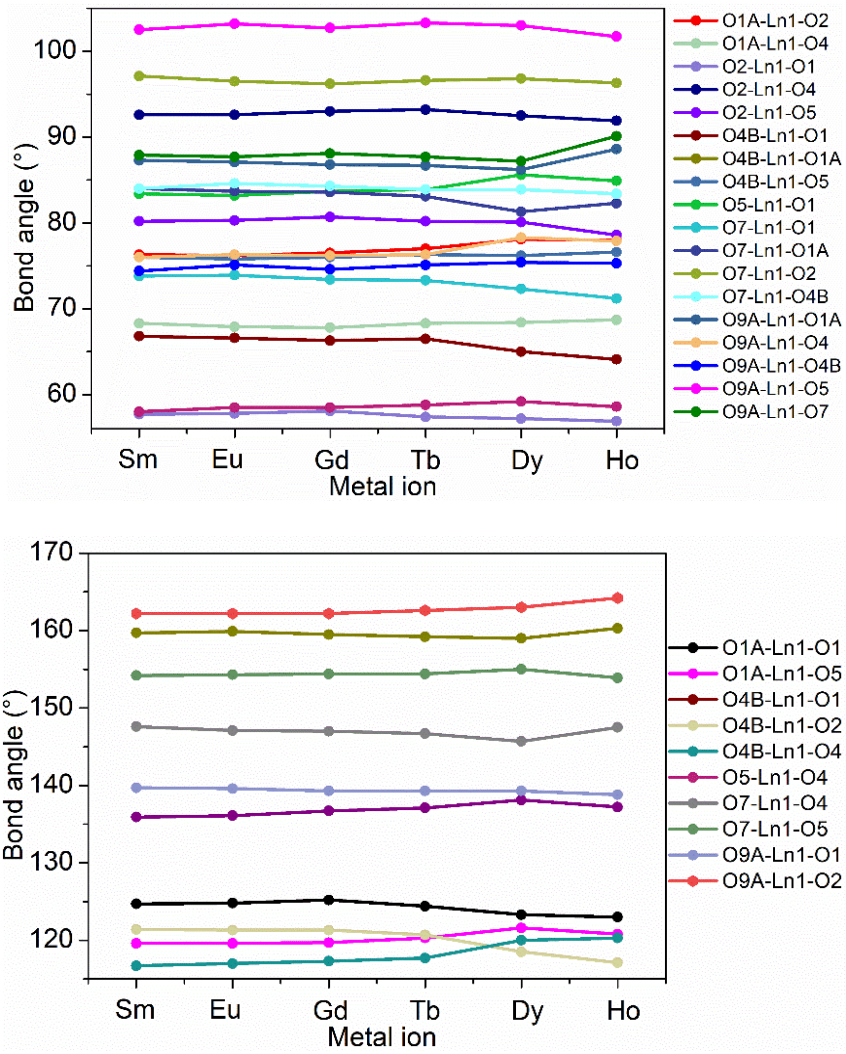

Figure S17. Variation of O-Ln-O bond lengths in ***R*-3r-Ln** with lanthanide ions.

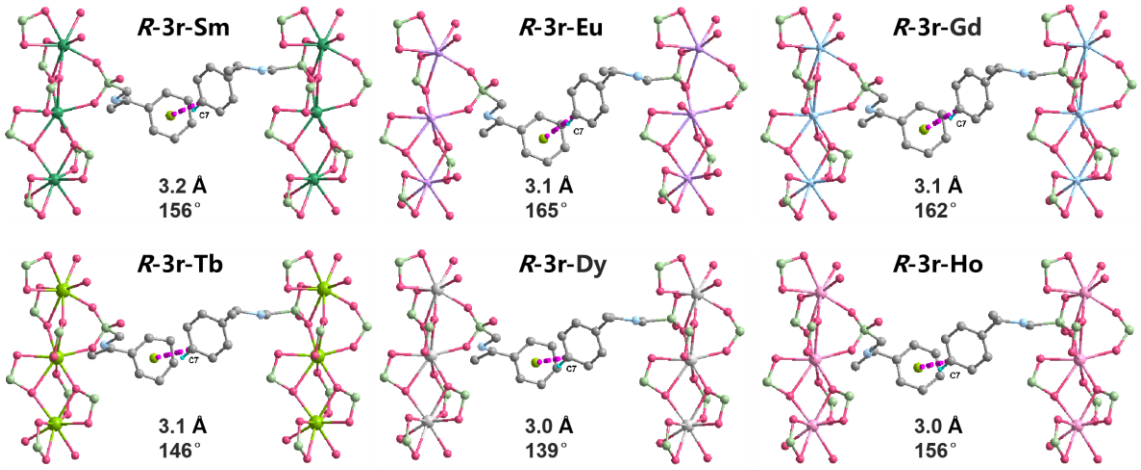

Figure S18. The C7(H7)···π distances and angles in adjacent chains of ***R*-3r-Ln**.

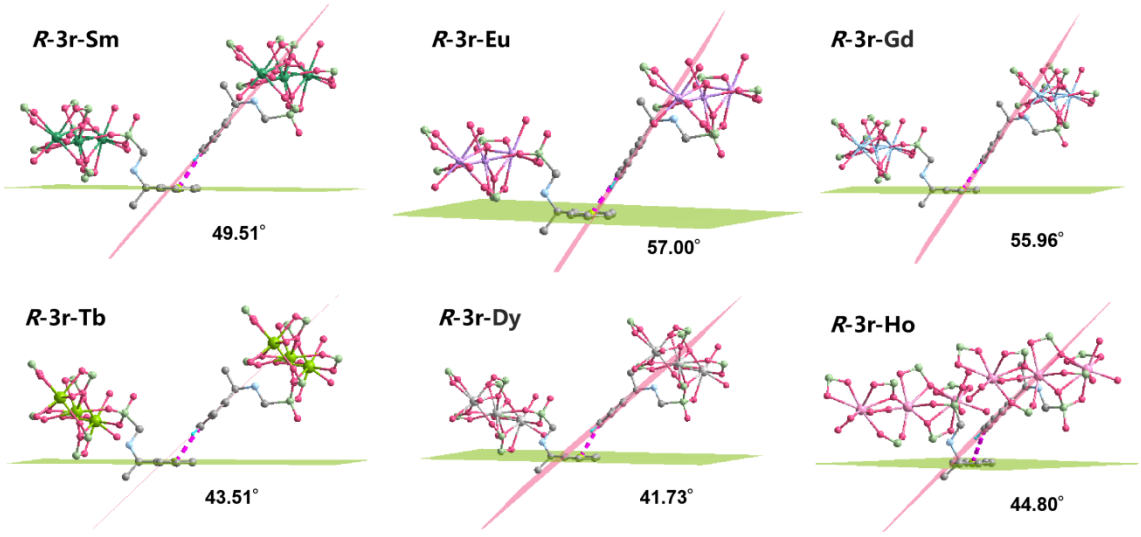

Figure S19. The dihedral angles of aromatic rings in adjacent chains of ***R*-3r-Ln**.

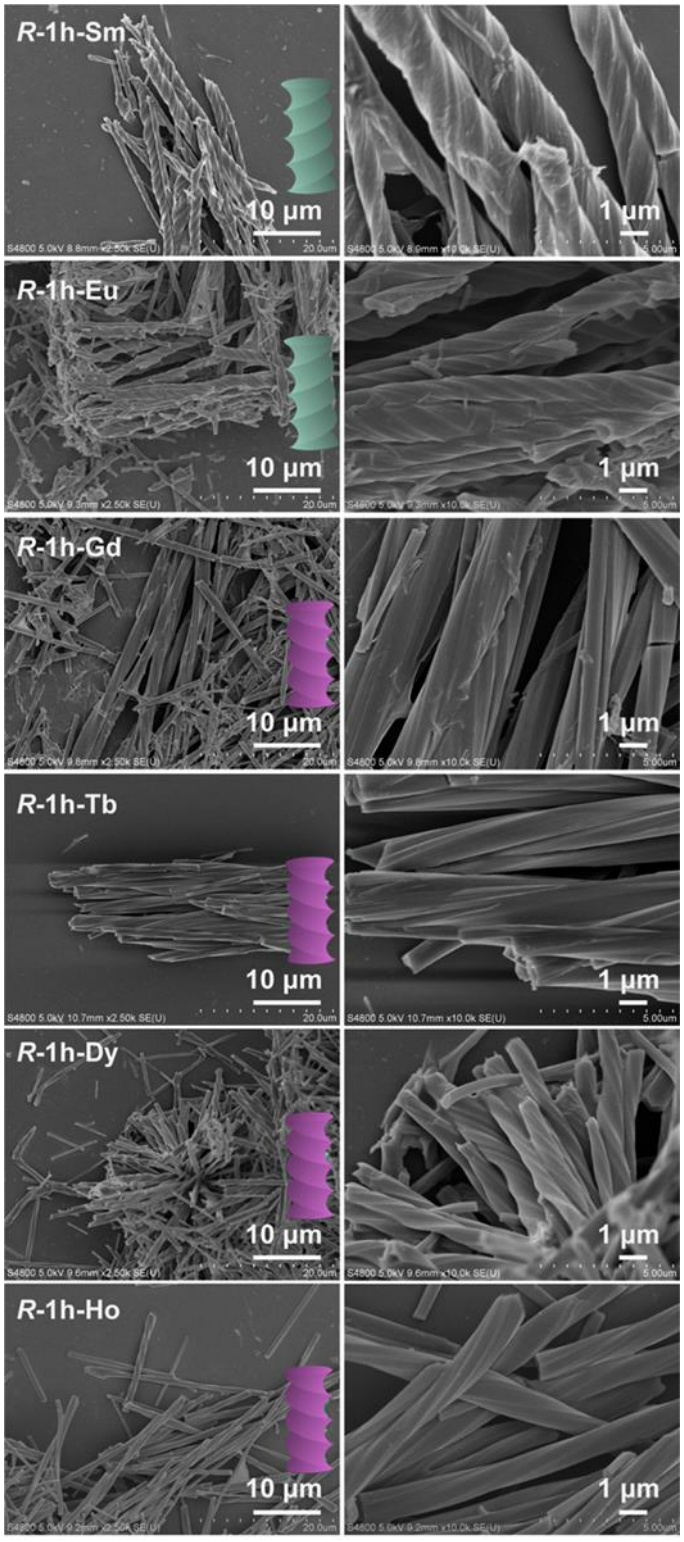

Figure S20. SEM morphologies of helical products ***R*-1h-Ln** (Ln = Sm, Eu, Gd, Tb, Dy, Ho) obtained after hydrothermal reactions of $Ln(NO_3)_3$ and *R*-pempH$_2$ (M:L molar ratio 1:6, pH 3.5, autoclave filling degree 60 %) at 120 °C for 24 h.

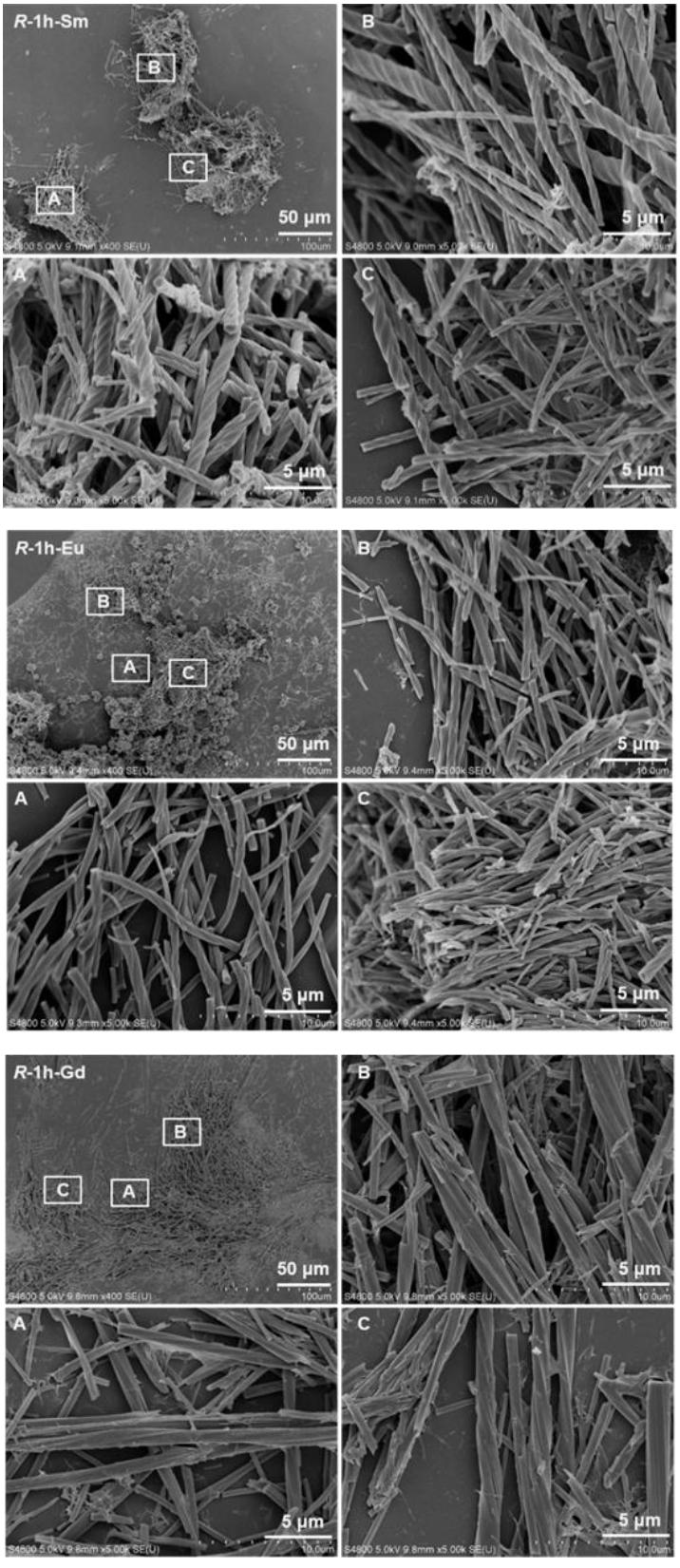
R-1h-Sm
B
C
A
50 μm
B
5 μm
A
5 μm
C
5 μm
R-1h-Eu
B
A
C
50 μm
B
5 μm
A
5 μm
C
5 μm
R-1h-Gd
B
C
A
50 μm
B
5 μm
A
5 μm
C
5 μm

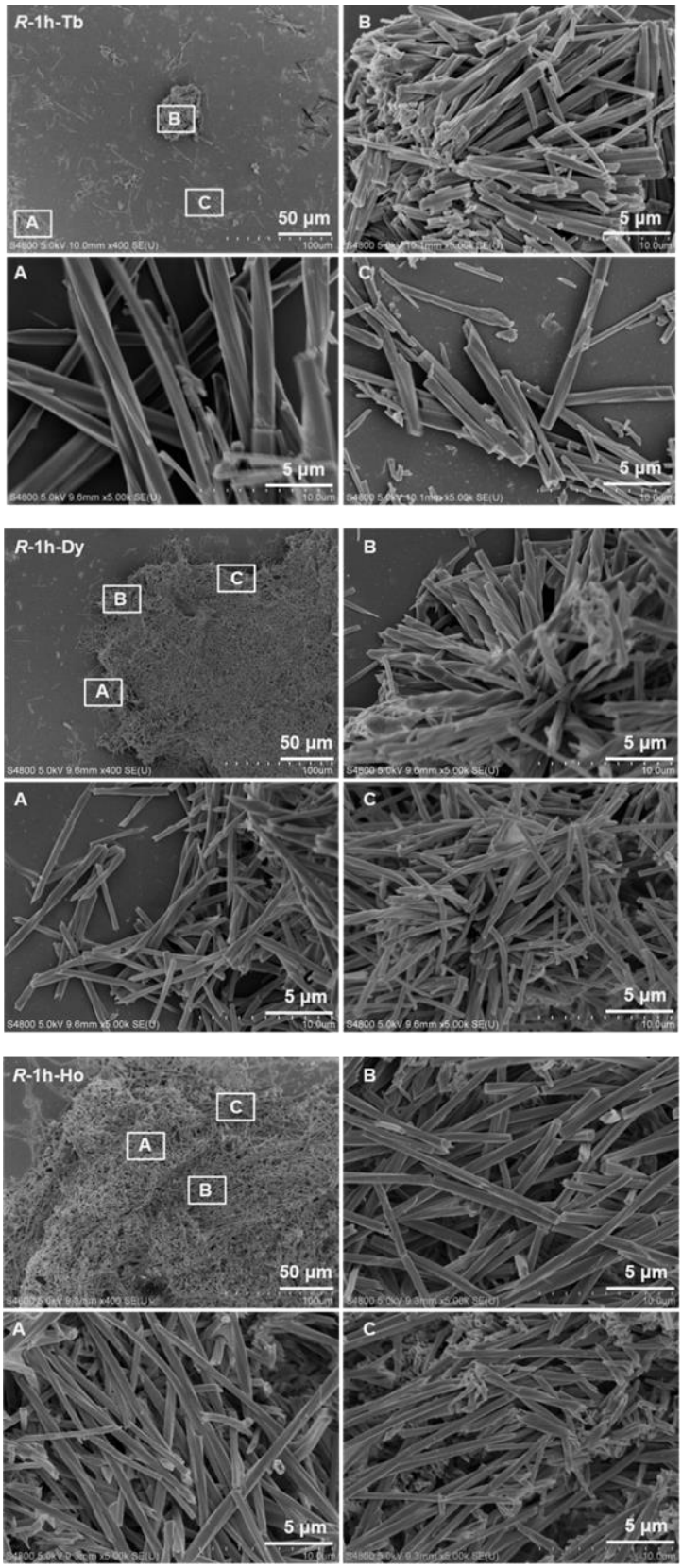

Figure S21. The SEM images of helices ***R*-1h-Ln** (Ln = Sm, Eu, Gd, Tb, Dy, Ho) obtained after hydrothermal reactions of $Ln(NO_3)_3$ and *R*-pempH$_2$ (M:L molar ratio 1:6, pH 3.5, autoclave filling degree 60 %) at 120 °C for 24 h. We selected three distinct regions (A, B, C) from the same sample and found that these helical structures shared the same handedness.

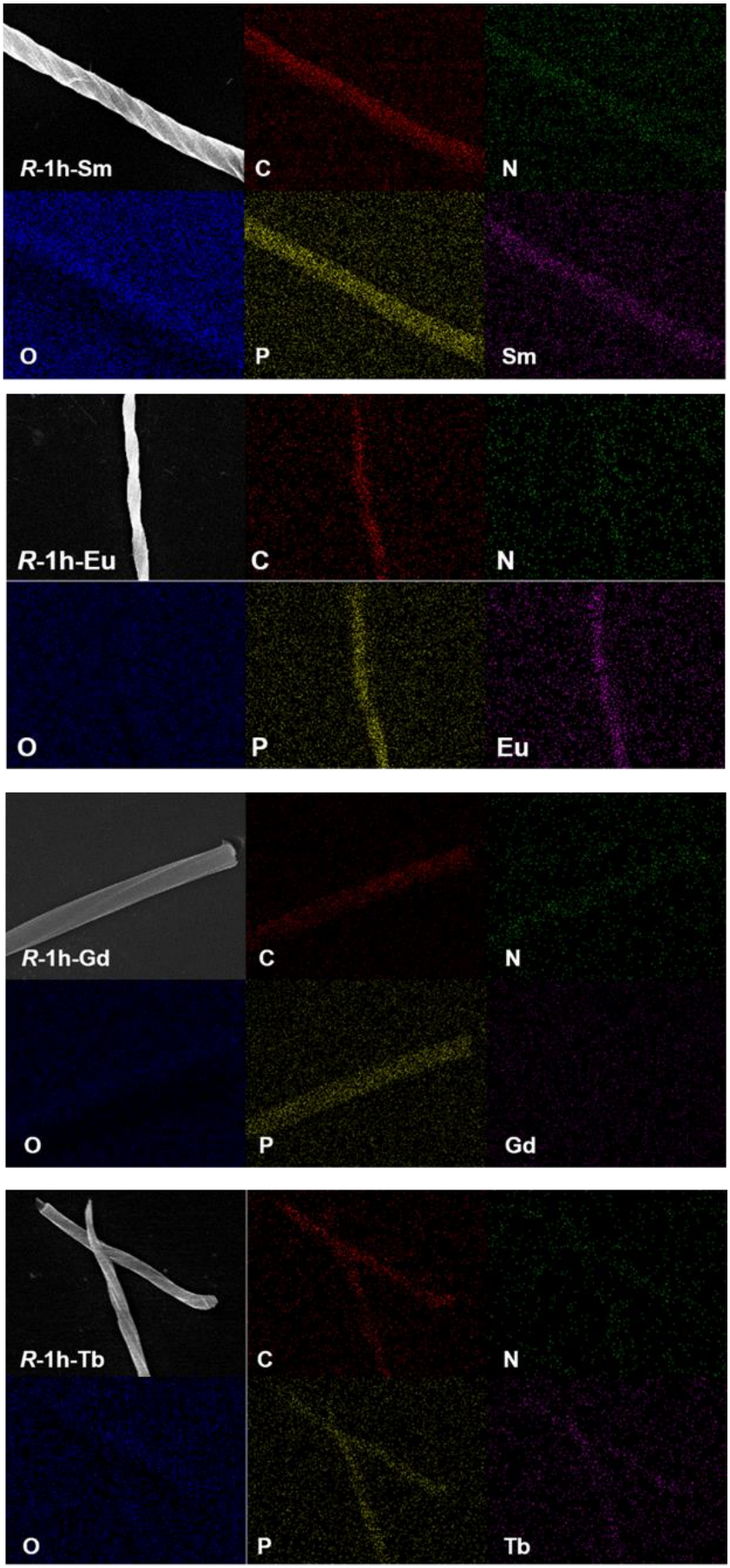
R-1h-Sm
C
N
O
P
Sm
R-1h-Eu
C
N
O
P
Eu
R-1h-Gd
C
N
O
P
Gd
R-1h-Tb
C
N
O
P
Tb

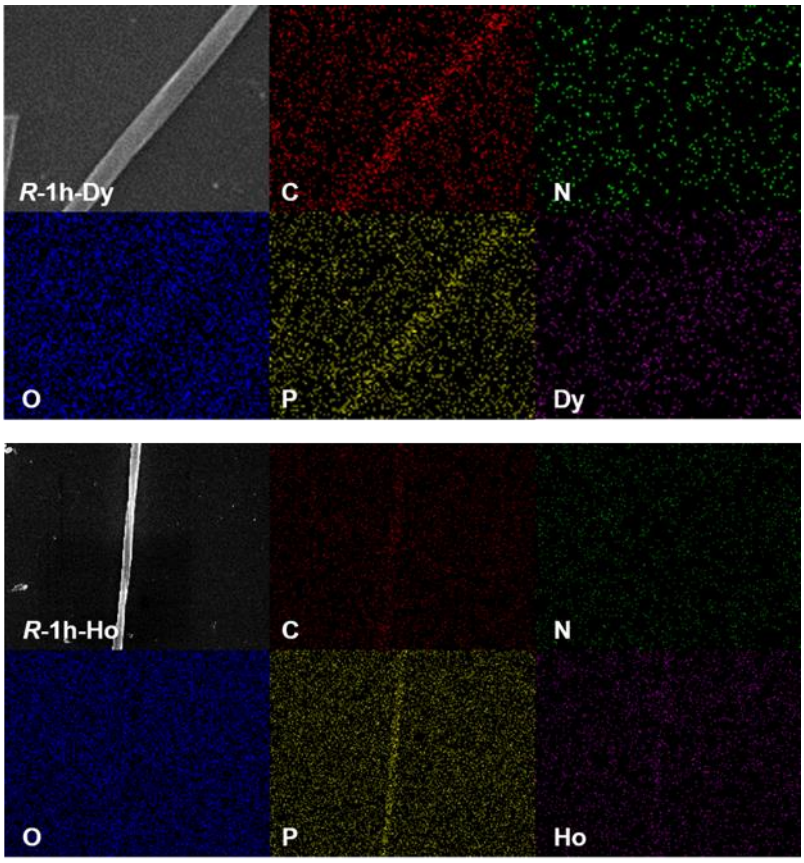

Figure S22. EDX mapping of helices ***R*-1h-Ln** (Ln = Sm, Eu, Gd, Tb, Dy, Ho) obtained after hydrothermal reactions of $Ln(NO_3)_3$ and *R*-pempH$_2$ (M:L molar ratio 1:6, pH 3.5, autoclave filling degree 60 %) at 120 °C for 24 h.

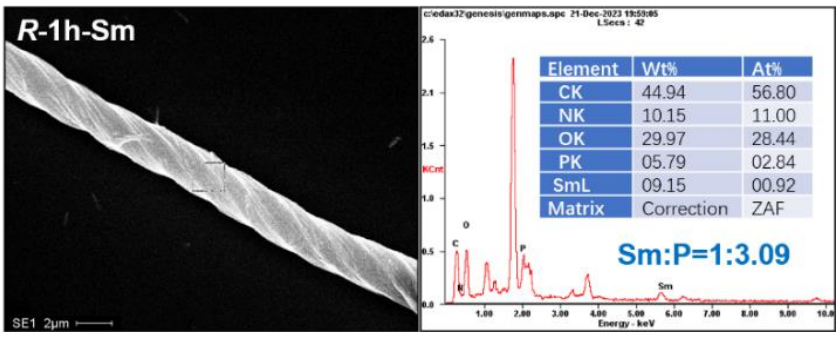
R-1h-Sm
SE1 2μm
Element Wt% At%
CK 44.94 56.80
NK 10.15 11.00
OK 29.97 28.44
PK 05.79 02.84
SmL 09.15 00.92
Matrix Correction ZAF
Sm:P=1:3.09
Energy - keV

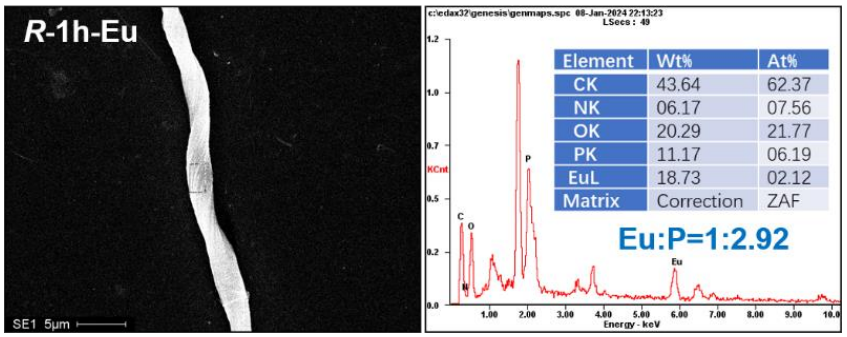
R-1h-Eu
SE1 5μm
Element Wt% At%
CK 43.64 62.37
NK 06.17 07.56
OK 20.29 21.77
PK 11.17 06.19
EuL 18.73 02.12
Matrix Correction ZAF
Eu:P=1:2.92
Energy - keV

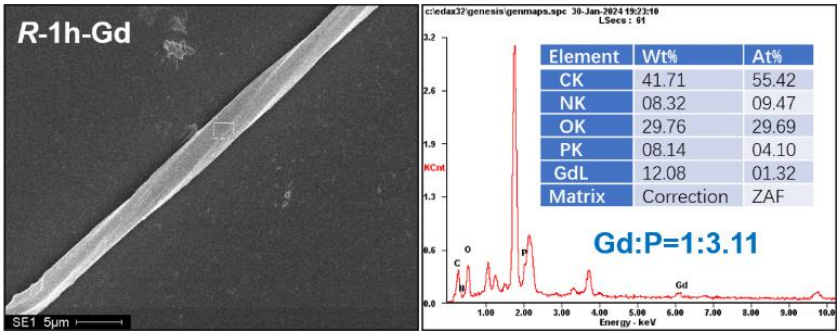
R-1h-Gd
SE1 5μm
Element Wt% At%
CK 41.71 55.42
NK 08.32 09.47
OK 29.76 29.69
PK 08.14 04.10
GdL 12.08 01.32
Matrix Correction ZAF
Gd:P=1:3.11
Energy - keV

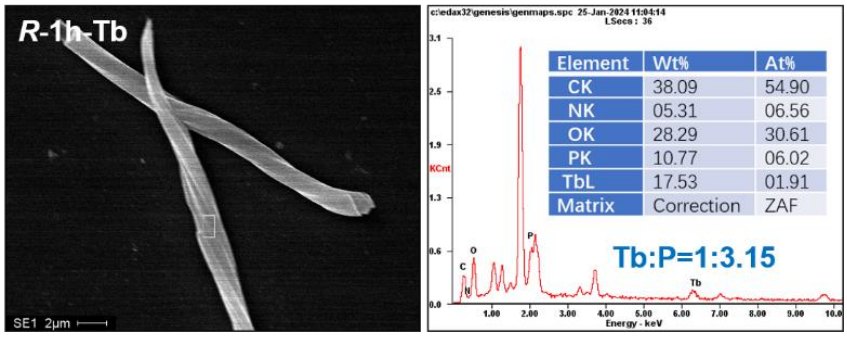
R-1h-Tb
SE1 2μm
Element Wt% At%
CK 38.09 54.90
NK 05.31 06.56
OK 28.29 30.61
PK 10.77 06.02
TbL 17.53 01.91
Matrix Correction ZAF
Tb:P=1:3.15
Energy - keV

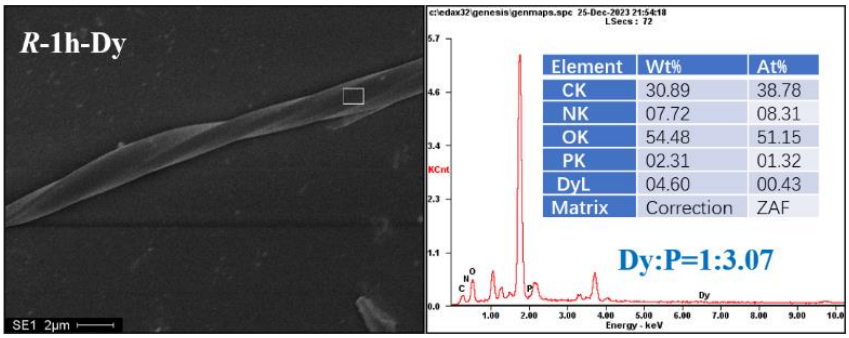
R-1h-Dy
SE1 2μm
Element Wt% At%
CK 30.89 38.78
NK 07.72 08.31
OK 54.48 51.15
PK 02.31 01.32
DyL 04.60 00.43
Matrix Correction ZAF
Dy:P=1:3.07
Energy - keV

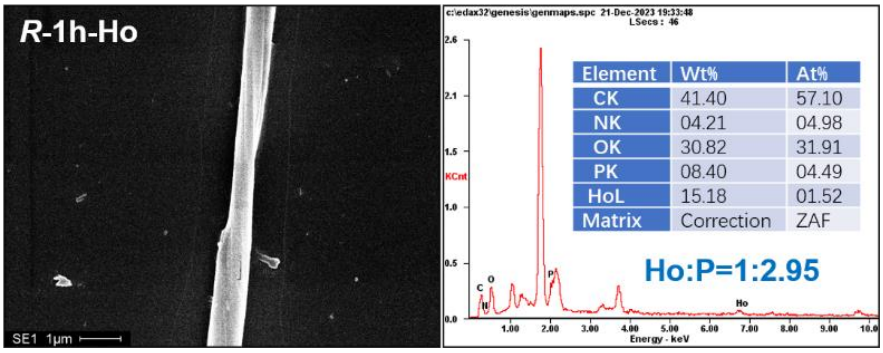

Figure S23. EDX spectra of helices ***R*-1h-Ln** (Ln = Sm, Eu, Gd, Tb, Dy, Ho) obtained after hydrothermal reactions of $Ln(NO_3)_3$ and *R*-pempH$_2$ (M:L molar ratio 1:6, pH 3.5, autoclave filling degree 60 %) at 120 °C for 24 h.

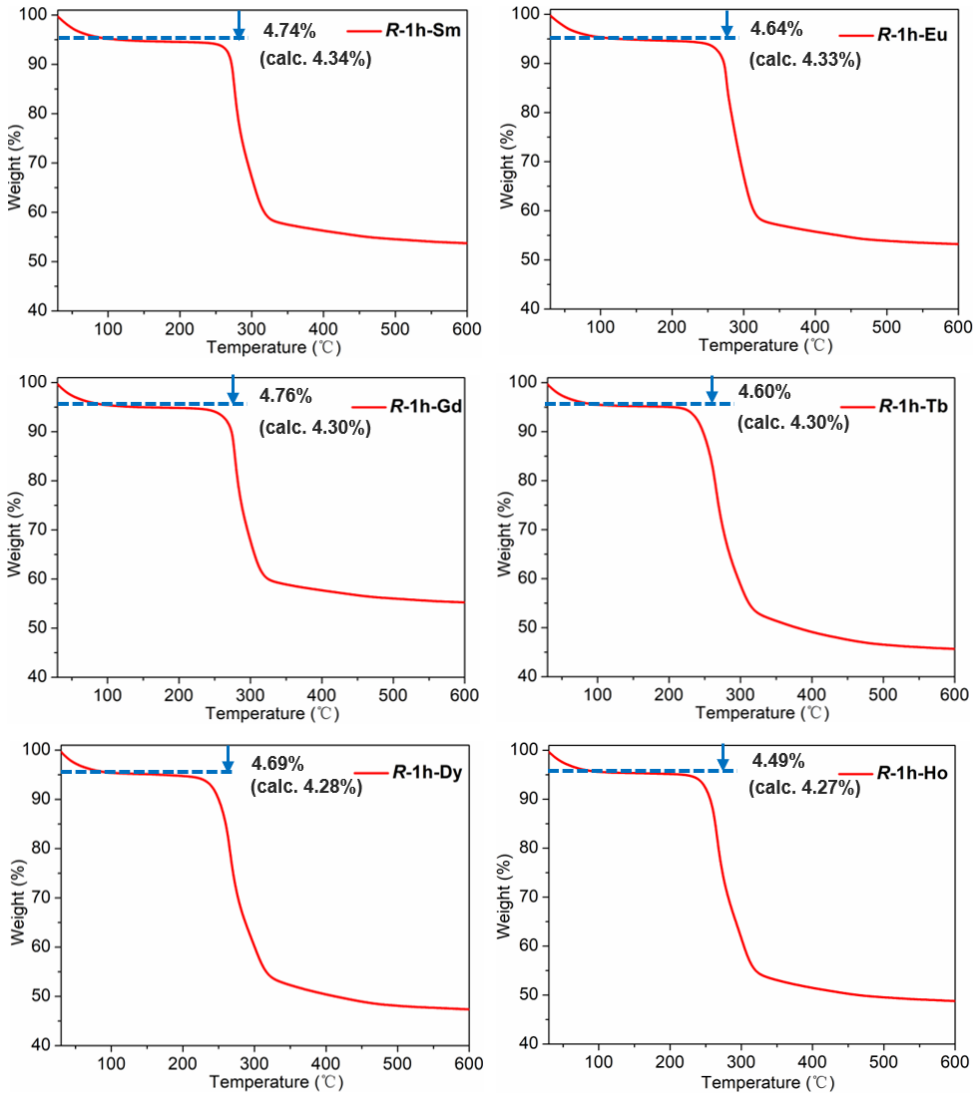

Figure S24. TGA curves of the helices ***R*-1h-Ln** (Ln = Sm, Eu, Gd, Tb, Dy, Ho) obtained after hydrothermal reactions of $Ln(NO_3)_3$ and *R*-pempH$_2$ (M:L molar ratio 1:6, pH 3.5, autoclave filling degree 60 %) at 120 °C for 24 h. The weight losses in the temperature 30-110 °C agree well with the valued expected for the removal of two lattice water molecules.

Table S7. The Elemental analyses, TG and molecular formula of ***R*-1h-Ln** (Ln = Sm, Eu, Gd, Tb, Dy, Ho).

Compound	Elemental analyses						TG		Molecular formula
	C%		H%		N%		H_2O%		
	Calcd (%)	Found (%)	Calcd (%)	Found (%)	Calcd (%)	Found (%)	Calcd (%)	Found (%)	
***R*-1h-Sm**	39.12	38.71	5.19	5.33	5.07	5.14	4.34	4.74	**Sm(*R*-pempH)$_3$·2H$_2$O**
									$C_{27}H_{39}N_3O_9P_3Sm·2H_2O$
***R*-1h-Eu**	39.05	38.79	5.18	5.29	5.06	5.17	4.33	4.64	**Eu(*R*-pempH)$_3$·2H$_2$O**
									$C_{27}H_{39}N_3O_9P_3Eu·2H_2O$
***R*-1h-Gd**	38.80	38.71	5.14	5.28	5.03	5.13	4.30	4.76	**Gd(*R*-pempH)$_3$·2H$_2$O**
									$C_{27}H_{39}N_3O_9P_3Gd·2H_2O$
***R*-1h-Tb**	38.72	38.50	5.13	5.24	5.02	5.13	4.30	4.60	**Tb(*R*-pempH)$_3$·2H$_2$O**
									$C_{27}H_{39}N_3O_9P_3Tb·2H_2O$
***R*-1h-Dy**	38.56	38.72	5.11	5.36	5.00	5.13	4.28	4.69	**Dy(*R*-pempH)$_3$·2H$_2$O**
									$C_{27}H_{39}N_3O_9P_3Dy·2H_2O$
***R*-1h-Ho**	38.45	38.45	5.10	5.20	4.98	5.13	4.27	4.49	**Ho(*R*-pempH)$_3$·2H$_2$O**
									$C_{27}H_{39}N_3O_9P_3Ho·2H_2O$

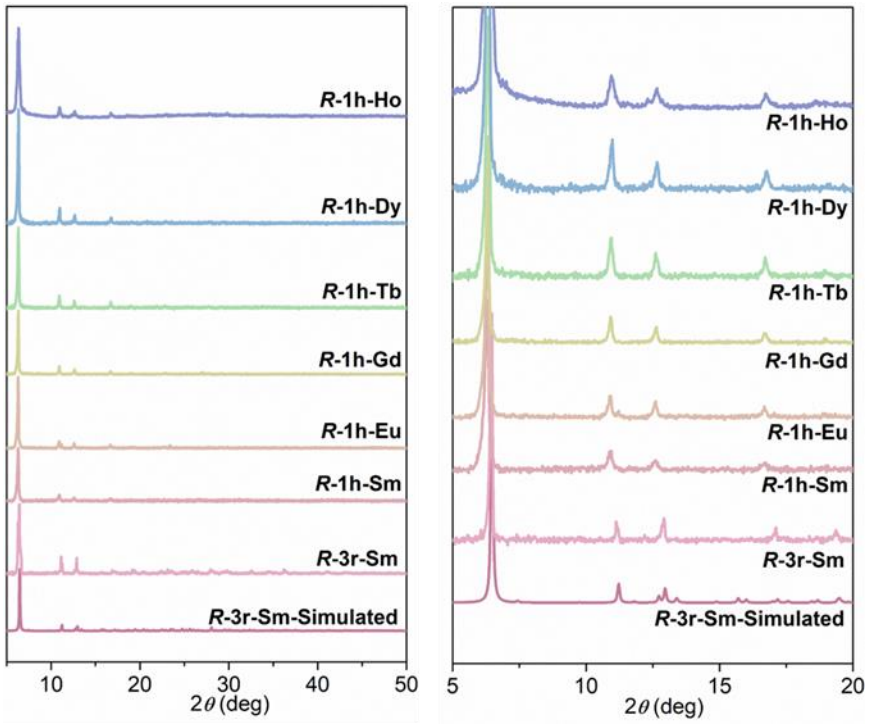

Figure S25 %) at 120 °C for 24 h. The pattern simulated from single crystal data of ***R*-3r-Sm** is given for comparison.

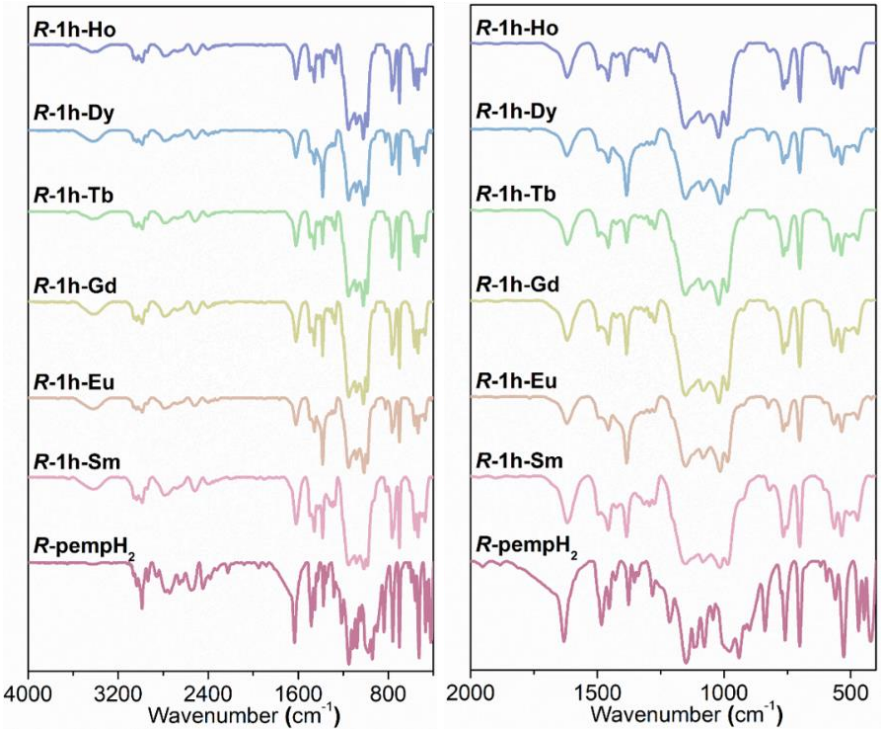

Figure S26. IR spectra of helical products ***R*-1h-Ln** (Ln = Sm, Eu, Gd, Tb, Dy, Ho) obtained after hydrothermal reactions of $Ln(NO_3)_3$ and *R*-pempH$_2$ (M:L molar ratio 1:6, pH 3.5, autoclave filling degree 60 %) at 120 °C for 24 h.

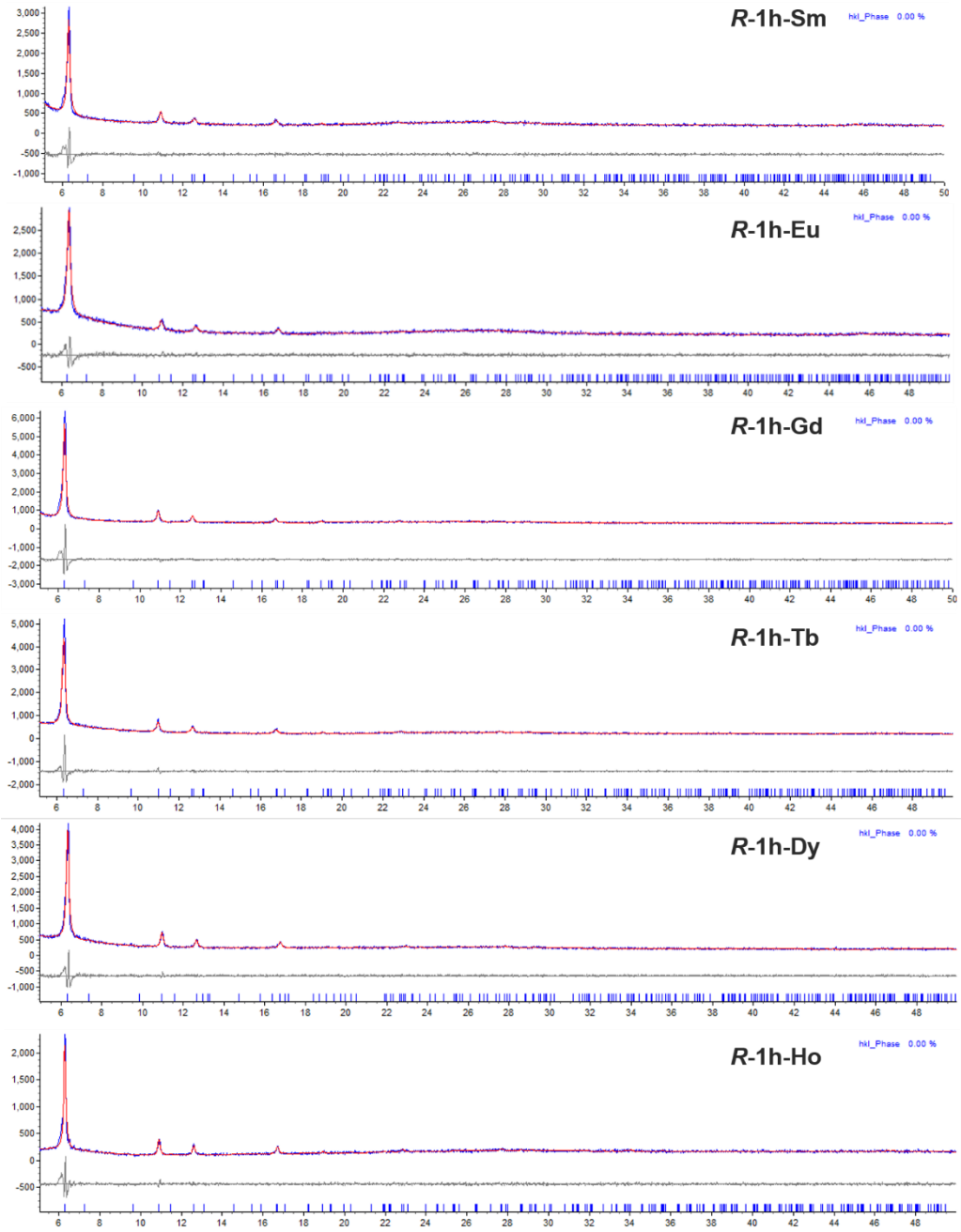

Figure S27. Pawley fit of the PXRD patterns of the powder samples of ***R*-1h-Ln** using TOPAS 5.0 program.

Fitted cell parameters for ***R*-1h-Sm**: $P6_5$, a = 16.248 Å, c = 24.658 Å, V = 5637.3 Å^3 (Rwp = 7.72).

Fitted cell parameters for ***R*-1h-Eu**: $P6_5$, a = 16.204 Å, c = 24.296 Å, V = 5522.9 Å^3 (Rwp = 6.96).

Fitted cell parameters for ***R*-1h-Gd**: $P6_5$, a = 16.230 Å, c = 24.090 Å, V = 5495.7 Å^3 (Rwp = 8.60).

Fitted cell parameters for ***R*-1h-Tb**: $P6_5$, a = 16.098 Å, c = 24.350 Å, V = 5464.7 Å^3 (Rwp = 8.03).

Fitted cell parameters for ***R*-1h-Dy**: $P6_5$, a = 16.164 Å, c = 23.445 Å, V = 5304.8 Å^3 (Rwp = 7.44).

Fitted cell parameters for ***R*-1h-Ho**: $P6_5$, a = 16.132 Å, c = 23.440 Å, V = 5282.8 Å^3 (Rwp = 8.62).

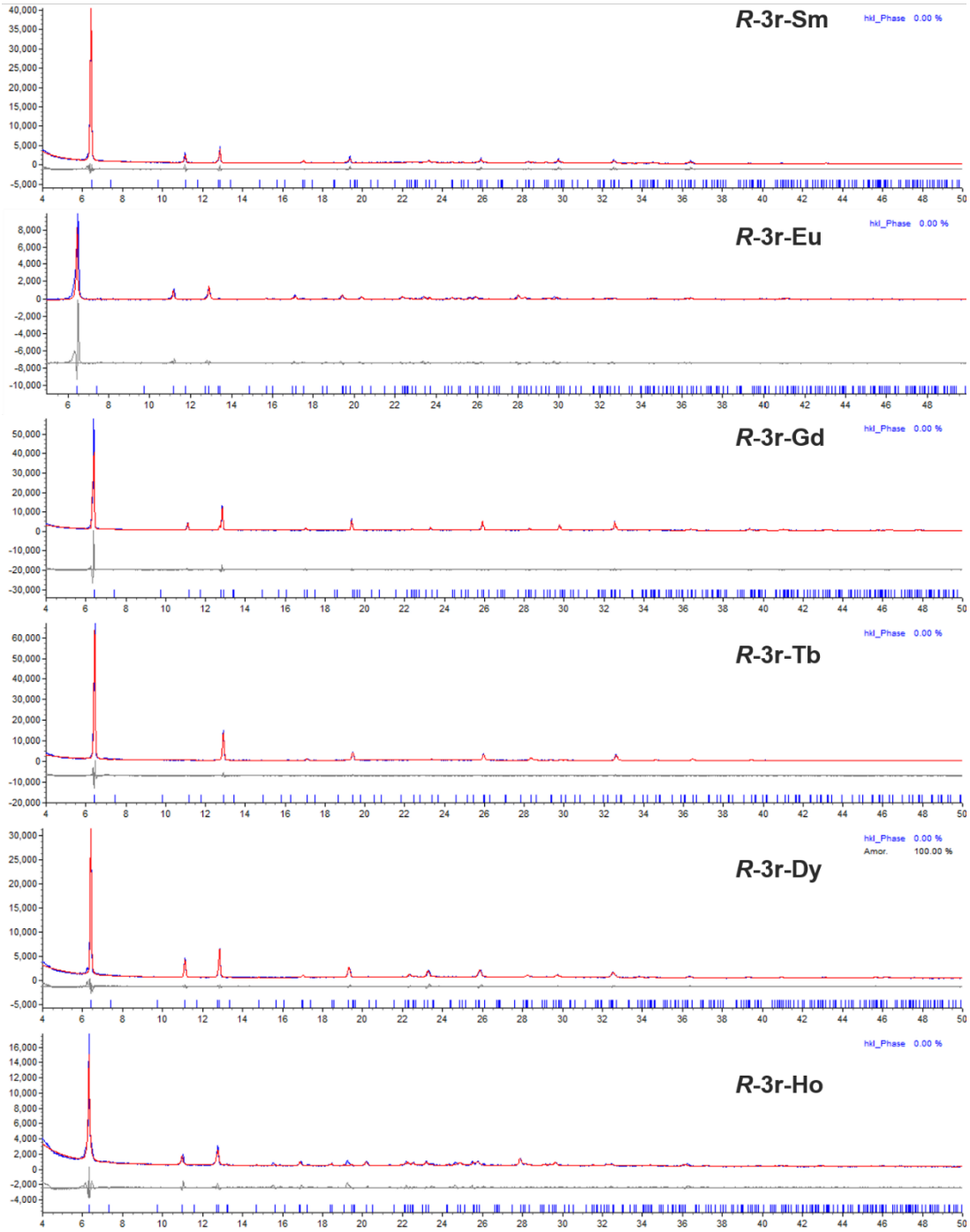

Figure S28. Pawley fit of the PXRD patterns of the powder samples of ***R*-3r-Ln** using TOPAS 5.0 program.

Fitted cell parameters for ***R*-3r-Sm:** $P6_5$, a = 15.848 Å, c = 23.993 Å, V = 5218.4 Å^3 (Rwp = 8.45).

Fitted cell parameters for ***R*-3r-Eu:** $P6_5$, a = 15.832 Å, c = 24.231 Å, V = 5260.0 Å^3 (Rwp = 9.51).

Fitted cell parameters for ***R*-3r-Gd:** $P6_5$, a = 15.846 Å, c = 24.108 Å, V = 5242.4 Å^3 (Rwp = 10.03).

Fitted cell parameters for ***R*-3r-Tb:** $P6_5$, a = 15.832 Å, c = 24.733 Å, V = 5151.6 Å^3 (Rwp = 9.89).

Fitted cell parameters for ***R*-3r-Dy:** $P6_5$, a = 15.915 Å, c = 24.069 Å, V = 5279.5 Å^3 (Rwp = 7.84).

Fitted cell parameters for ***R*-3r-Ho:** $P6_5$, a = 16.091 Å, c = 23.923 Å, V = 5264.2 Å^3 (Rwp = 8.31).

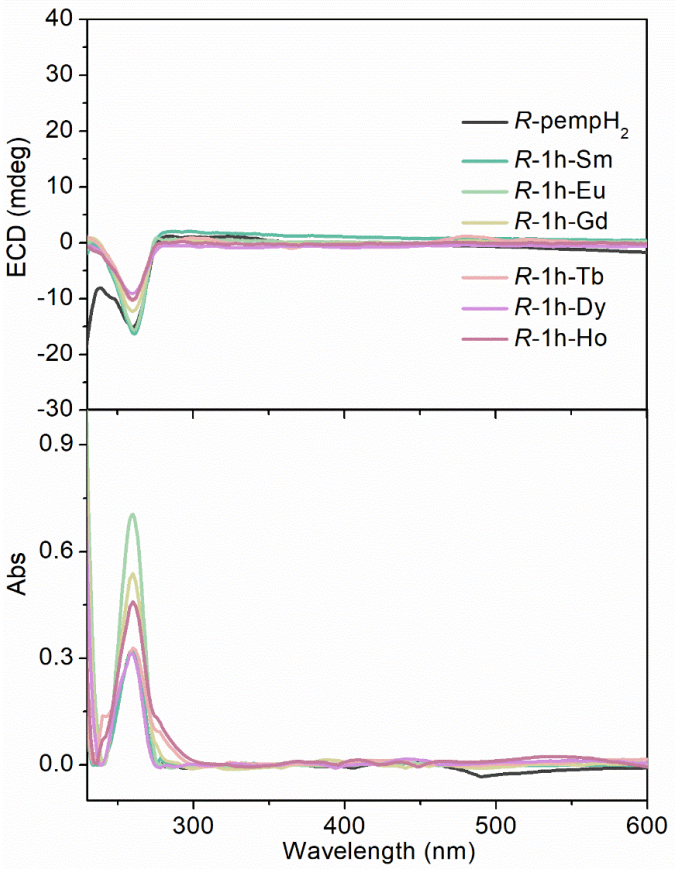

Figure S29. ECD spectra of helical products of ***R*-1h-Ln** (Ln = Sm, Eu, Gd, Tb, Dy, Ho) obtained after hydrothermal reactions of $Ln(NO_3)_3$ and *R*-pempH$_2$ (M:L molar ratio 1:6, pH 3.5, autoclave filling degree 60 %) at 120 °C for 24 h.

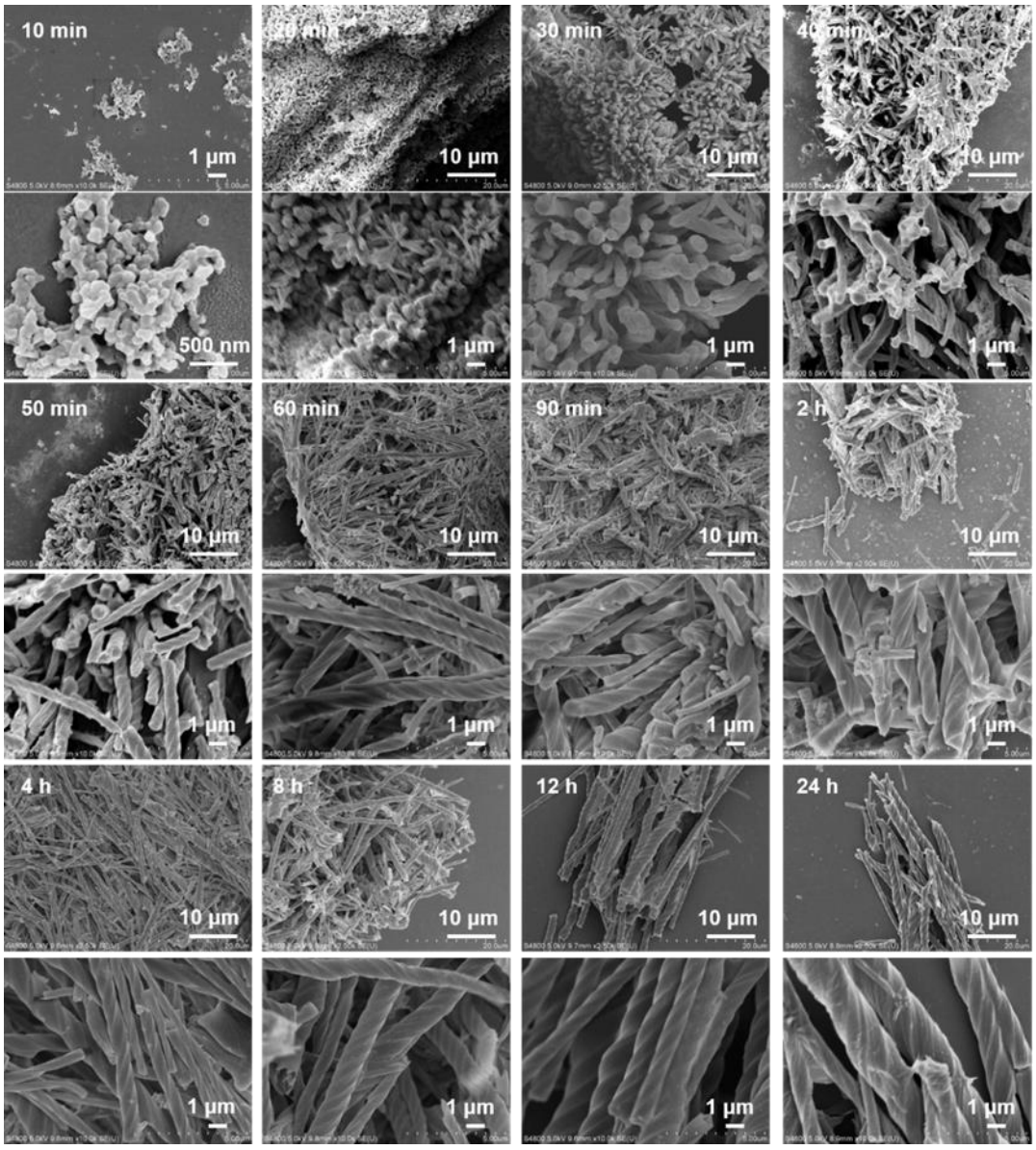

Figure S30. SEM images of the reaction products after hydrothermal reactions of $Sm(NO_3)_3$ and *R*-pempH$_2$ (molar ratio 1:6, autoclave filling degree 60 %) under pH 3.5 at 120 °C for different period of time.

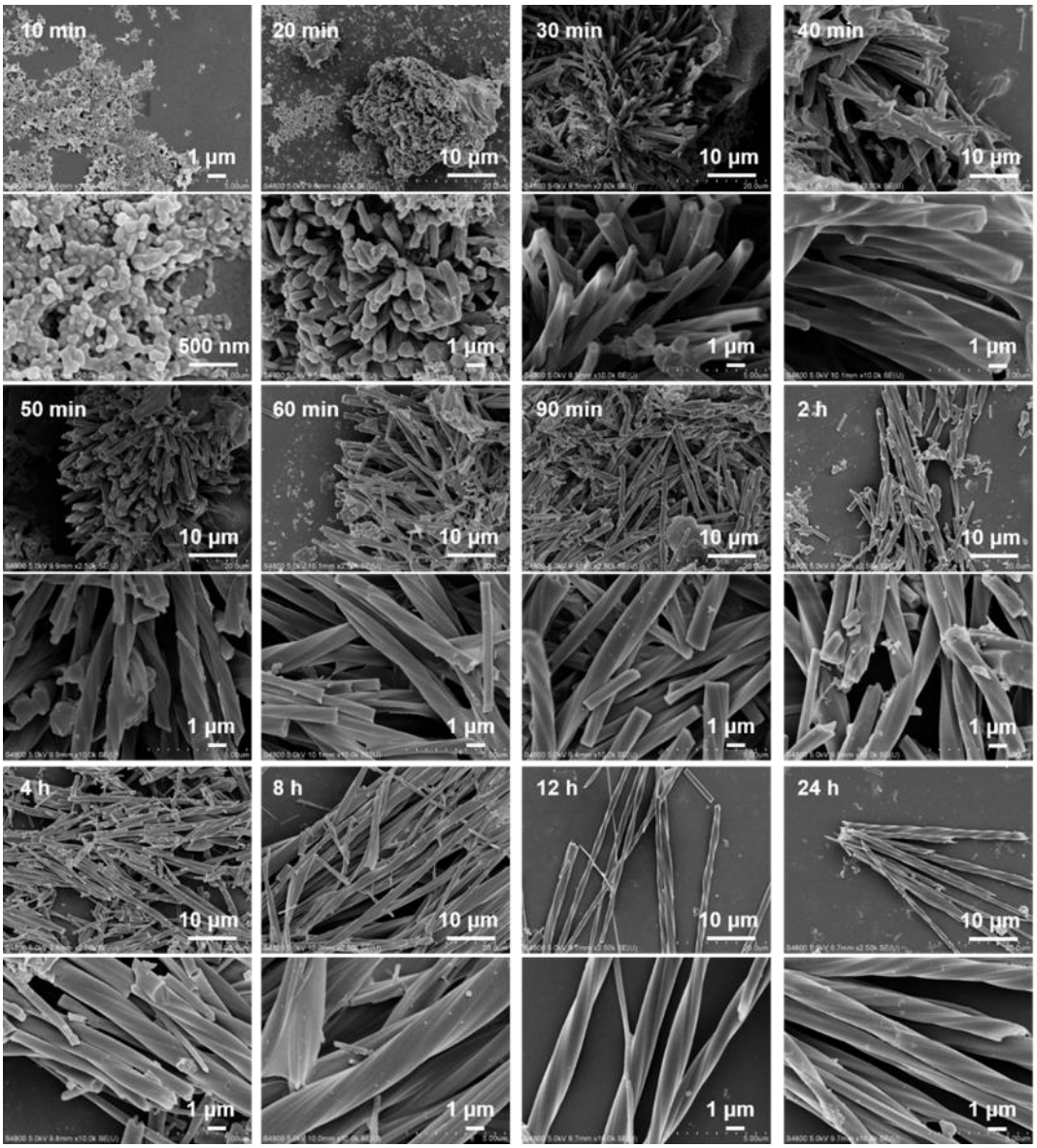

Figure S31. SEM images of the reaction products after hydrothermal reactions of $Dy(NO_3)_3$ and *R*-pempH$_2$ (molar ratio 1:6, autoclave filling degree 60 %) under pH 3.5 at 120 °C for different period of time.

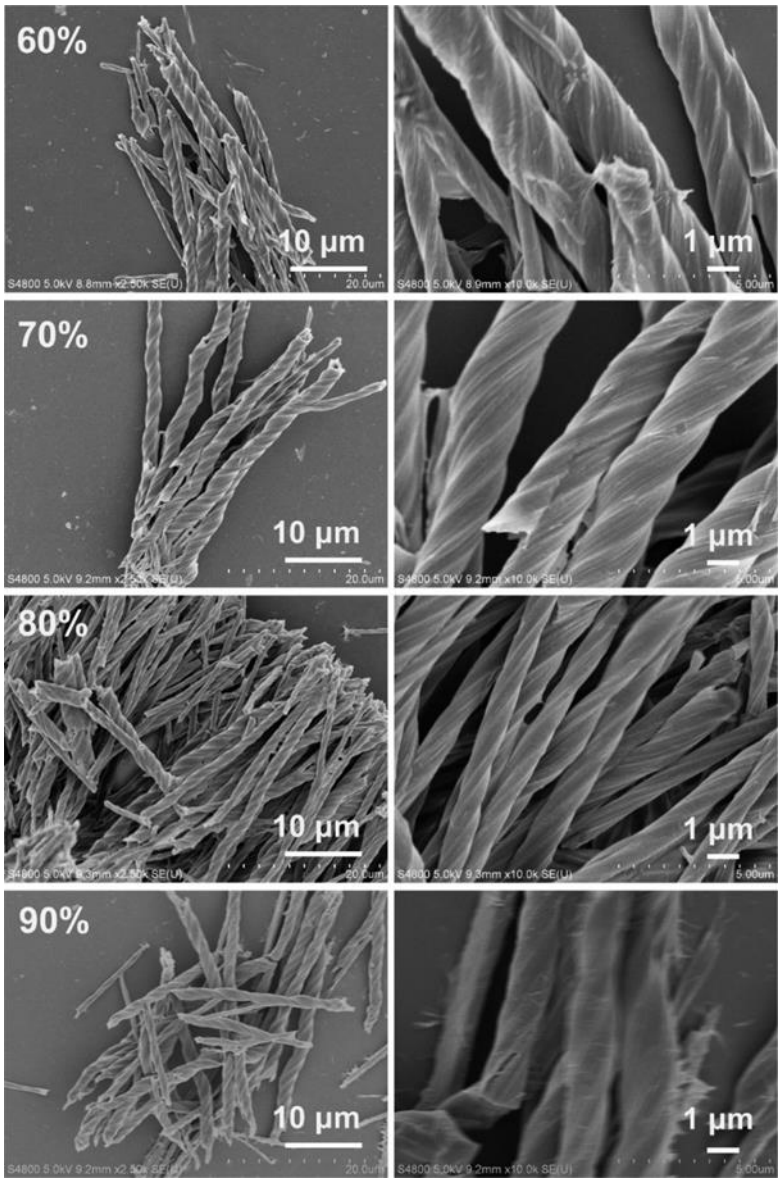

Figure S32. SEM images of the reaction products after hydrothermal reactions of $Sm(NO_3)_3$ and *R*-pempH$_2$ (molar ratio 1:6, autoclave filling degree 60-90 %) under pH 3.5 at 120 °C for 24 h.

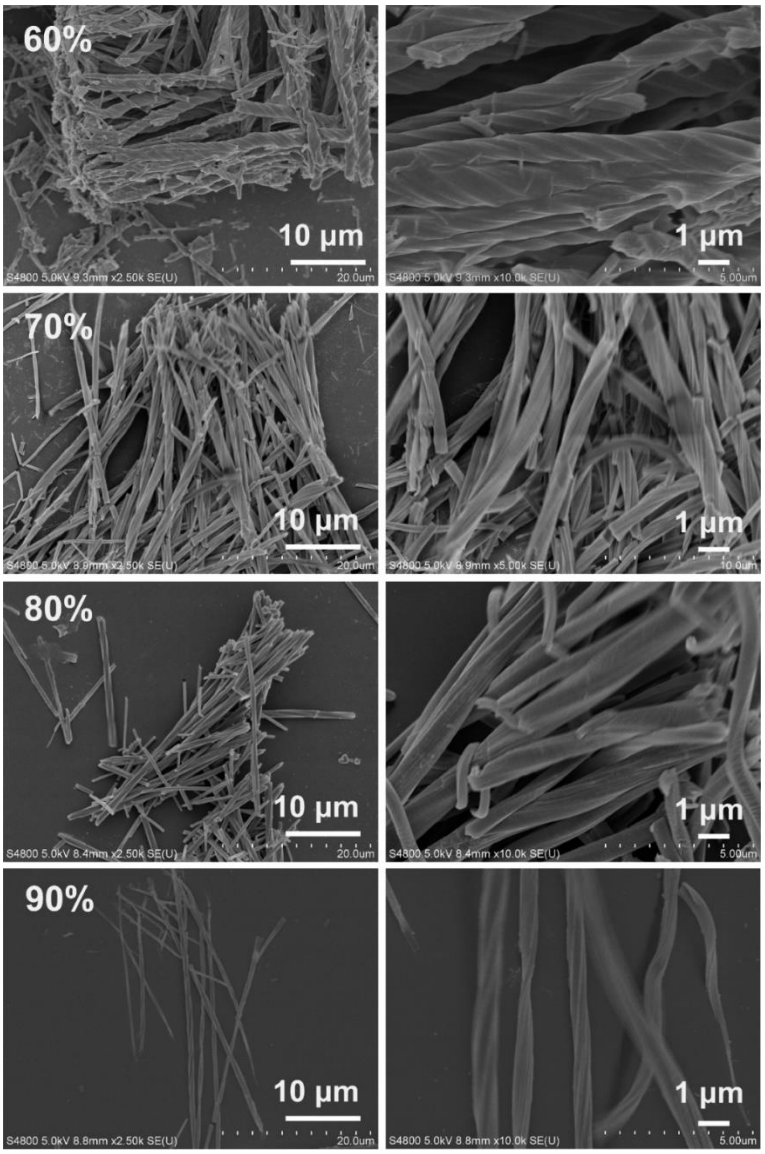

Figure S33. SEM images of the reaction products after hydrothermal reactions of $Eu(NO_3)_3$ and *R*-pempH$_2$ (molar ratio 1:6, autoclave filling degree 60-90 %) under pH 3.5 at 120 °C for 24 h.

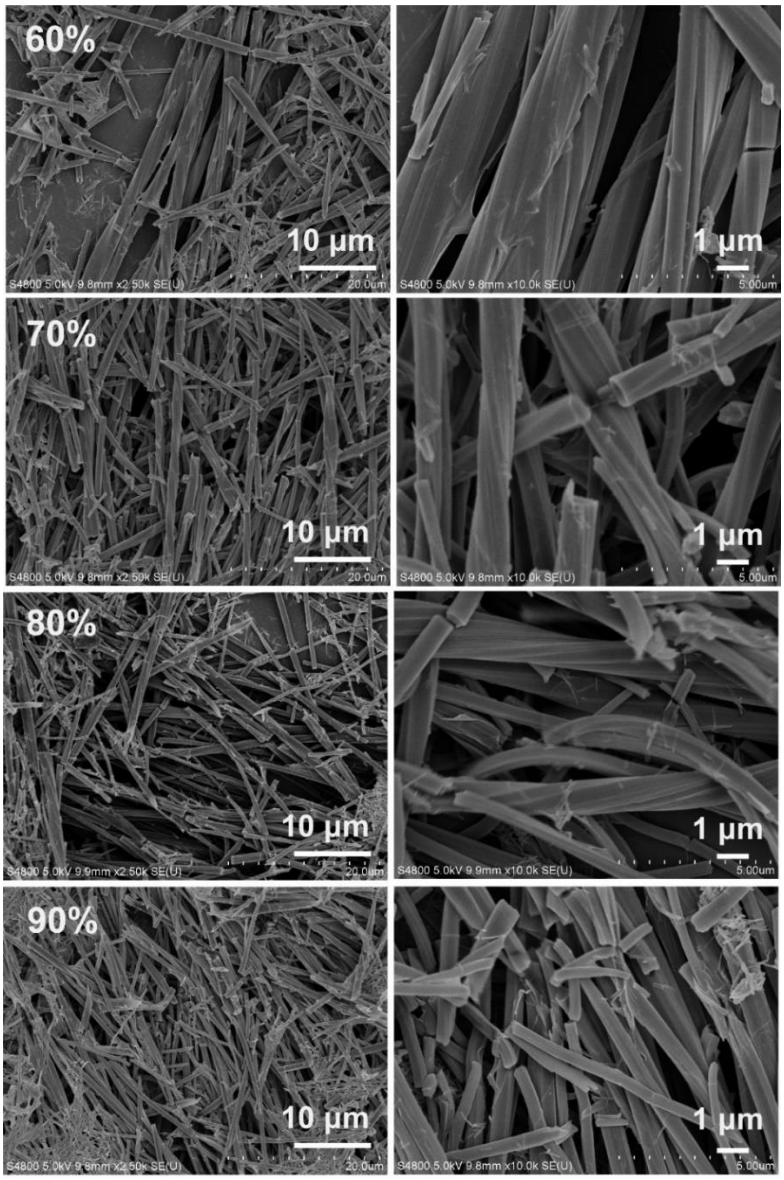

Figure S34. SEM images of the reaction products after hydrothermal reactions of $Gd(NO_3)_3$ and *R*-pempH$_2$ (molar ratio 1:6, autoclave filling degree 60-90 %) under pH 3.5 at 120 °C for 24 h.

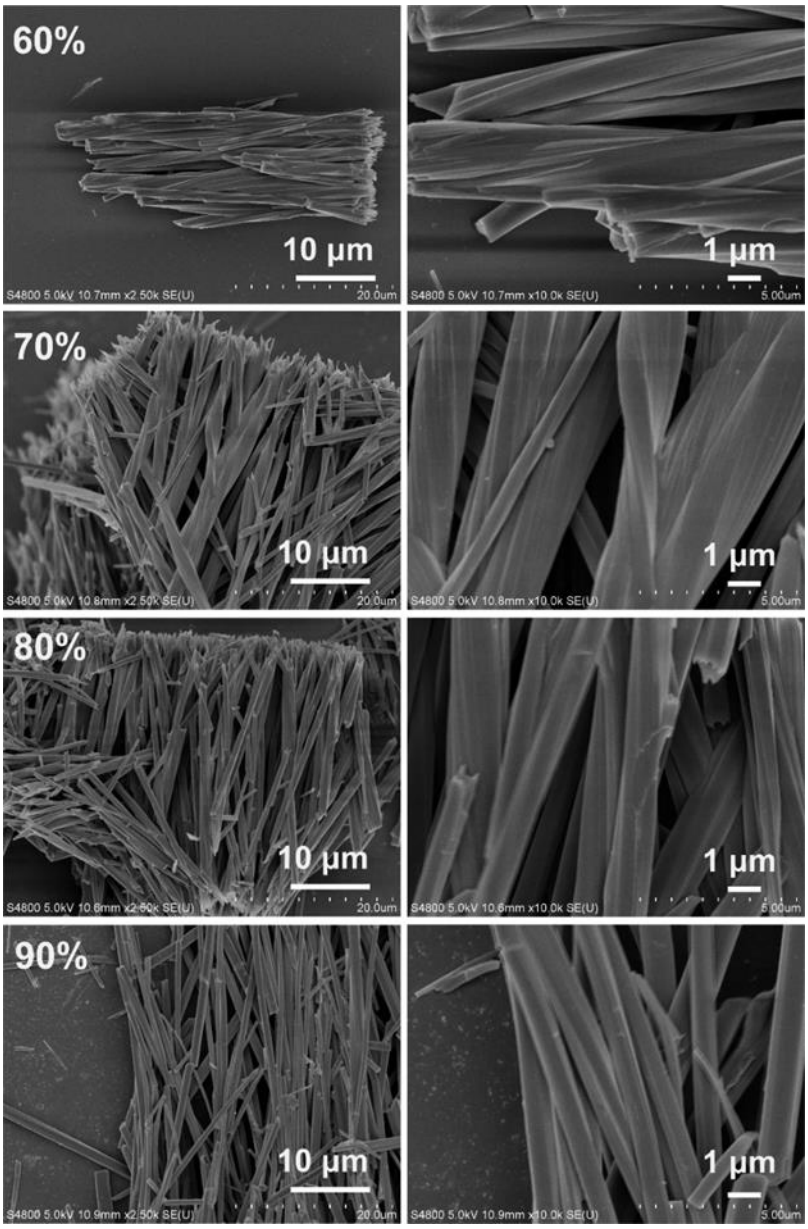

Figure S35. SEM images of the reaction products after hydrothermal reactions of $Tb(NO_3)_3$ and *R*-pempH$_2$ (molar ratio 1:6, autoclave filling degree 60-90 %) under pH 3.5 at 120 °C for 24 h.

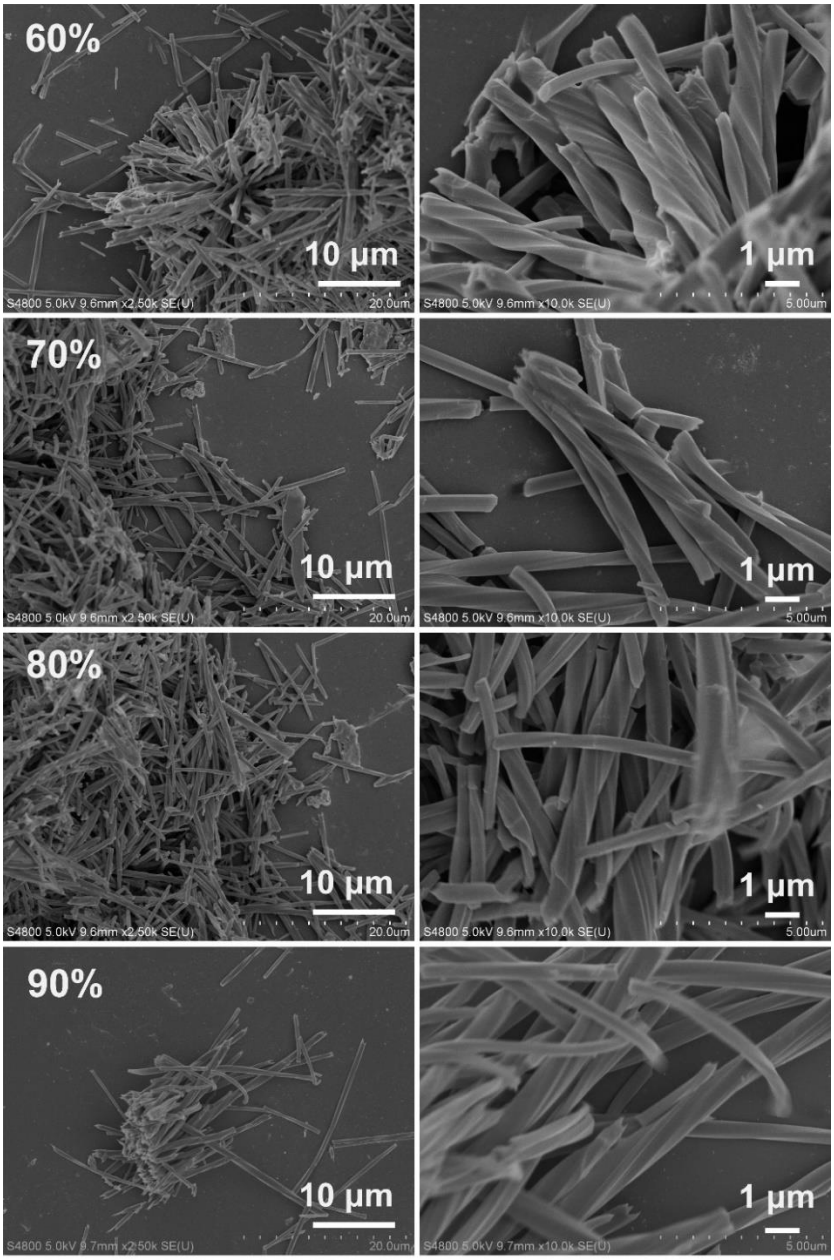

Figure S36. SEM images of the reaction products after hydrothermal reactions of $Dy(NO_3)_3$ and *R*-pempH$_2$ (molar ratio 1:6, autoclave filling degree 60-90 %) under pH 3.5 at 120 °C for 24 h.

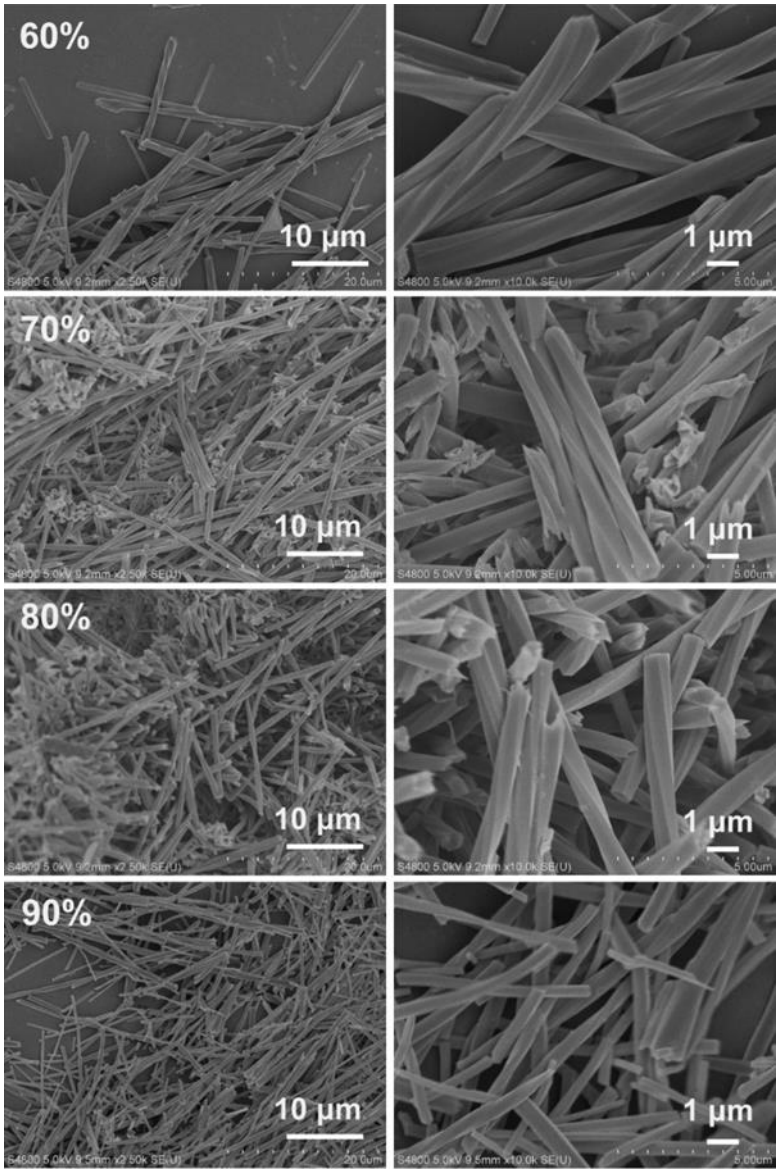

Figure S37. SEM images of the reaction products after hydrothermal reactions of $Ho(NO_3)_3$ and *R*-pempH$_2$ (molar ratio 1:6, autoclave filling degree 60-90 %) under pH 3.5 at 120 °C for 24 h.

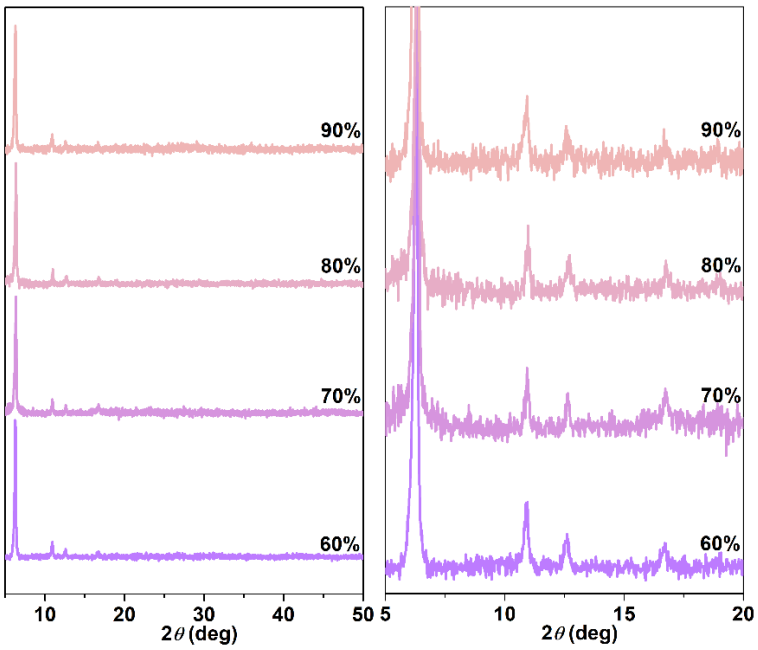

Figure S38. The PXRD patterns of the reaction products after hydrothermal reactions of $Sm(NO_3)_3$ and *R*-pempH$_2$ (molar ratio 1:6, autoclave filling degree 60-90 %) under pH 3.5 at 120 °C for 24 h.

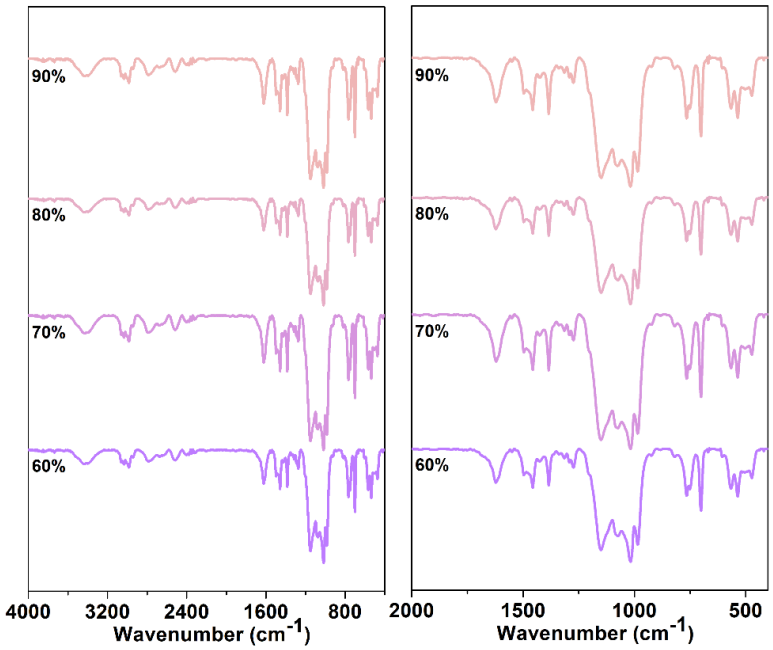

Figure S39. The IR spectra of the reaction products after hydrothermal reactions of $Sm(NO_3)_3$ and *R*-pempH$_2$ (molar ratio 1:6, autoclave filling degree 60-90 %) under pH 3.5 at 120 °C for 24 h. (Left: 4000-400, Right: 2000-400 cm^{-1}).

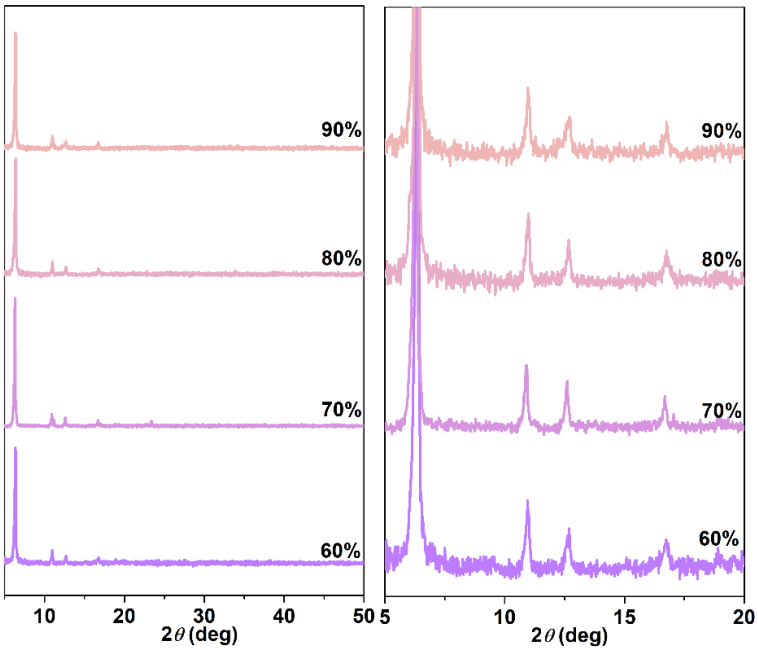

Figure S40. The PXRD patterns of the reaction products after hydrothermal reactions of $Eu(NO_3)_3$ and *R*-pempH$_2$ (molar ratio 1:6, autoclave filling degree 60-90 %) under pH 3.5 at 120 °C for 24 h.

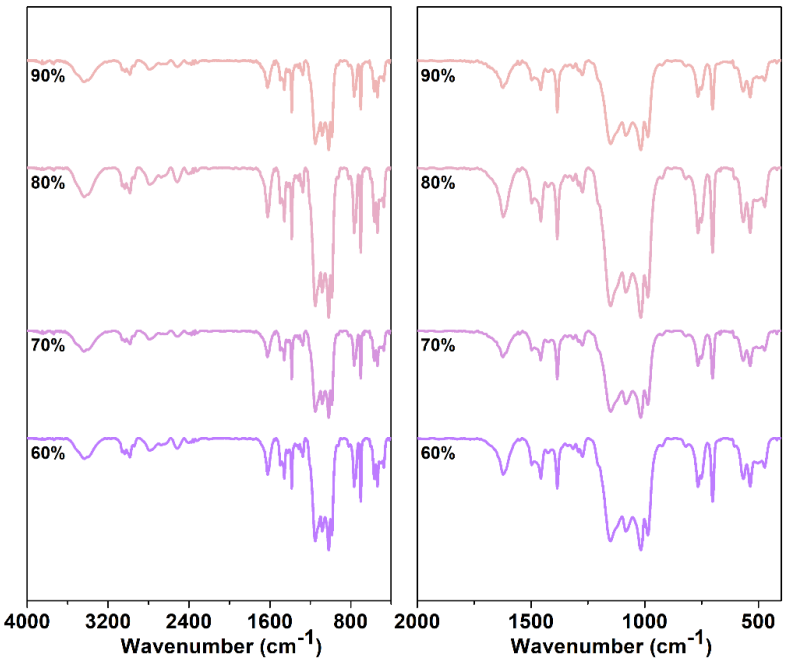

Figure S41. The IR spectra of the reaction products after hydrothermal reactions of $Eu(NO_3)_3$ and *R*-pempH$_2$ (molar ratio 1:6, autoclave filling degree 60-90 %) under pH 3.5 at 120 °C for 24 h. (Left: 4000-400, Right: 2000-400 cm^{-1}).

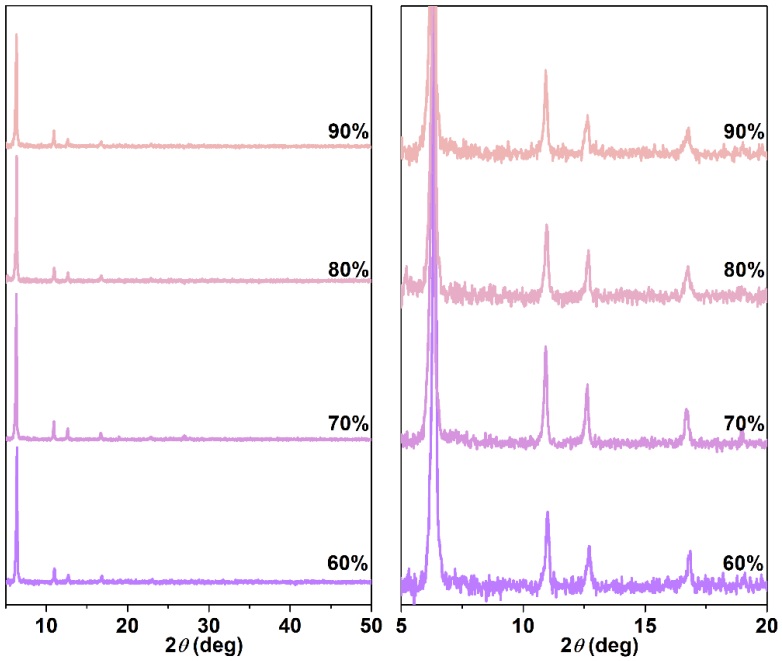

Figure S42. The PXRD patterns of the reaction products after hydrothermal reactions of $Gd(NO_3)_3$ and *R*-pempH$_2$ (molar ratio 1:6, autoclave filling degree 60-90 %) under pH 3.5 at 120 °C for 24 h.

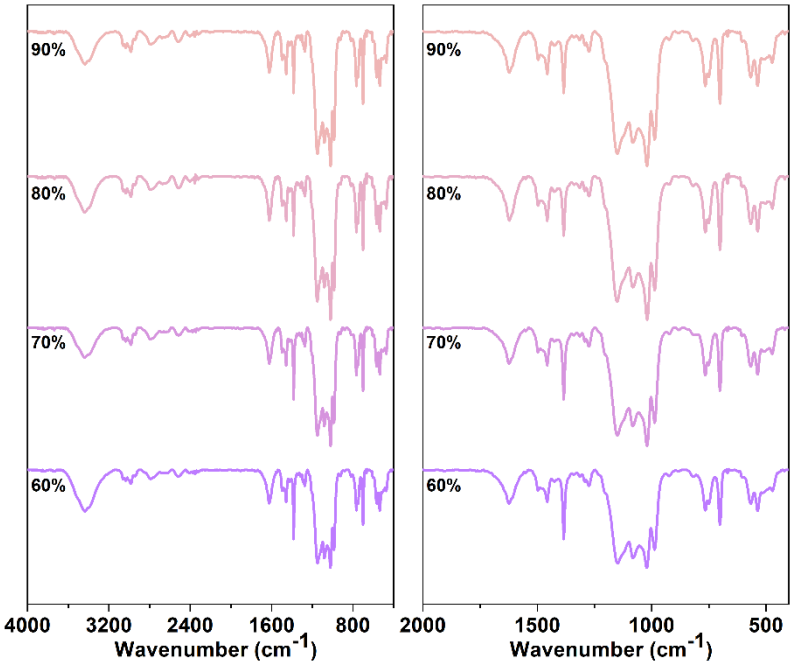

Figure S43. The IR spectra of the reaction products after hydrothermal reactions of $Gd(NO_3)_3$ and *R*-pempH$_2$ (molar ratio 1:6, autoclave filling degree 60-90 %) under pH 3.5 at 120 °C for 24 h. (Left: 4000-400, Right: 2000-400 cm^{-1}).

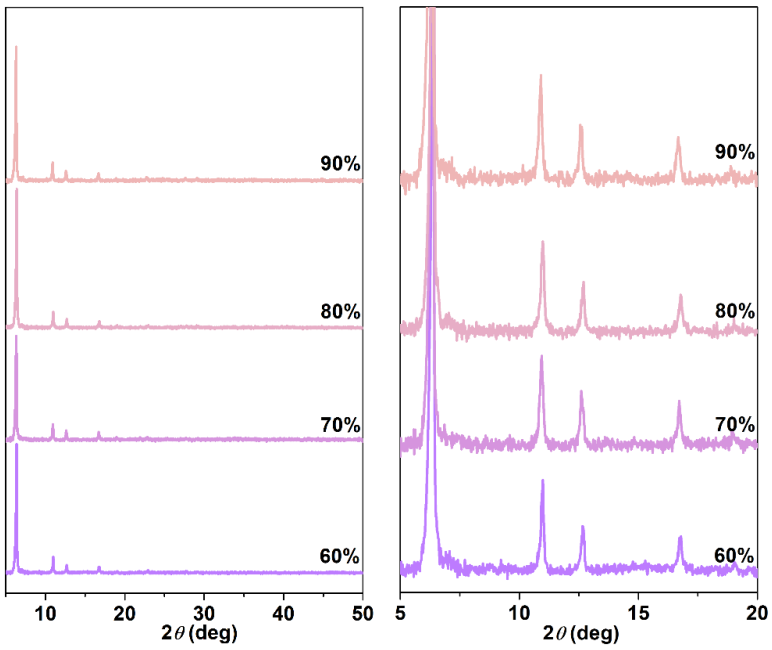

Figure S44. The PXRD patterns of the reaction products after hydrothermal reactions of $Tb(NO_3)_3$ and *R*-pempH$_2$ (molar ratio 1:6, autoclave filling degree 60-90 %) under pH 3.5 at 120 °C for 24 h.

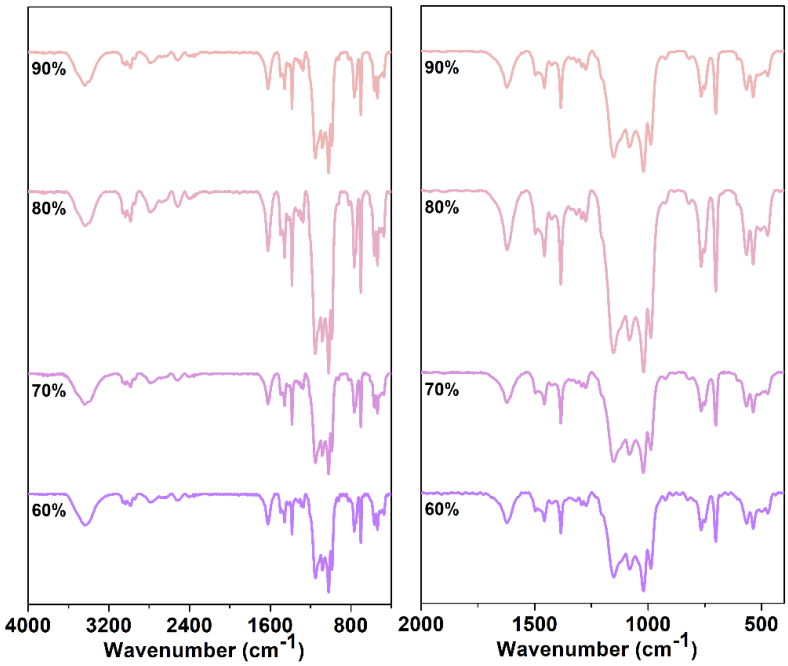

Figure S45. The IR spectra of the reaction products after hydrothermal reactions of $Tb(NO_3)_3$ and *R*-pempH$_2$ (molar ratio 1:6, autoclave filling degree 60-90 %) under pH 3.5 at 120 °C for 24 h. (Left: 4000-400, Right: 2000-400 cm^{-1}).

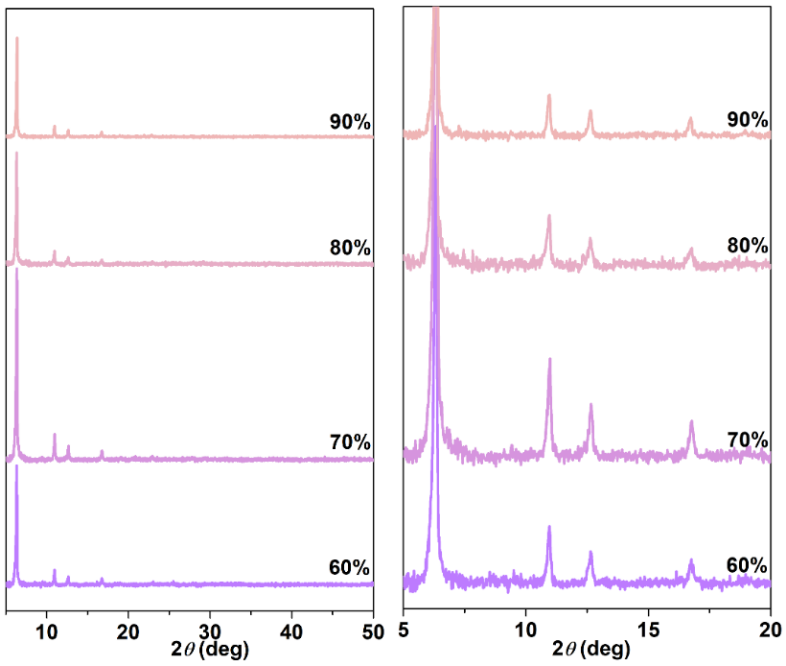

Figure S46. The PXRD patterns of the reaction products after hydrothermal reactions of $Dy(NO_3)_3$ and *R*-pempH$_2$ (molar ratio 1:6, autoclave filling degree 60-90 %) under pH 3.5 at 120 °C for 24 h.

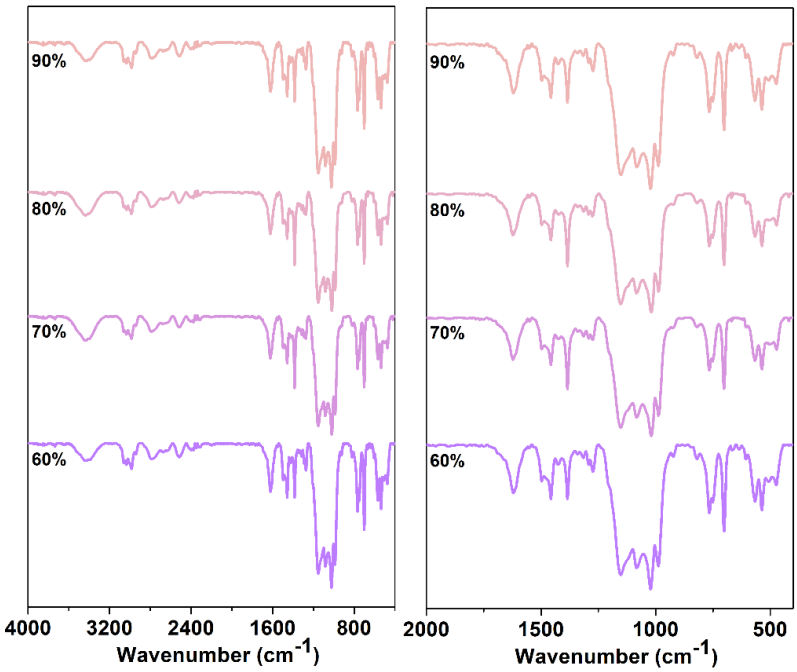

Figure S47. The IR spectra of the reaction products after hydrothermal reactions of $Dy(NO_3)_3$ and *R*-pempH$_2$ (molar ratio 1:6, autoclave filling degree 60-90 %) under pH 3.5 at 120 °C for 24 h. (Left: 4000-400, Right: 2000-400 cm^{-1}).

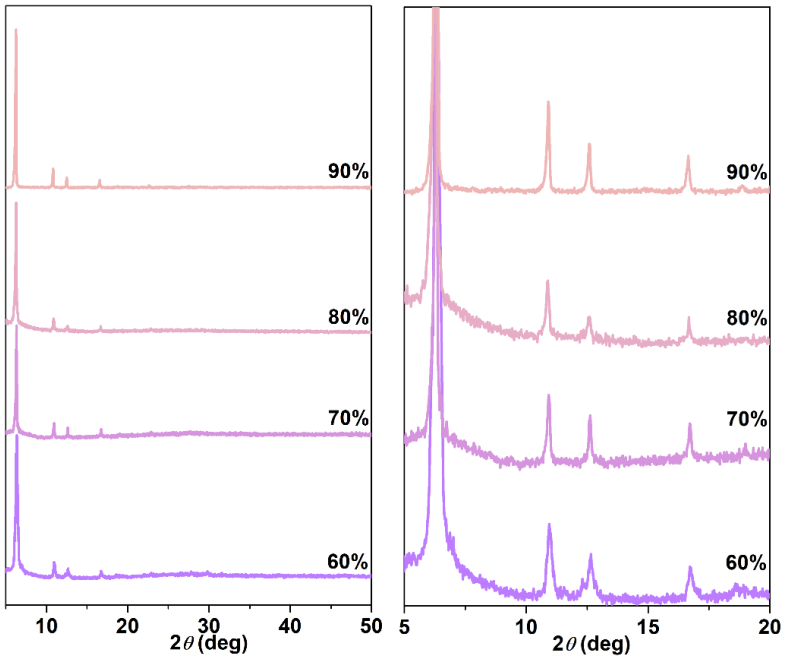

Figure S48. The PXRD patterns of the reaction products after hydrothermal reactions of $Ho(NO_3)_3$ and *R*-pempH$_2$ (molar ratio 1:6, autoclave filling degree 60-90 %) under pH 3.5 at 120 °C for 24 h.

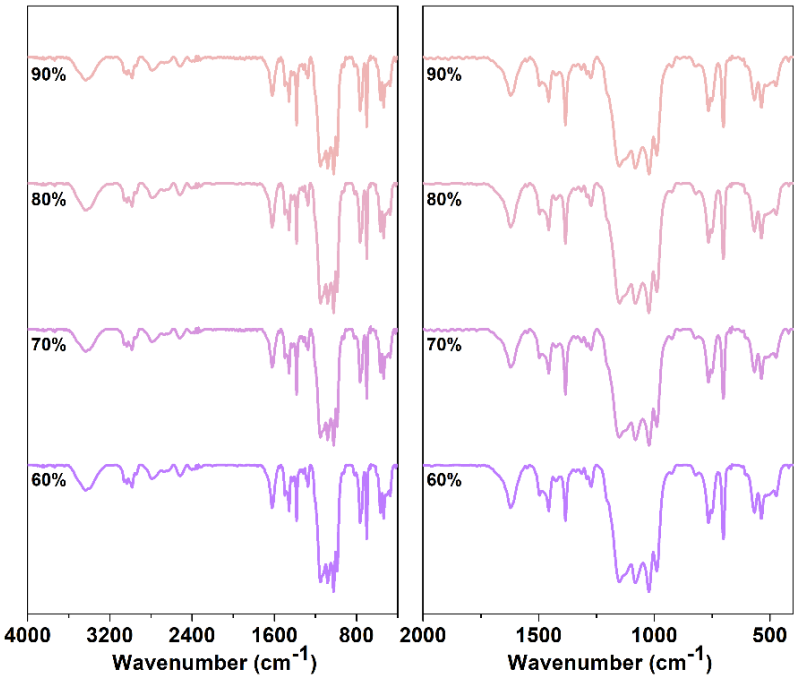

Figure S49. The IR spectra of the reaction products after hydrothermal reactions of $Ho(NO_3)_3$ and *R*-pempH$_2$ (molar ratio 1:6, autoclave filling degree 60-90 %) under pH 3.5 at 120 °C for 24 h. (Left: 4000-400, Right: 2000-400 cm^{-1}).

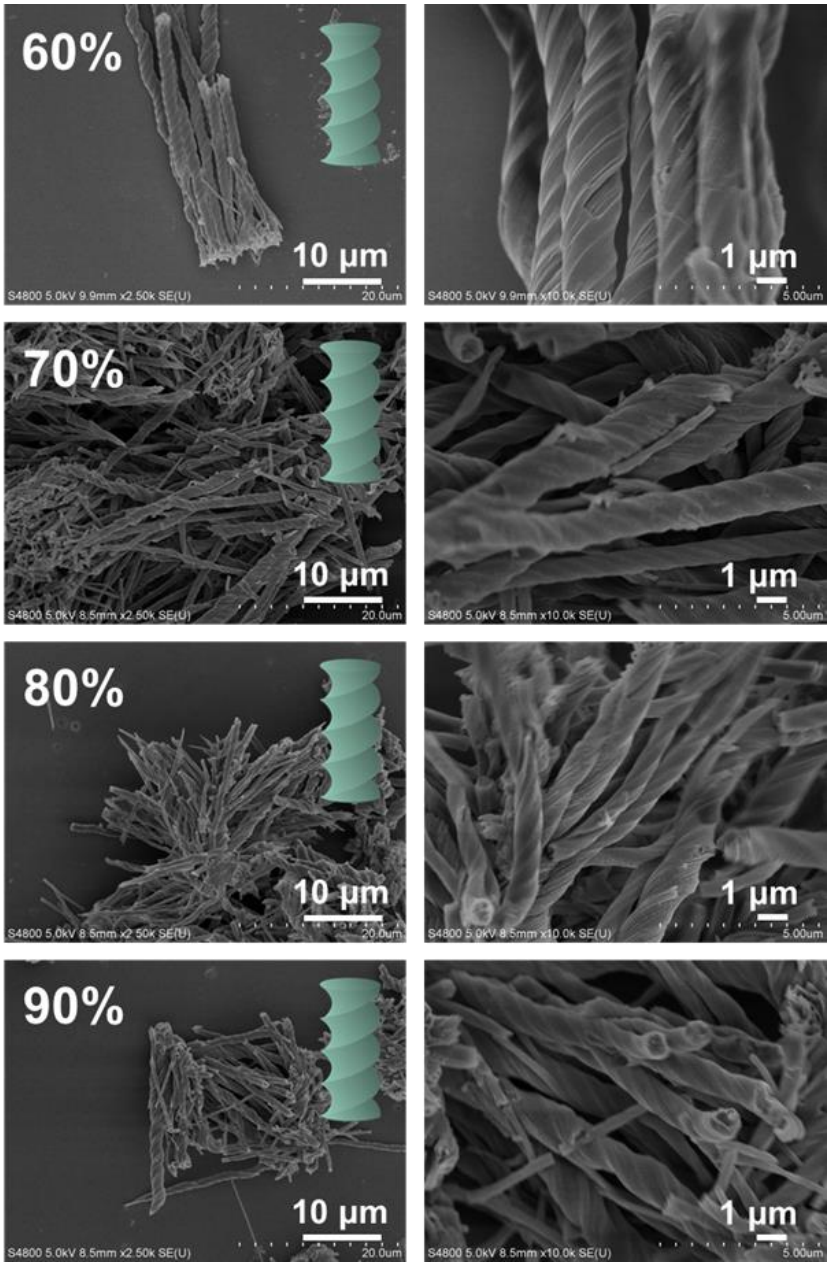

Figure S50. SEM images of the reaction products after hydrothermal reactions of $Sm(NO_3)_3$ and *R*-pempH$_2$ (molar ratio 1:5, autoclave filling degree 60-90%) under pH 3.5 at 120 °C for 24 h.

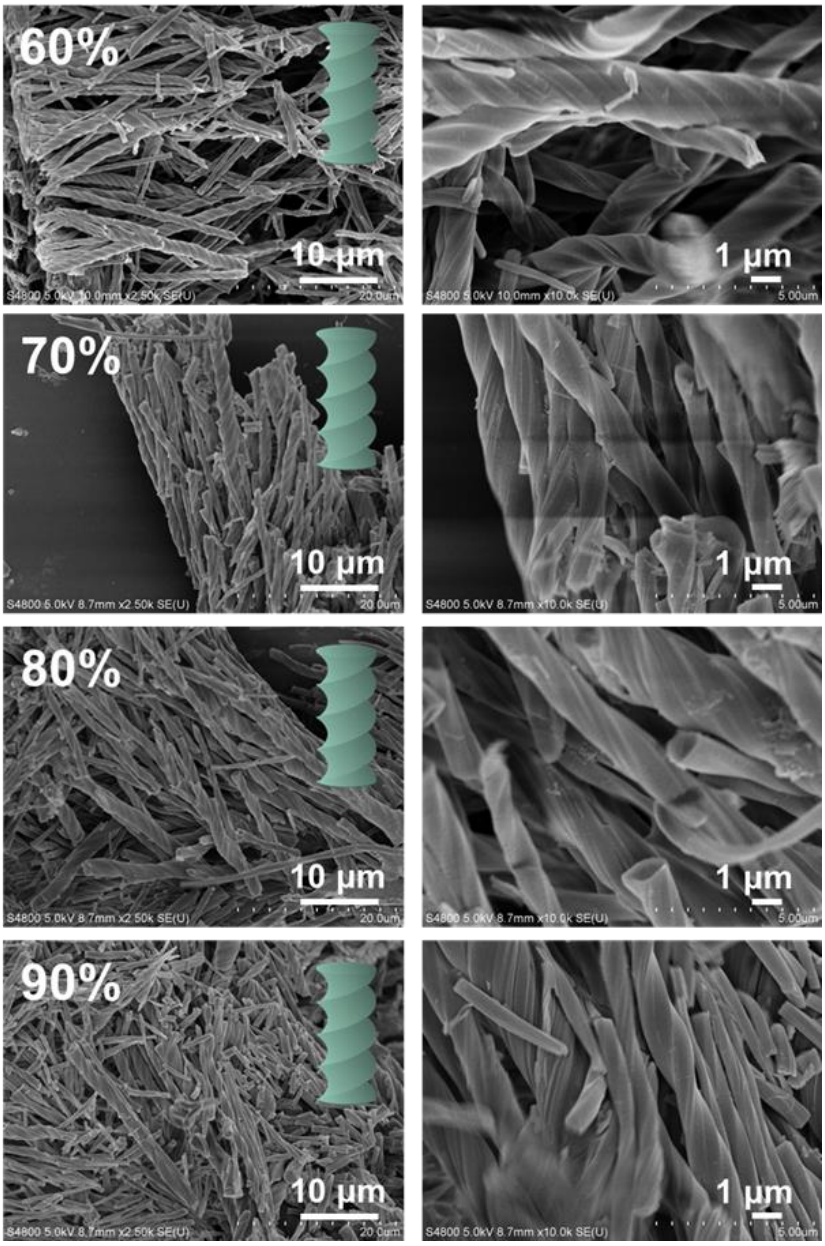

Figure S51. SEM images of the reaction products after hydrothermal reactions of $Eu(NO_3)_3$ and *R*-pempH_2 (molar ratio 1:5, autoclave filling degree 60-90 %) under pH 3.5 at 120 °C for 24 h.

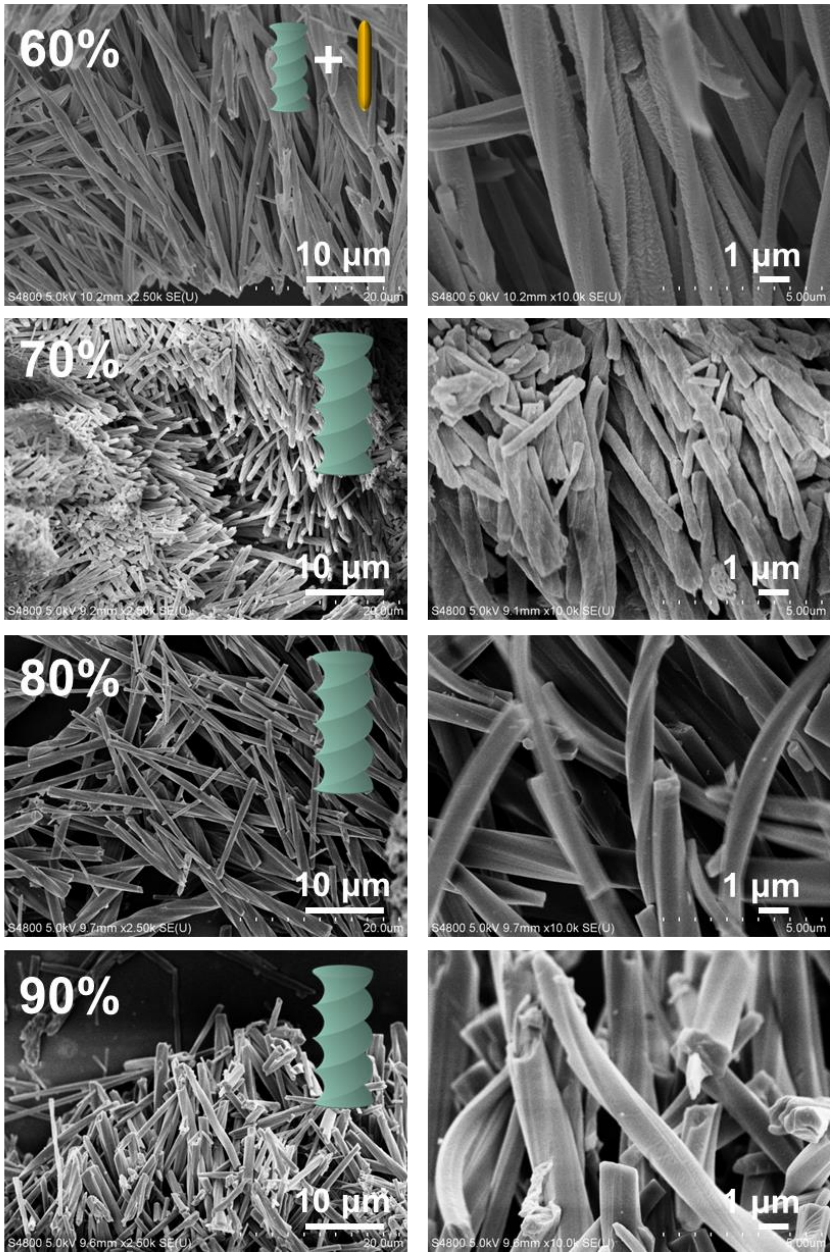

Figure S52. SEM images of the reaction products after hydrothermal reactions of $Gd(NO_3)_3$ and *R*-pempH$_2$ (molar ratio 1:5, autoclave filling degree 60-90 %) under pH 3.5 at 120 °C for 24 h.

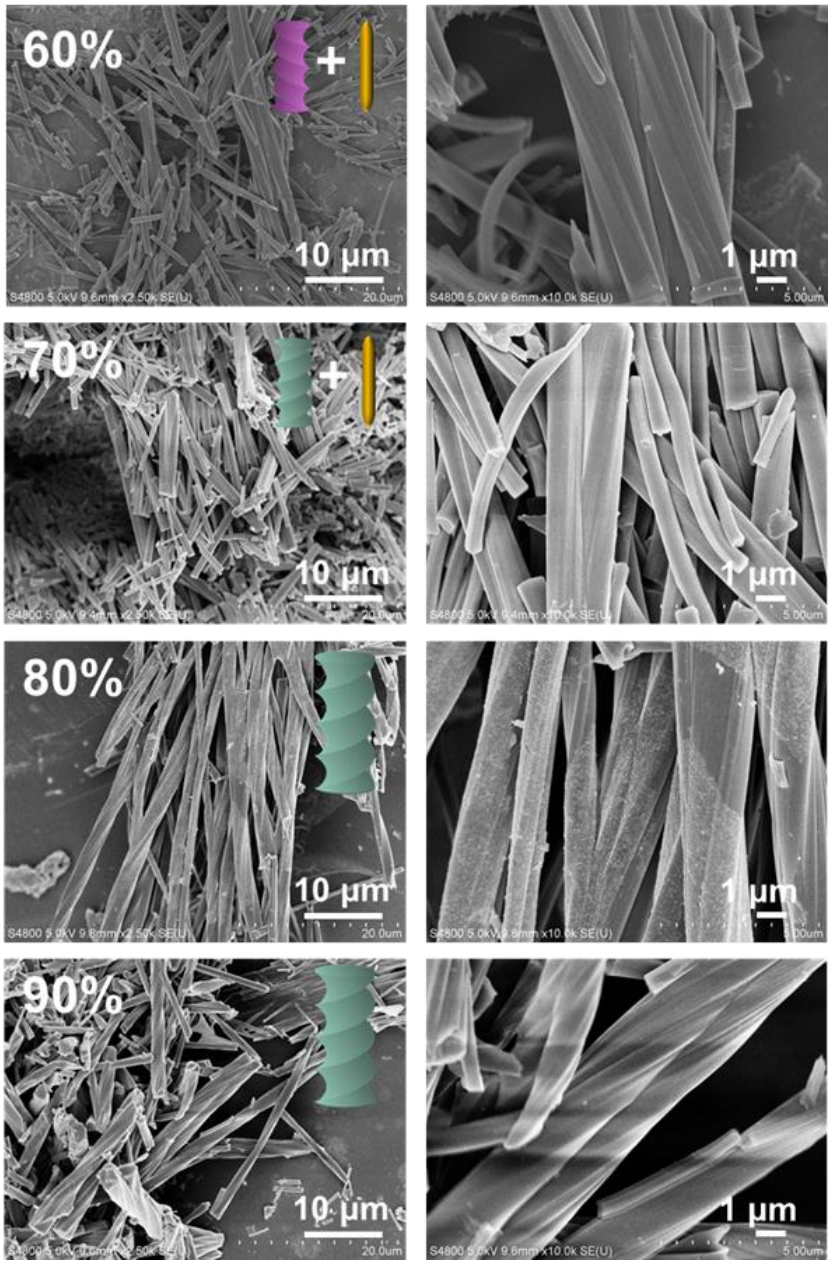

Figure S53. SEM images of the reaction products after hydrothermal reactions of $Tb(NO_3)_3$ and *R*-pempH$_2$ (molar ratio 1:5, autoclave filling degree 60-90 %) under pH 3.5 at 120 °C for 24 h.

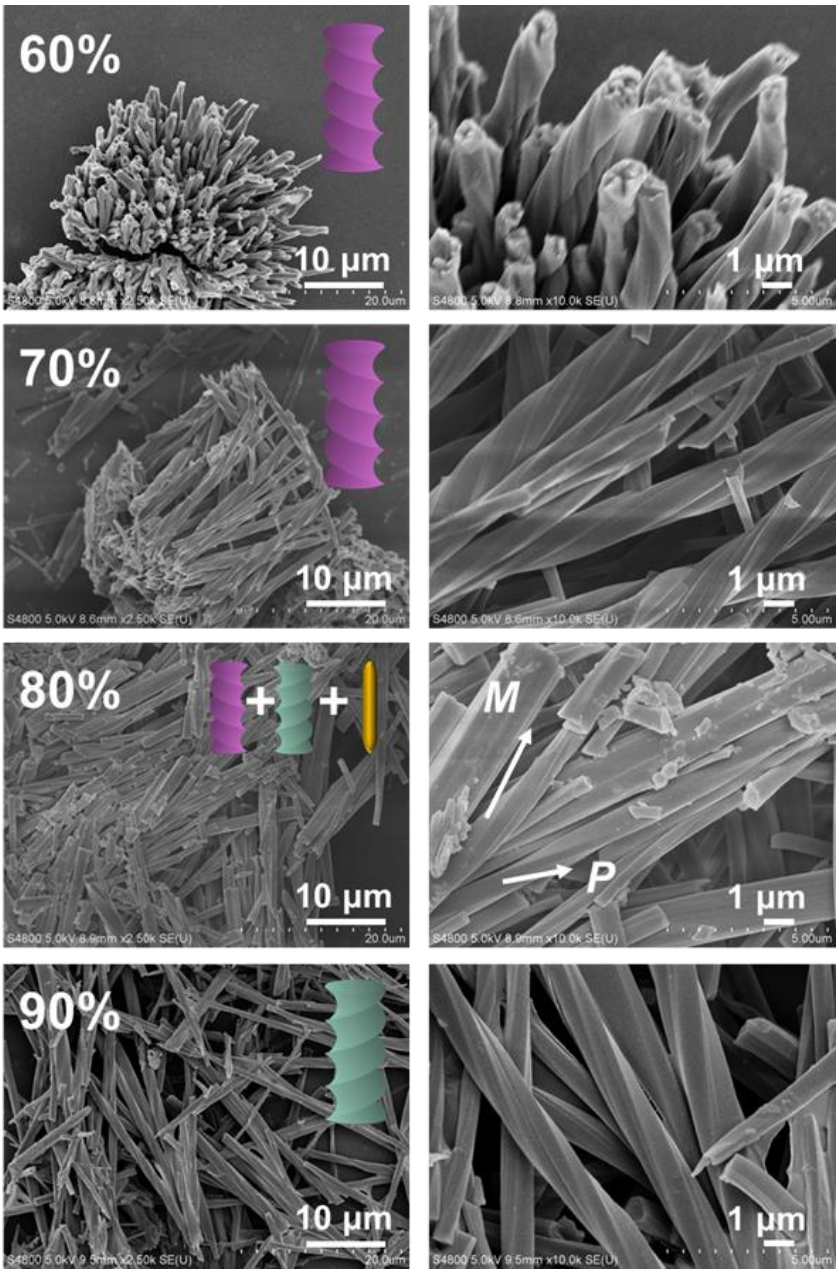

Figure S54. SEM images of the reaction products after hydrothermal reactions of $Dy(NO_3)_3$ and *R*-pempH$_2$ (molar ratio 1:5, autoclave filling degree 60-90 %) under pH 3.5 at 120 °C for 24 h.

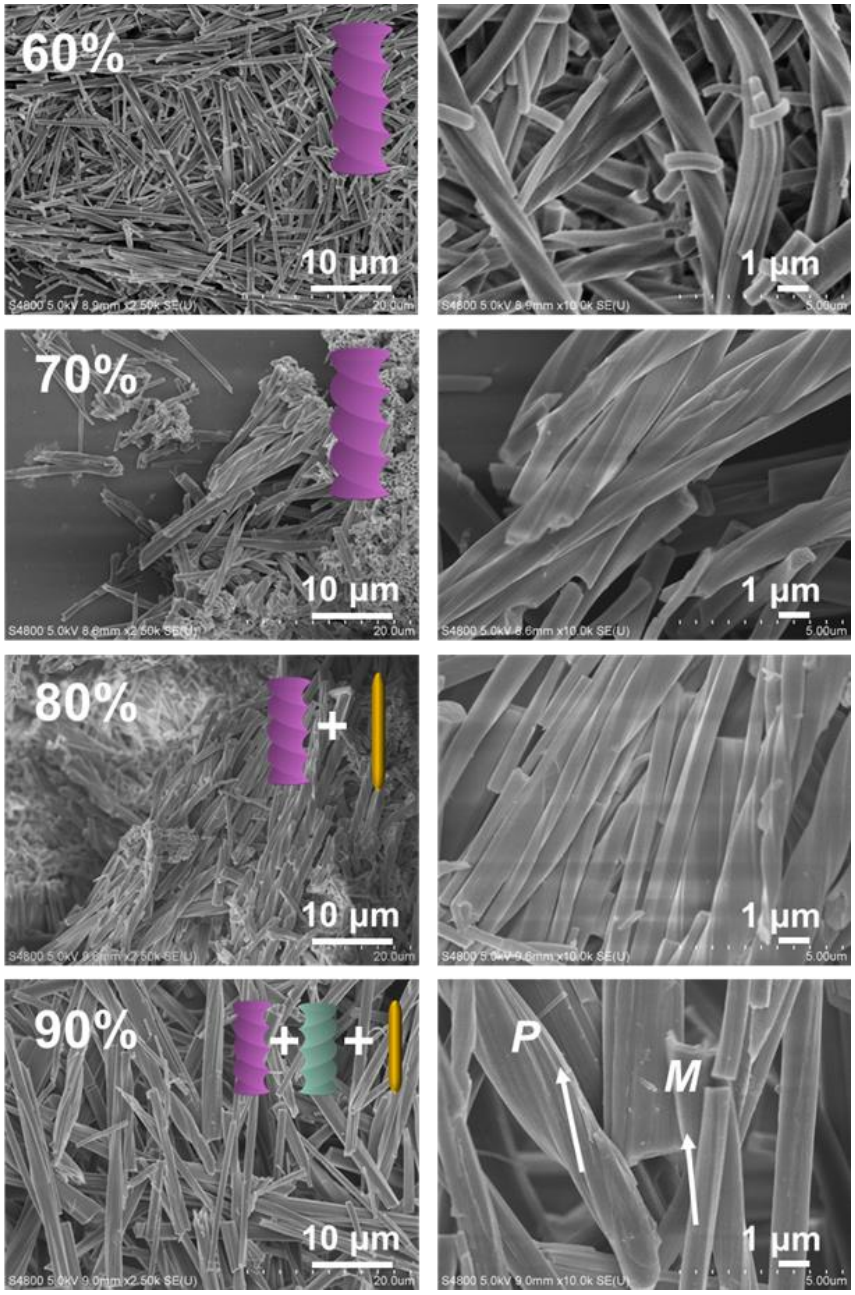

Figure S55. SEM images of the reaction products after hydrothermal reactions of $Ho(NO_3)_3$ and *R*-pempH$_2$ (molar ratio 1:5, autoclave filling degree 60-90 %) under pH 3.5 at 120 °C for 24 h.

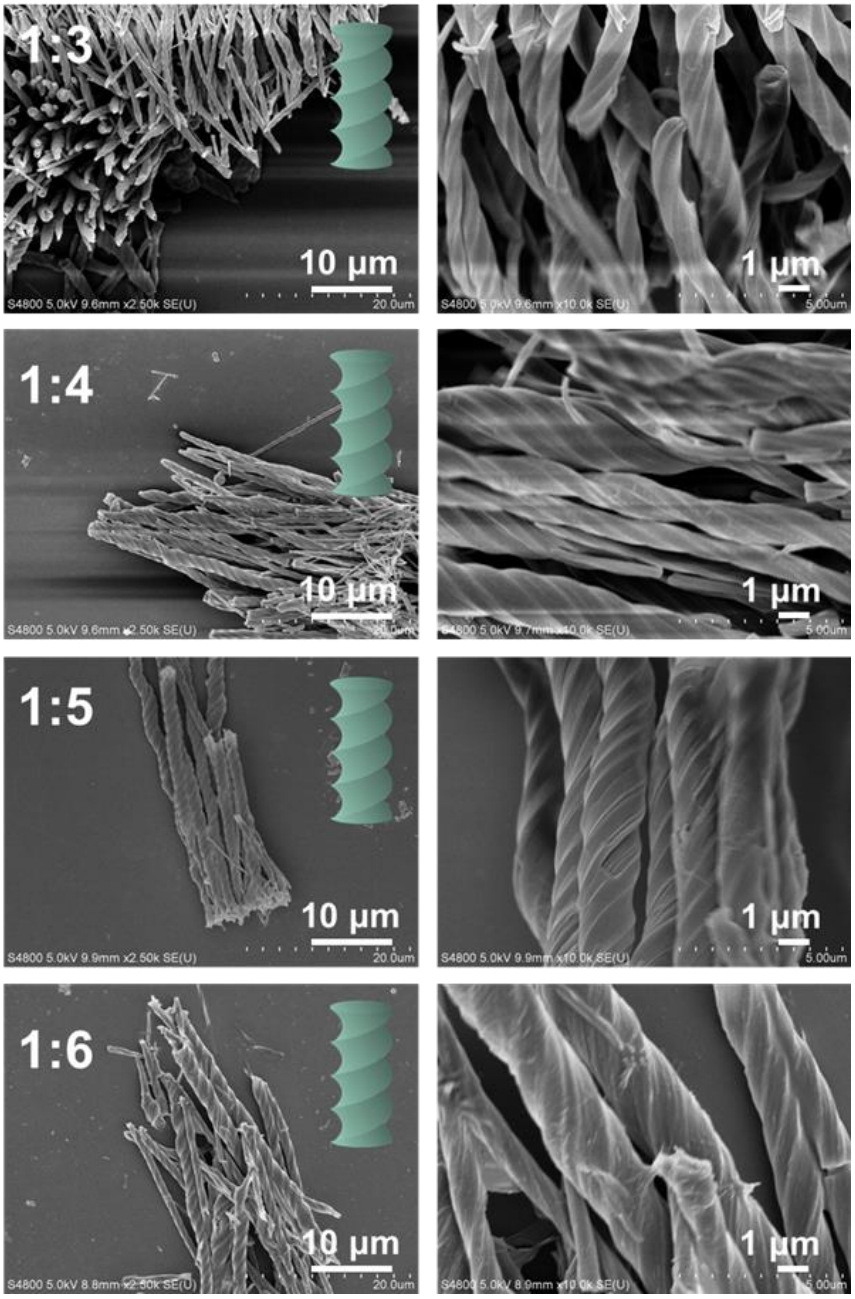

Figure S56. SEM images of the reaction products after hydrothermal reactions of $Sm(NO_3)_3$ and *R*-pempH$_2$ with different molar ratio (1:3-6) (autoclave filling degree 60%) under pH 3.5 at 120 °C for 24 h.

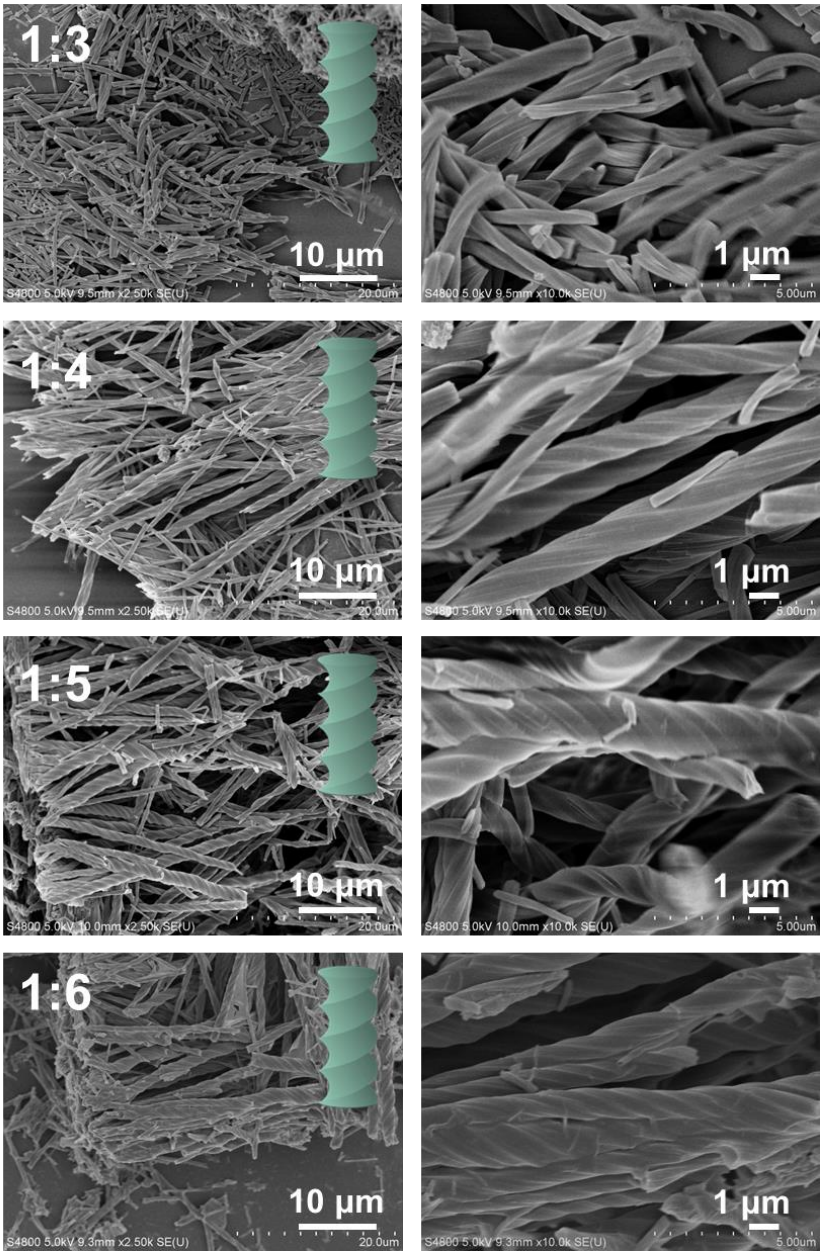

Figure S57. SEM images of the reaction products after hydrothermal reactions of $Eu(NO_3)_3$ and *R*-pempH$_2$ with different molar ratio (1:3-6) (autoclave filling degree 60 %) under pH 3.5 at 120 °C for 24 h.

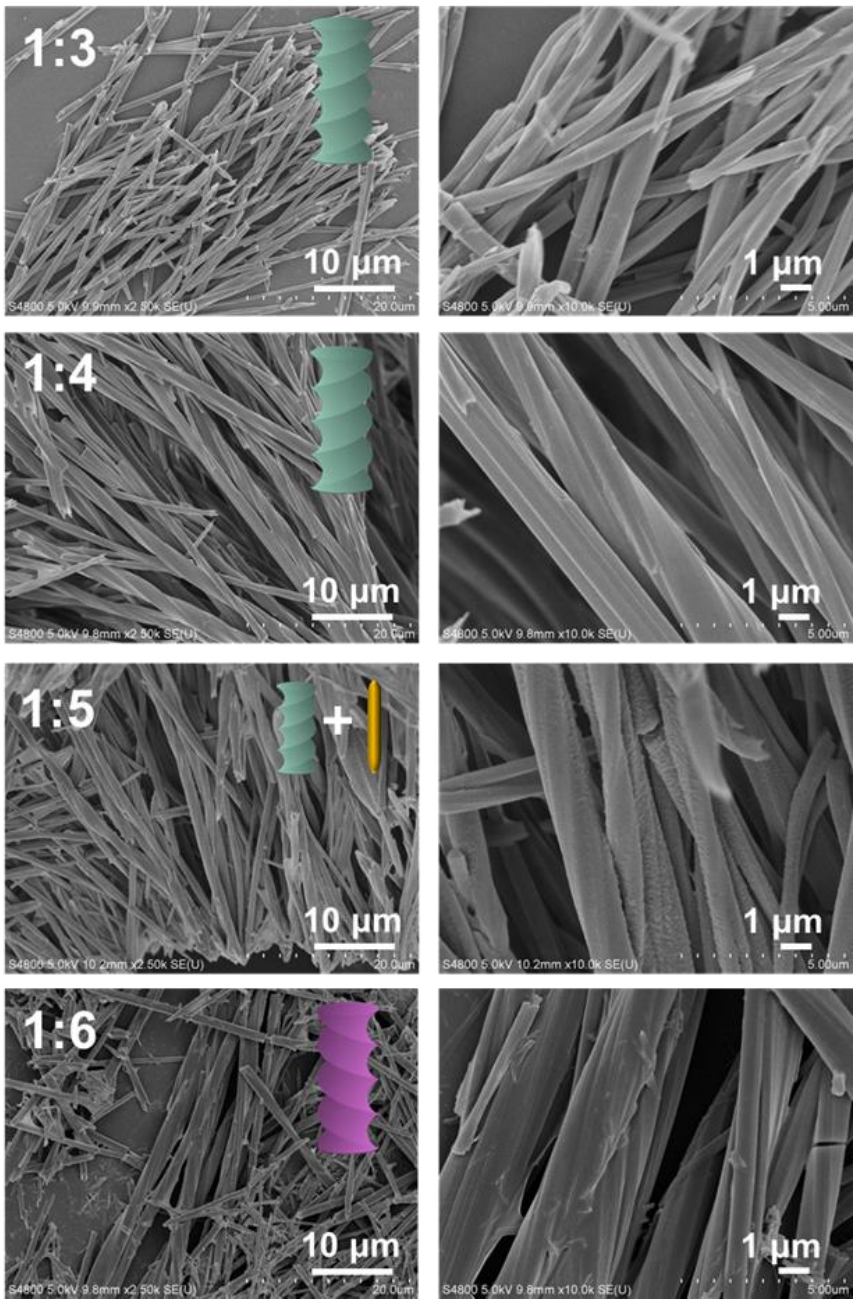

Figure S58. SEM images of the reaction products after hydrothermal reactions of $Gd(NO_3)_3$ and *R*-pempH$_2$ with different molar ratio (1:3-6) (autoclave filling degree 60 %) under pH 3.5 at 120 °C for 24 h.

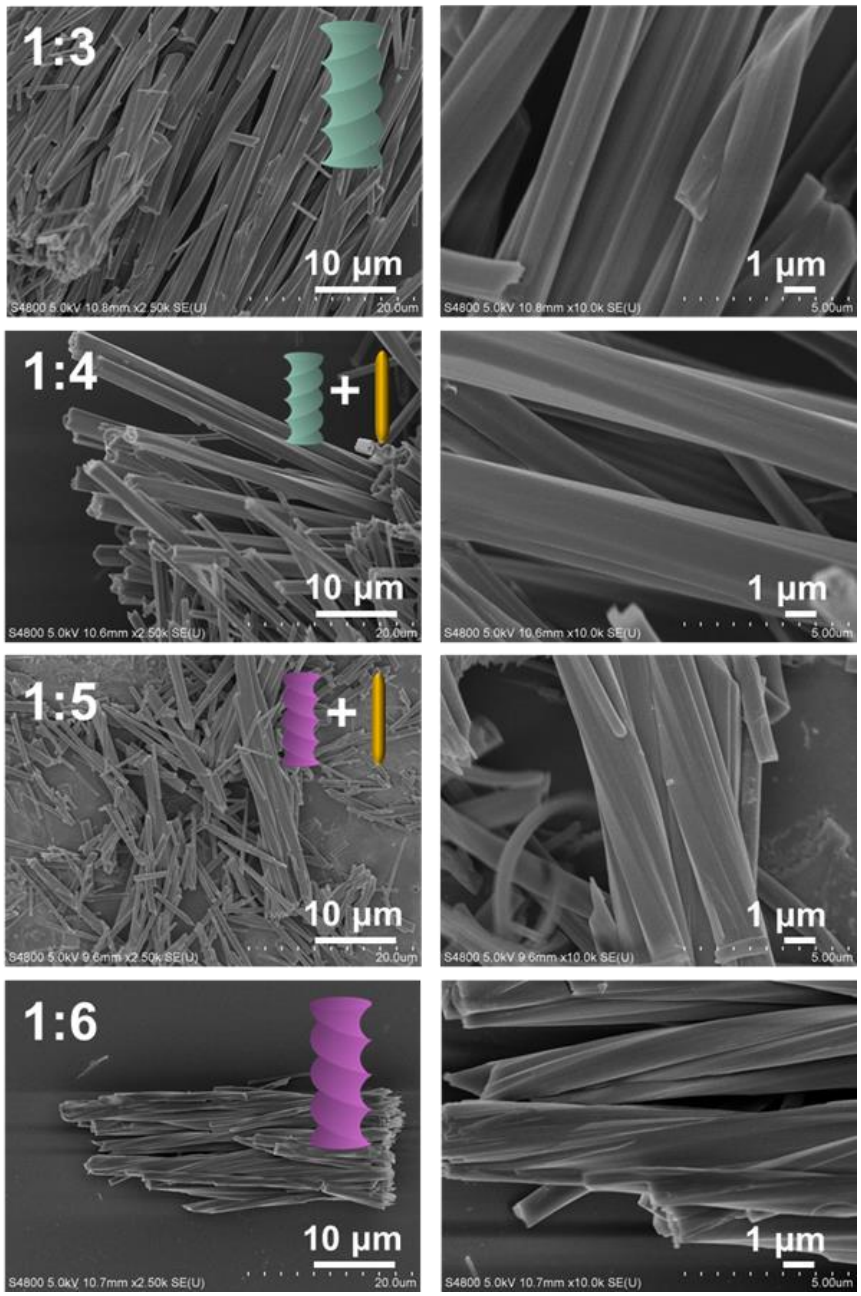

Figure S59. SEM images of the reaction products after hydrothermal reactions of $Tb(NO_3)_3$ and *R*-pempH$_2$ with different molar ratio (1:3-6) (autoclave filling degree 60 %) under pH 3.5 at 120 °C for 24 h.

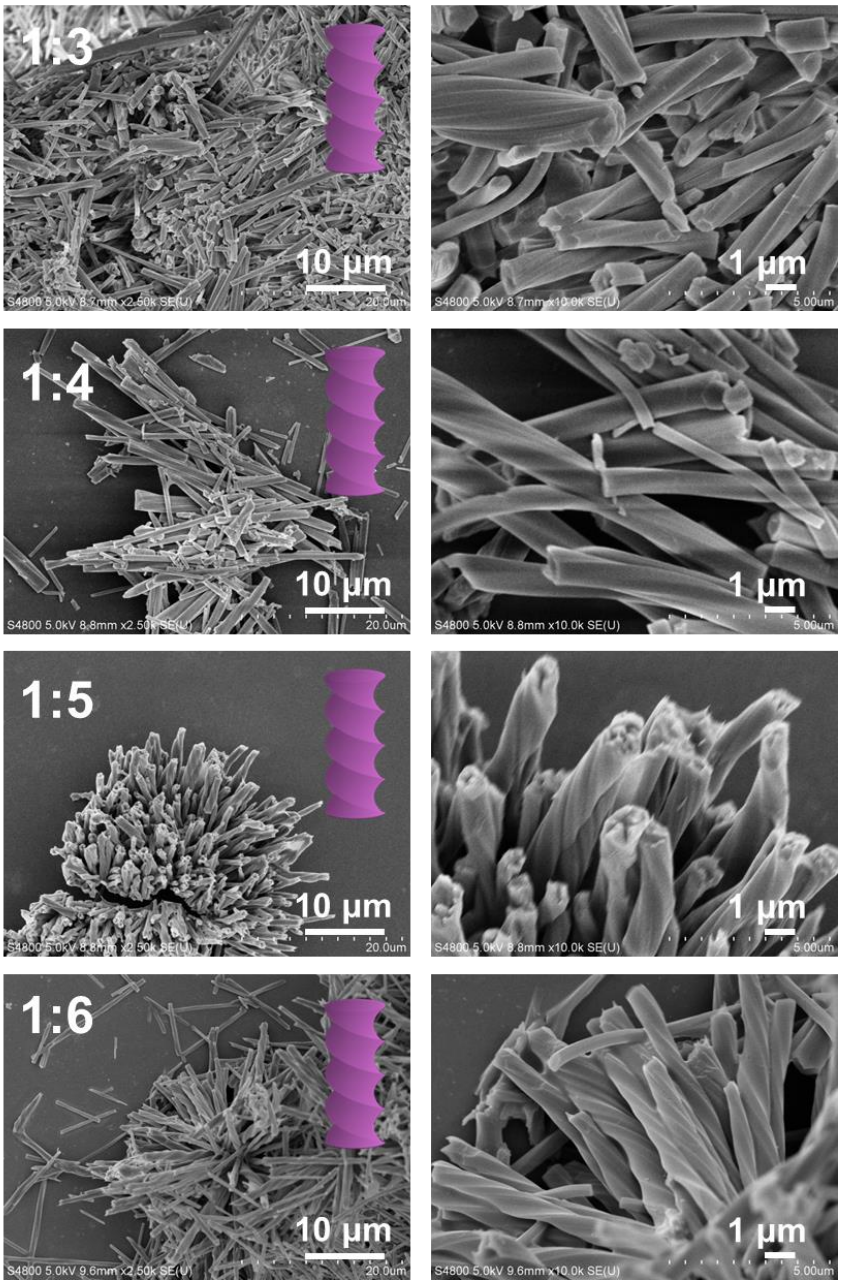

Figure S60. SEM images of the reaction products after hydrothermal reactions of $Dy(NO_3)_3$ and *R*-pempH$_2$ with different molar ratio (1:3-6) (autoclave filling degree 60 %) under pH 3.5 at 120 °C for 24 h.

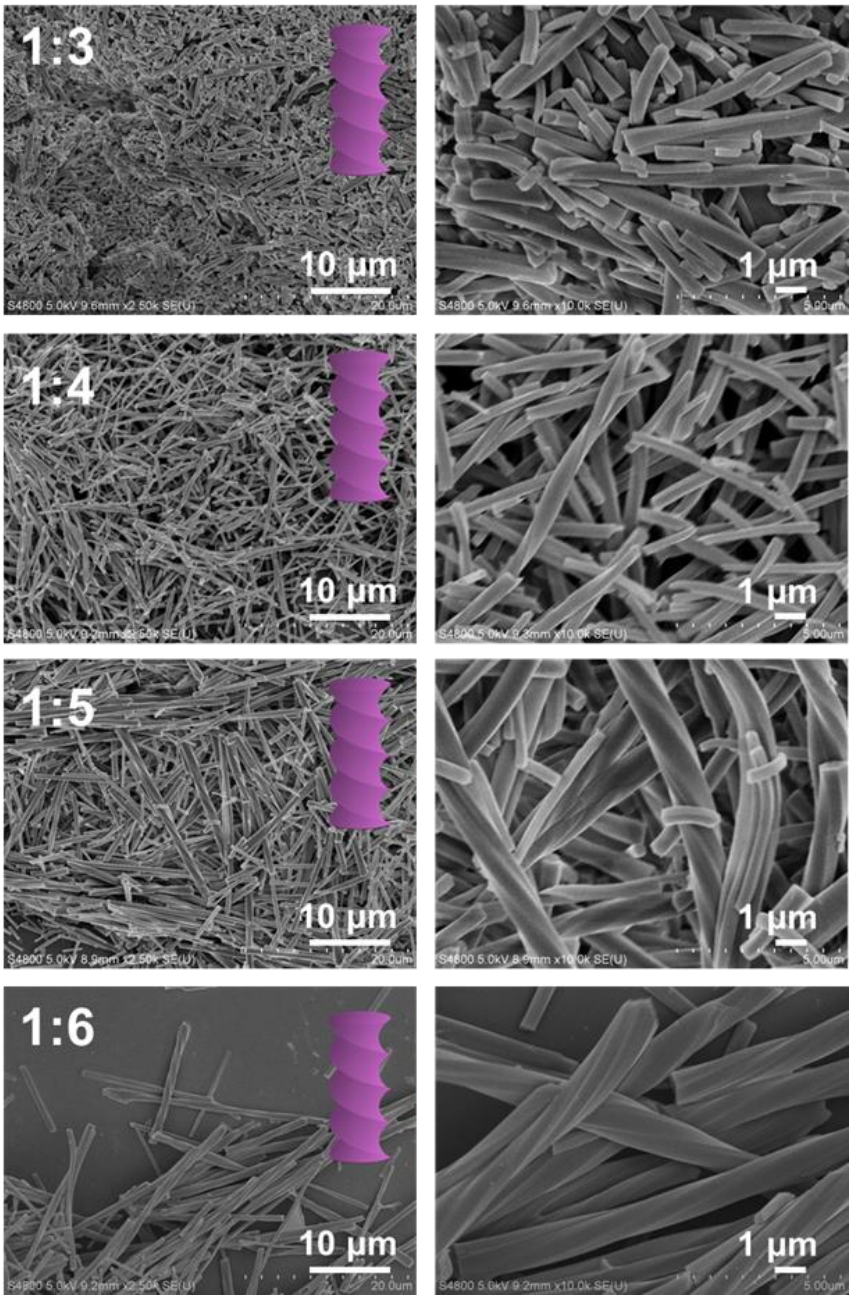

Figure S61. SEM images of the reaction products after hydrothermal reactions of $Ho(NO_3)_3$ and *R*-pempH$_2$ with different molar ratio (1:3-6) (autoclave filling degree 60 %) under pH 3.5 at 120 °C for 24 h.

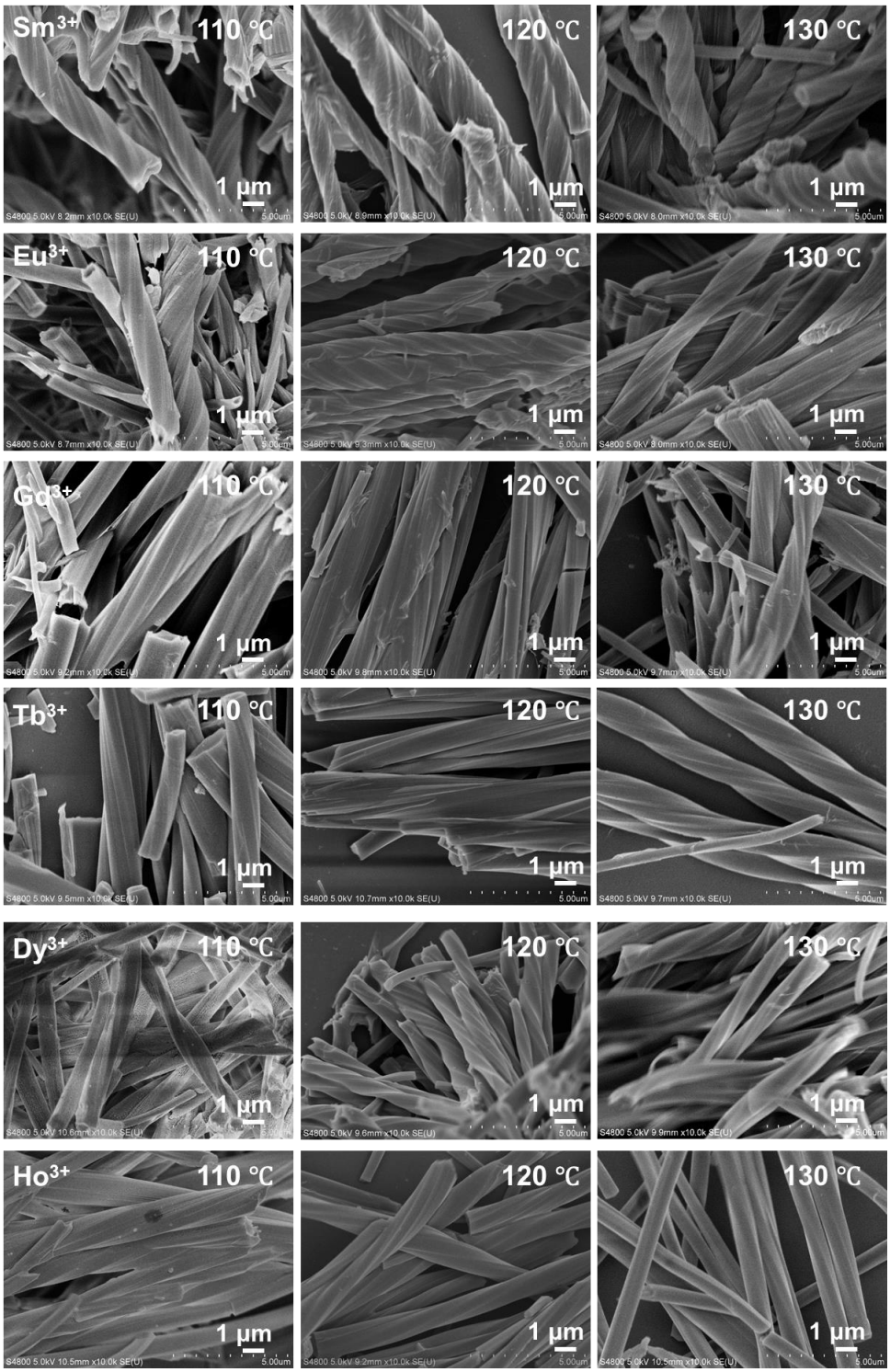

Figure S62. SEM images of the products after hydrothermal reactions of $Ln(NO_3)_3$ and *R*-pempH$_2$ for 24 h at different temperatures (110–130 °C).

Table S8. Summary of the morphology of the hydrothermal reaction products of $Ln(NO_3)_3 \cdot 6H_2O$ and *R*-pempH_2 at different reaction conditions (pH = 3.5).

pH	M:L ratio	Autoclave filling (%)	Products	Helical direction	pH	M:L ratio	Autoclave filling (%)	Products	Helical direction
3.5	1: 6	60	***R*-1h-Sm**	***P***	3.5	1: 3	60	***R*-1h-Sm**	***P***
3.5	1: 6	70	***R*-1h-Sm**	***P***	3.5	1: 4	60	***R*-1h-Sm**	***P***
3.5	1: 6	80	***R*-1h-Sm**	***P***	3.5	1: 5	60	***R*-1h-Sm**	***P***
3.5	1: 6	90	***R*-1h-Sm**	***P***	3.5	1: 6	60	***R*-1h-Sm**	***P***
3.5	1: 6	60	***R*-1h-Eu**	***P***	3.5	1: 3	60	***R*-1h-Eu**	***P***
3.5	1: 6	70	***R*-1h-Eu**	***P***	3.5	1: 4	60	***R*-1h-Eu**	***P***
3.5	1: 6	80	***R*-1h-Eu**	***P***	3.5	1: 5	60	***R*-1h-Eu**	***P***
3.5	1: 6	90	***R*-1h-Eu**	***P***	3.5	1: 6	60	***R*-1h-Eu**	***P***
3.5	1: 6	60	***R*-1h-Gd**	***M***	3.5	1: 3	60	***R*-1h-Gd**	***P***
3.5	1: 6	70	***R*-1h-Gd**	***M***	3.5	1: 4	60	***R*-1h-Gd**	***P***
3.5	1: 6	80	***R*-1h-Gd**	***M***	3.5	1: 5	60	***R*-1h-Gd**	***P + N***
3.5	1: 6	90	***R*-1h-Gd**	***M***	3.5	1: 6	60	***R*-1h-Gd**	***M***
3.5	1: 6	60	***R*-1h-Tb**	***M***	3.5	1: 3	60	***R*-1h-Tb**	***P***
3.5	1: 6	70	***R*-1h-Tb**	***M***	3.5	1: 4	60	***R*-1h-Tb**	***P+N***
3.5	1: 6	80	***R*-1h-Tb**	***M***	3.5	1: 5	60	***R*-1h-Tb**	***M + N***
3.5	1: 6	90	***R*-1h-Tb**	***M***	3.5	1: 6	60	***R*-1h-Tb**	***M***
3.5	1: 6	60	***R*-1h-Dy**	***M***	3.5	1: 3	60	***R*-1h-Dy**	***M***
3.5	1: 6	70	***R*-1h-Dy**	***M***	3.5	1: 4	60	***R*-1h-Dy**	***M***
3.5	1: 6	80	***R*-1h-Dy**	***M***	3.5	1: 5	60	***R*-1h-Dy**	***M***
3.5	1: 6	90	***R*-1h-Dy**	***M***	3.5	1: 6	60	***R*-1h-Dy**	***M***
3.5	1: 6	60	***R*-1h-Ho**	***M***	3.5	1: 3	60	***R*-1h-Ho**	***M***
3.5	1: 6	70	***R*-1h-Ho**	***M***	3.5	1: 4	60	***R*-1h-Ho**	***M***
3.5	1: 6	80	***R*-1h-Ho**	***M***	3.5	1: 5	60	***R*-1h-Ho**	***M***
3.5	1: 6	90	***R*-1h-Ho**	***M***	3.5	1: 6	60	***R*-1h-Ho**	***M***

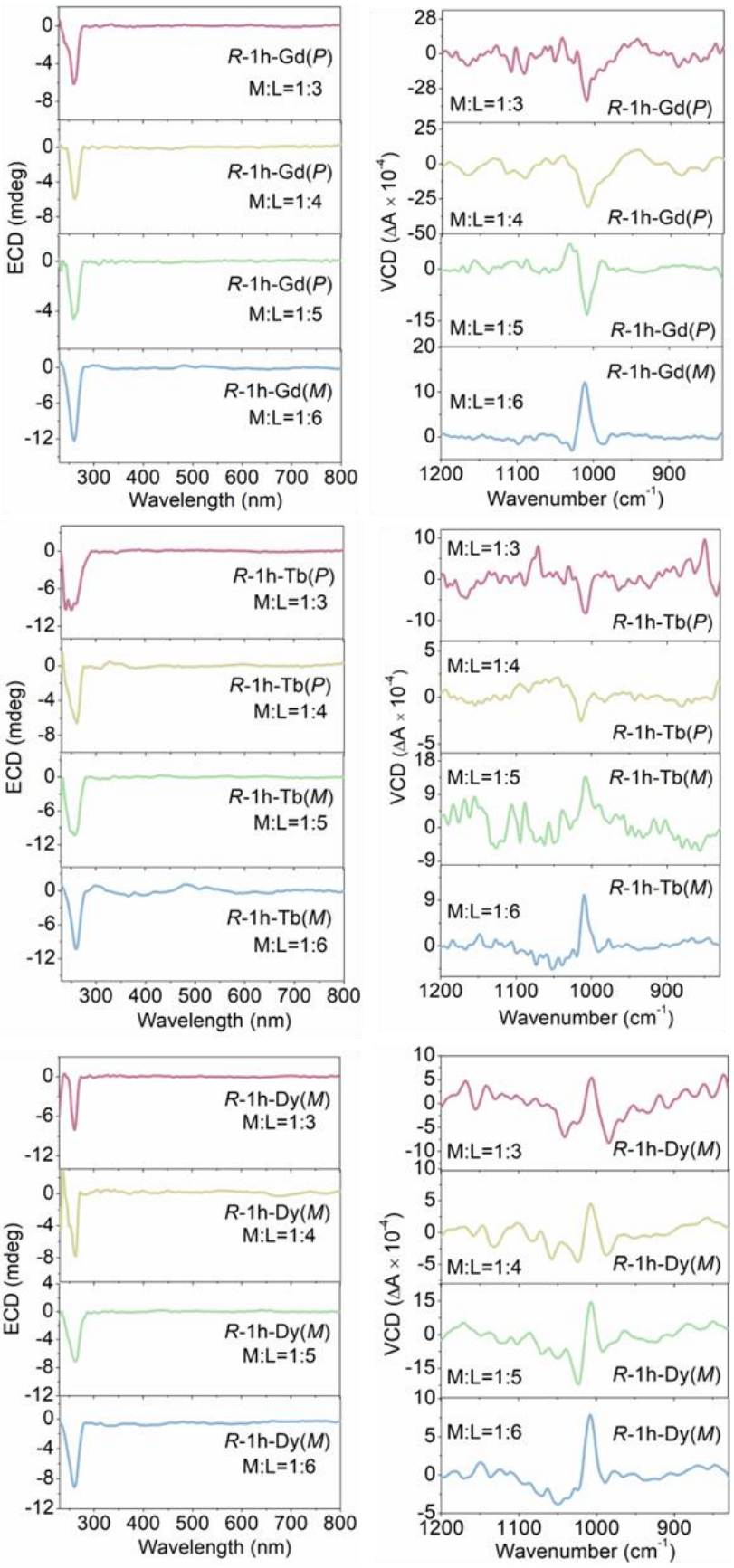

Figure S63. The ECD and VCD spectra of helical products ***R*-1h-Gd**, ***R*-1h-Tb** and ***R*-1h-Dy** in different M:L molar ratio.

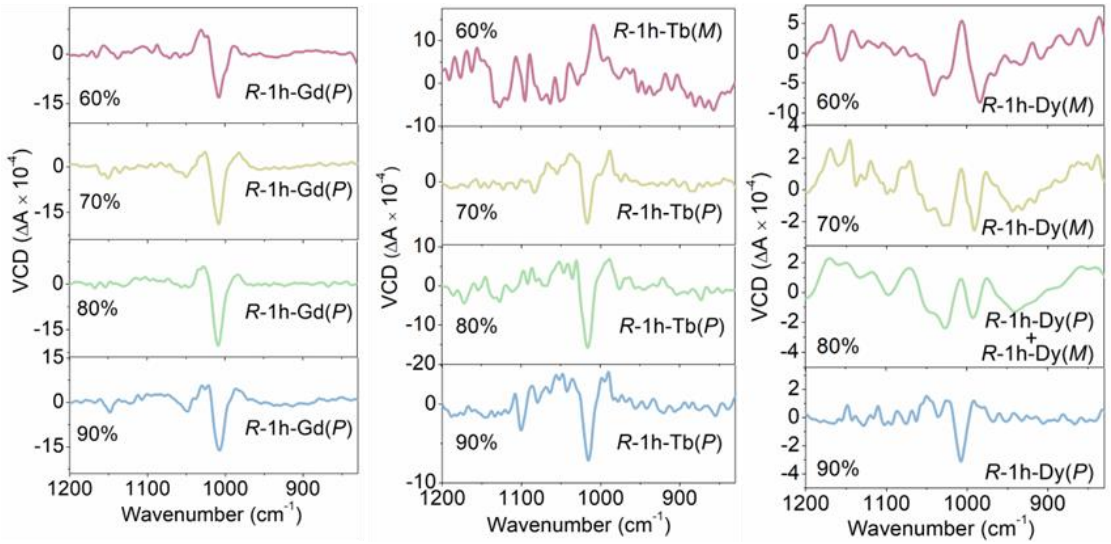

Figure S64. The VCD spectra of helical products ***R*-1h-Gd**, ***R*-1h-Tb** and ***R*-1h-Dy** in different autoclave filling degree (60-90 %) when M:L molar ratio is 1:5.

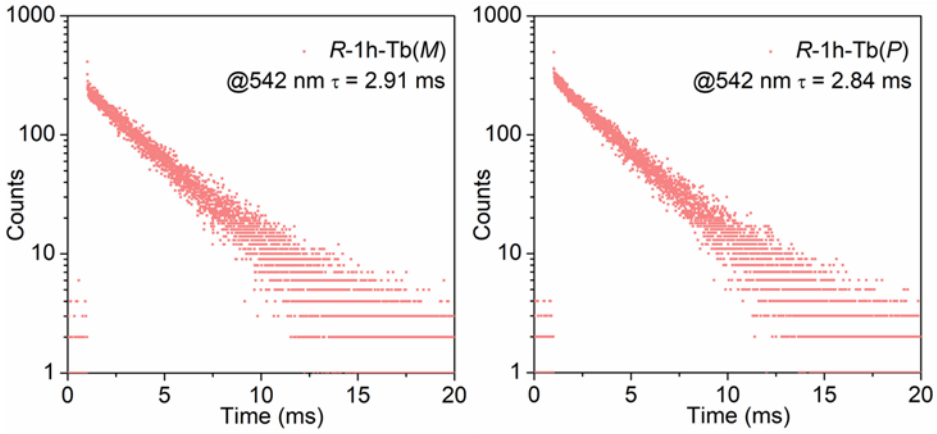

Figure S65. The luminescence decay curves of ***R*-1h-Tb(*M*)** and ***R*-1h-Tb(*P*)**. (λ_{ex} = 260 nm)

References

[1] a) X.-G. Liu, S.-S. Bao, Y.-Z. Li, L.-M. Zheng. Polymorphism in homochiral zinc phosphonates. *Inorg. Chem*., 2008, **47**, 5525–5527.

[2] Z.-M. Zhai, Ting Hou, Y. Xu, Q. Teng, S.-S. Bao, L.-M. Zheng. Hollow Superhelices Based on Chiral Europium Coordination Polymers. *Chem. Eur. J*. 2024, **31**, e202403699.

[3] T. Hou, L.-Q. Wu, Y. Xu, S.-S. Bao, L.-M. Zheng, pH and Salt-Assisted Macroscopic Chirality Inversion of Gadolinium Coordination Polymer. *Molecules,* 2023, **28**, 163.

[4] J. Huang, H.-M. Ding, Y. Xu, D. Zeng, H. Zhu, D.-M. Zang, S.-S. Bao, Y.-Q. Ma, L.-M. Zheng, Chiral expression from molecular to macroscopic level via pH modulation in terbium coordination polymers. *Nat. Commun.* 2017, **8**, 2131.

[5] Y. Xu, Y.-S. Yu, X.-D. Huang, S.-S. Bao, H.-M. Ding, Y.-Q. Ma, L.-M. Zheng, Counteranion Modulated Crystal Growth and Function of One-Dimensional Homochiral Coordination Polymers: Morphology,Structures, and Magnetic Properties. *Inorg. Chem*., 2018, **57**, 12143−12154.

[6] L.-Q. Wu, Y. Xu, T. Hou, J.-G. Jia, X.-D. Huang, G.-G. Weng, S.-S. Bao, L.-M. Controllable Macroscopic Chirality of Coordination Polymers through pH and Anion-Mediated Weak Interactions. *Chem. Eur. J*. 2021, **27**, 16722–16734.